

**NOVEL METHOD FOR DETECTING UNIFORM AND PARTIAL
DEMAGNETIZATION IN LINE START PERMANENT MAGNET
SYNCHRONOUS MOTORS**

BY

ABDULAZIZ SALEH MILHEM

A Thesis Presented to the
DEANSHIP OF GRADUATE STUDIES

KING FAHD UNIVERSITY OF PETROLEUM & MINERALS

DHAHRAN, SAUDI ARABIA

1963 ١٣٨٣

In Partial Fulfillment of the
Requirements for the Degree of

MASTER OF SCIENCE

In

ELECTRICAL ENGINEERING

MAY 2017

KING FAHD UNIVERSITY OF PETROLEUM & MINERALS

DHAHRAN- 31261, SAUDI ARABIA

DEANSHIP OF GRADUATE STUDIES

This thesis, written by **ABDULAZIZ SALEH MILHEM** under the direction his thesis advisor and approved by his thesis committee, has been presented and accepted by the Dean of Graduate Studies, in partial fulfillment of the requirements for the degree of **MASTER OF SCIENCE IN ELECTRICAL ENGINEERING.**



Dr. Ali A. Al-Shaikhi
Department Chairman



Dr. Zakariya M. Al-Hmouz
(Advisor)



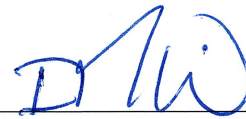
Dr. Salam A. Zummo
Dean of Graduate Studies



Dr. Mohammad A. Abido
(Member)

6/6/17

Date



Dr. Ibrahim M. El-Amin
(Member)

© ABDULAZIZ SALEH MILHEM

2017

This Thesis is dedicated to

The soul of my Father

My Dear Mother

My Wife

My Children Shahd, Omar and Noor

My Holy Homeland Palestine

ACKNOWLEDGMENTS

All praise and glory to Allah the most merciful, the most beneficent, who gave me the health, strength, and courage to complete my Master's degree.

I would like to express my deep appreciation to my advisor Prof. Zakariya Al-Hamouz for giving me the opportunity to become one of his students. I thank him for his efficient and constant support, help, motivation, and immense knowledge. His precious advices and thorough guidance played a critical role in completing this thesis.

I also would like to extend my appreciation to my dissertation committee members Prof. Mohammed Abido and Prof. Ibrahim El-Amin for their insightful comments, support, and profitable questions which incited me to enhance my work.

I would like to thank our research group members supervised by Prof. Zakariya Al-Hamouz, they include Mr. Luqman Marraba for his massive support and help, Mr. Khalid Baradiah and Mr. Ibrahim Hussein.

I am very grateful to Mr. Osama Hussain the General Manager and Mr. Samir Al-Hourani the Procurement Manager from Al-Osais Contracting Co. for their continuous support and understanding during the study period.

I am thankful to the King Fahd University of Petroleum and Minerals (KFUPM) for providing me with the research facilities, precious resources and an environment conducive to intellectual growth for my master research

TABLE OF CONTENTS

ACKNOWLEDGMENTS	V
TABLE OF CONTENTS	VI
LIST OF TABLES.....	IX
LIST OF FIGURES.....	X
LIST OF ABBREVIATIONS	XII
NOMENCLATURE	XIII
ABSTRACT	XVI
ملخص الرسالة.....	XVIII
CHAPTER ONE INTRODUCTION.....	1
1.1 Background.....	1
1.2 Thesis Motivations	2
1.3 Thesis Objectives.....	4
1.4 Thesis Organization	5
CHAPTER TWO LITERATURE REVIEW.....	6
2.1 Configuration of LSPMSM	6
2.2 B-H Curve of Permanent Magnet in LSPMSM	6
2.3 Permanent Magnet Material.....	8
2.4 LSPMSM Modelling Methods	9
2.4.1 Two-axes Reference Frame Model.....	9
2.4.2 Equivalent circuit mathematical model	10
2.4.3 Finite Element Method (FEM)	10
2.5 Faults in LSPMSM	10

2.5.1	Stator Faults	11
2.5.2	Rotor Faults	11
2.6	Summary of Literature Review	16
 CHAPTER THREE MATHEMATICAL MODELLING AND PARAMETER DETERMINATION OF LSPMSM		18
3.1	Introduction	18
3.2	Mathematical Model Description	18
3.2.1	Stator and Rotor Voltage Equations	19
3.3	Transformation to qd0 Reference Frame	20
3.3.1	Stator and Rotor Voltage Equations in qd0 Reference Frame	22
3.3.2	Flux Linkage Equations in qd0 Reference Frame:.....	23
3.3.3	Equation of Motion and Electromagnetic Torque.....	25
3.3.4	Healthy Model Summary.....	26
3.4	Parameter Determination of LSPMSM	27
3.4.1	DC Test	27
3.4.2	Open Circuit Test.....	28
3.4.3	Synchronous Speed Loading Test.....	28
3.4.4	Blocked Rotor Test	31
3.4.5	Single-phase AC Test	32
3.5	Behavior of LSPMSM	33
 CHAPTER FOUR MODELLING OF LSPMSM USING JMAG (FEM BASED SOFTWARE).....		39
4.1	Introduction	39
4.2	Modeling Demagnetization Fault	41
4.2.1	Healthy Model.....	42
4.2.2	Demagnetization Mechanism in LSPMSM	47
4.2.3	Indexing of Demagnetization	50
4.2.4	Demagnetization Through Three Phase Currents	54
4.2.5	Sudden Rotation Reversal Model.....	55
4.2.6	Sudden increase in supply voltage Model.....	58
 CHAPTER FIVE PROPOSED DIAGNOSTICS TECHNIQUE FOR DEMAGNETIZATION FAULTS IN LSPMSM.....		61
5.1	Introduction	61

5.2 Artificial Neural Network (ANN)	61
5.3 Fault Detection	63
5.3.1 Features Extraction	65
5.3.2 Features Selection	66
5.4 Possible Inputs	67
5.5 Feature Selection	68
5.5.1 Transient Versus. Steady State	68
5.5.2 Stator Current Behavior	70
5.5.3 Input Power	71
5.6 Simulation of ANN	76
5.6.1 ANN Configuration and Selected Parameters	76
5.6.2 Input / Output Training Lists	79
5.6.3 Test Cases:	80
5.6.4 Results of Testing the ANN	80
CHAPTER SIX CONCLUSIONS AND FUTURE WORK	84
6.1 Conclusions	84
6.2 Recommendations for Future Work	85
REFERENCES	86
APPENDICES	94
Appendix A MOTOR PARAMETERS	95
Appendix B JMAG-DESIGNER VERSION 16	98
Appendix C Matlab Code for Healthy Case	112
Appendix D Training Cases	113
Appendix E Testing Cases	121
VITAE	123

LIST OF TABLES

Table 2-1 Ordering by measures useful in motor applications [10]	9
Table 2-2 Causes and effects of broken rotor bars [46].....	12
Table 2-3 Summary for causes of demagnetization faults.....	16
Table 2-4 Summary of Literature Review	17
Table 3-1 Summary of parameter tests	27
Table 3-2: LSPMS motor specifications.....	34
Table 4-1 Summary for motor parameter	43
Table 4-2 Summary of study properties.....	43
Table 4-3 Categories of Demagnetization	53
Table 5-1 Demagnetization Percentage Classification	61
Table 5-2 Motor Variables.....	67
Table 5-3 Configuration of ANN.....	78
Table 5-4 Sample of training Cases	79
Table 5-5 Sample of Testing Cases	80
Table 5-6 Result of ANN Test Cases.....	80
Table 5-7 Summary for test results	83

LIST OF FIGURES

Figure 2-1 Construction of LSPMSM.....	6
Figure 2-2 Typical BH curve for LSPMSM	7
Figure 3-1 Stator and rotor circuits of LSPMS motor	19
Figure 3-2 qd reference frame attached to rotor	21
Figure 3-3 Phasor diagram of a salient pole PMSM.....	31
Figure 3-4 dq-axis equivalent circuit model of a LSPMSM in the rotor reference frame	32
Figure 3-5 Analysis for starting torque in LSPMSM.....	33
Figure 3-6: Stator current under different loading conditions	35
Figure 3-7: Electromagnetic torque under different loading conditions.....	35
Figure 3-8 Motor speed under different loading conditions	36
Figure 3-9 Motor speed under 3.99 NM load	36
Figure 3-10 Motor current with 50% and 10% value of the magnet flux.....	37
Figure 3-11 Motor torque with 50% and 10% value of the magnet flux	37
Figure 3-12 Motor speed with 50% and 10% value of the magnet flux	38
Figure 4-1 JMag Work Process Flowchart	41
Figure 4-2 Final LSPMSM Model.....	42
Figure 4-3 Rotational speed for healthy case.....	44
Figure 4-4 Induced torque for healthy case	44
Figure 4-5 Phase A current for healthy case.....	45
Figure 4-6 Comparison of motor speed at full load between Jmag and Matlab models ...	46
Figure 4-7 Comparison of motor current at full load between Jmag and Matlab models	46
Figure 4-8 Comparison of motor torque at full load between Jmag and Matlab models .	47
Figure 4-9 Demagnetization curve and recoil line of LSPMSM	48
Figure 4-10 Measurement Location of Operating Point in the magnet	49
Figure 4-11 Values of operating points	50
Figure 4-12 Summary of demagnetization indexes	51
Figure 4-13 B-H curve for LSPMSM	52
Figure 4-14 Circuit for Demagnetization by current	54
Figure 4-15 Residual magnetic flux density (T).....	55
Figure 4-16 Circuit for rotation reverse	55
Figure 4-17 Rotational speed during phase reversal.....	56
Figure 4-18 Rotor magnets before rotation reversal	57
Figure 4-19 Rotor magnets during rotation reversal.....	58
Figure 4-20 Circuit for supply voltage sudden increase	59
Figure 4-21 Rotational speed during supply voltage increase	59
Figure 4-22 Rotor magnets during normal operation	60
Figure 4-23 Rotor magnets during voltage increase	60
Figure 5-1: Basic structure of neuron.	62
Figure 5-2: A single layer in neural networks.	63

Figure 5-3: Detection scheme using ANN.....	65
Figure 5-4 Rotational speed under various rotor initial position	69
Figure 5-5 Phase current for various rotor initial positions	70
Figure 5-6 RMS stator phase current with load	71
Figure 5-7 Instantaneous apparent power	72
Figure 5-8 Instantaneous apparent power FFT	72
Figure 5-9 Partial Demagnetization for 60°C	73
Figure 5-10 Partial Demagnetization for 120 °C	73
Figure 5-11 Partial Demagnetization for 150 °C	74
Figure 5-12 Uniform Demagnetization for 60 °C	74
Figure 5-13 Uniform Demagnetization for 120 °C	75
Figure 5-14 Uniform Demagnetization for 150 °C	75
Figure 5-15 Configuration no.1 for ANN	76
Figure 5-16 Flow chart for ANN Detection.....	77
Figure 5-17 Matlab training process of ANN	78

LIST OF ABBREVIATIONS

ANNs	:	Artificial Neural Networks
FEA	:	Finite Element Analysis
FEM	:	Finite Element Method
FFNN	:	Feedforward neural network
ICCG	:	incomplete Cholesky conjugate gradient
IVS	:	Input variable selection
LSPMS	:	Line Start Permanent Magnet Synchronous
LSPMSM	:	Line Start Permanent Magnet Synchronous Motor
MCSA	:	Motor Current Signature Analysis
MMF	:	Magneto-motive Force
PM	:	Permanent Magnets
PMSM	:	Permanent Magnet Synchronous Motor
RMS	:	Root mean square error

NOMENCLATURE

g_0	:	Airgap length
H	:	Magnetic field intensity
i_A	:	Current in coil A
i_d	:	Direct current
$i_{r,abc}$:	Rotor circuit currents per each phase
$i_{r,qd0}$:	Rotor circuit currents in qd0 reference frame
$i_{s,abc}$:	Stator circuit currents per each phase
$i_{s,qd0}$:	Stator circuit currents in qd0 reference frame
i_q	:	Quadrature current
J	:	Motor moment of inertia
K_s	:	Park transformation matrix
K_r	:	Clark transformation matrix
l	:	Motor stack length
l_{ls}	:	Stator winding leakage inductance
l_{lr}	:	Rotor winding leakage inductance
L_{rr}	:	Rotor winding self-inductance
L_{rs}	:	Rotor to stator mutual inductance
L_s	:	Stator winding self-inductance
L_{sr}	:	Stator to rotor mutual inductance
$L_{r,qd0}$:	Rotor winding self-inductance in qd0 reference frame
$L_{rs,qd0}$:	Rotor to stator mutual inductance in qd0 reference frame
$L_{s,qd0}$:	Stator winding self-inductance in qd0 reference frame
$L_{sr,qd0}$:	Stator to rotor mutual inductance in qd0 reference frame

N	:	Number of samples or operating conditions
N_s	:	Number of stator winding turns
N_r	:	Number of rotor winding turns
N_e	:	Number of equivalent winding turns
p	:	The permeance in flux path
P	:	Number of poles
P_p	:	Number of pole pairs
R_s	:	Radius of stator inner race
r	:	Average radius of the motor airgap
T_{damp}	:	Damping torque
T_{em}	:	The developed electromechanical torque
T_{mech}	:	Input load torque
$V_{r,abc}$:	Rotor circuit terminal voltages
$V_{r,qd0}$:	Rotor circuit terminal voltages in qd0 reference frame
$V_{s,abc}$:	Stator terminal voltages
$V_{s,qd0}$:	Stator circuit terminal voltages in qd0 reference frame
ω	:	Angular speed
ω_r	:	Rotor angular speed
$\lambda_{r,abc}$:	Flux linkage of rotor windings
$\lambda_{r,qd0}$:	Flux linkage of rotor windings in qd0 reference frame
$\lambda_{s,abc}$:	Flux linkage of stator windings
$\lambda_{s,qd0}$:	Flux linkage of stator windings in qd0 reference frame
λ_m	:	Peak magnetic flux of the permanent magnets
$\lambda_{r,pm}$:	Rotor permanent magnets flux components

$\lambda_{s,pm}$:	Stator permanent magnets flux components
λ_d	:	Direct axis flux linkage
λ_q	:	Quadrature axis flux linkage
ϕ	:	Spatial reference angle from (as) stator winding axis

ABSTRACT

Full Name : [Abdulaziz Saleh Mustafa Milhem]
Thesis Title : [Novel Method for Detecting Uniform and Partial Demagnetization in Line Start Permanent Magnet Synchronous Motors]
Major Field : [Electrical Engineering]
Date of Degree : [May 2017]

Electrical Motors are widely employed in both industrial and domestic fields. Line Start-Permanent Magnet Synchronous Motor (LSPMSM) is one of the modern high efficiency motor introduced. This motor has a self-starting capability, the ability to reach a synchronous speed, and a premium efficiency. During the operation of electrical motors, various faults occur that lead to malfunction of the motor. Among these faults, demagnetization faults are important in the motors with permanent magnets. Demagnetization faults are known to be uniform or partial faults on the rotor magnets. These faults decrease the performance, the reliability and the efficiency of the LSPMSM drive systems.

The aim of this thesis is to investigate and identify the existence of demagnetization faults in LSPMSM on line without disturbing the normal operation of the system. A mathematical model for healthy case is derived based on the coupled magnetic circuit and Matlab/Simulink was used to simulate the results. Finite Element Method (FEM) analysis is used through JMAG-Designer to study the motor behavior and simulate the demagnetization faults. Both model shows very good agreement in the healthy case, while the mathematical model could not be used in the faulty case due to the existence of unsymmetrical q-axis magnet flux linkage in the faulty case.

Based on features extracted from the line current and voltage, Artificial Neural Network (ANN) is utilized successfully to predict the fault type and degree with an overall performance of 94.7%.

This study presents an on-line detection scheme with an ability to distinct between partial and uniform demagnetization while such scheme is not presented in the literature so far. Moreover, the scheme output provides classification for the degree of demagnetization, which is also not presented in the literature so far.

ملخص الرسالة

الاسم الكامل: عبد العزيز صالح مصطفى ملحم

عنوان الرسالة: طريقة جديدة للكشف عن فقد التمغط الجزئي والكلي في المحركات المتزامنة دائمة المغناطيسية باستخدام الشبكة العصبية الاصطناعية

التخصص: الهندسة الكهربائية

تاريخ الدرجة العلمية: أيار ٢٠١٧ م – شعبان ١٤٣٨ هـ

تستخدم المحركات الكهربائية بشكل واسع في القطاعات الصناعية والتجارية والسكنية. المحرك التزامني دائم المغناطيسية الذي يعمل من مصدر الجهد مباشرة، هو أحد المحركات حديث التصنيع والتطوير. يتمتع هذا المحرك بقدرته الذاتية على الحركة عند التشغيل، وعلى قدرته للوصول الى سرعة تزامنية ثابتة، ويتمتع ايضا بكفاءة استثنائية عن باقي المحركات الكهربائية. يتعرض هذا المحرك كما باقي الأجهزة الكهربائية الى مشاكل فنية كهربائية وميكانيكية تقلل من كفاءته وقد تتسبب في تعطيل عمل هذا المحرك. مشكلة فقد التمغط في المحركات التي تحتوي على مغناطيس دائم هي أحد المشاكل الرئيسة المؤثرة. تنقسم مشكلة فقد التمغط الى فقد تمغط كلي أو جزئي. ينتج عن فقد التمغط تناقص أداء وكفاءة وموثوقية الأنظمة التي تعمل فيها هذه المحركات.

هدف هذه الدراسة هو كشف وتحديد وجود مشاكل عدم التمغط في المحركات المتزامنة دائمة المغناطيسية أثناء عمل المحرك بدون تعطيله. لقد تم اشتقاق نموذج رياضي يوصف الحالة الطبيعية للمحرك بناءً على مبدأ الدائرة المغناطيسية المترابطة، وتم محاكاة سلوك المحول على برنامج (Matlab) باستخدام النموذج الرياضي. كما تم عمل نموذج للمحرك باستخدام برنامج (JAMG) القائم على مبدأ الأجزاء المحدودة لمحاكاة سلوك المحرك ومحاكاة مشكلة فقد التمغط. وقد اتفقت نتائج الحالة الطبيعية للنموذجين ولكن لم يستطع النموذج الرياضي وصف خطأ عدم التمغط نظرا لوجود قيمة للمجال المغناطيسي القادم من المغناطيس الدائم باتجاه المحور (q).

بناءً على الخصائص والسمات المشتقة من التيار والجهد، فقد تم تصميم شبكة عصبية اصطناعية لكشف حدوث فقدان التمغط تحت الظروف المختلفة وقد نجحت بدقة ٩٤,٧ بالمئة.

تقدم هذه الدراسة زيادة عما هو موجود في مراجع البحث العلمي، الية للكشف عن مشكلة فقد التمغط أثناء عمل المحرك وبدون الحاجة الى اطفائه. كما تقوم هذه الالية بتوضيح نوع عدم التمغط ونسبة عدم التمغط بطريقة لم تقدم من قبل.

CHAPTER ONE

INTRODUCTION

1.1 Background

High efficiency motors are being gradually exerted in many industrial applications of developed countries because of their positive impact on the environment by reducing energy consumption and CO₂ emission. The efficiency improvement of induction motors, which are the majority of the motors used in industry, was tried through an optimal design of induction motors. However, it is difficult to improve the induction motors efficiency significantly due to its inherent limitations. An alternative solution, which is of great interest, is to replace the induction motors with high efficiency permanent magnet (PM) motors. An important obstacle for ordinary PM motors is that this type of motor needs inverter for starting. Adding inverter is not economical for many single speed applications. To overcome this problem, the cage equipped PM motors; called Line Start Permanent Magnet Synchronous motors (LSPMSMs) have been introduced. A LSPMSM consists of a single or poly-phase stator as of the induction motors and a hybrid rotor involving squirrel cages and pairs of permanent magnet poles. Line start permanent magnet synchronous motors (LSPMSMs) allow reaching super premium efficiency levels due to the non-existence of rotor losses at synchronous speed.

In practical applications, electrical motors can experience different types of faults. In general, electrical motor failures can be categorized into electrical and mechanical faults. Electrical faults/asymmetries can be further categorized into rotor and stator faults. The rotor faults are broken rotor bars, rotor eccentricity, breakage of end-rings, rotor bow and demagnetizing of permanent magnet. The stator faults include stator windings defects, stator core defects and stator frame defects. Mechanical faults include bearing damage and shaft defects. As the number of LSPMSMs used in different fields is increasing, presence of maintenance scheme based on fault detection for this type of motor becomes important and vital. Early detection of irregularity in the motor with a proper fault diagnosis scheme will help in preventing high cost failures and hence reduces maintenance costs and more importantly prevents unscheduled downtimes that results in loss in production and financial income. The use of LSPMSMs in industry is in its infancy and no efficient scheme exists for faults detection in LSPMSMs yet. In this dissertation, a mathematical model for LSPMSM will be developed. In addition to a finite element analysis will be used to validate the developed model. The FEM model will be used to simulate the demagnetization faults under different loading conditions. Finally, an intelligent demagnetization fault detection algorithm based on Artificial Neural Network for LSPMS motor will be proposed.

1.2 Thesis Motivations

Electrical motors play a major role in industrial sectors around the world. They are the backbone of the industry and manufacturing. Their applications take place in our daily life with different classes of use such as industrial, commercial and residential utilization. Statistics indicates that electrical motors consumes about two-thirds of the total industrial power consumption in each society. Most of the developing countries

moved from rural and agriculture to industrialization. Moreover, machines are being utilized widely instead of the traditional manual processes in all sectors of our life. Therefore, demand for more efficient and robust electrical motors is a challenge.

Electric motors affect almost every aspect of modern life, such as washing machines, vacuum cleaners, refrigerators, air conditioners, computer hard drives, fans, cars, and a lot of other appliances and devices. Electric motors are also responsible for a very large portion of industrial processes. Electric motors are used at some point in the manufacturing process of nearly every conceivable product that is produced in modern factories. Because of the nearly unlimited number of applications for electric motors, it is possible to imagine that there are over 700 million motors of various sizes in operation across the world [1]. This enormous number of motors have a significant impact on the industry because of the expected faults, which may happen during the industrial process.

In general, motors are classified into two categories: AC Motors and DC Motors. AC motors, include Induction, Universal, Synchronous, and Shaded-Pole Motors. While DC motors, include Shunt-wound, Series-wound, Permanent Magnet, Separately Excited, Brushless, Stepper, and Coreless Ironless DC Motors [2]. The horsepower of these motors ranges up to 150,000 [3].

Induction motors constitute, by far, the largest portion of electrical motors in the market. However, motors that are more efficient have begun to appear as another alternative. In the last few years, powerful candidate in motor industry, which is Line-Start Permanent Magnet Synchronous Motor (LS-PMSM), has been promoted in industrial, commercial and residential applications. This motor has many desirable features, which open the door for more penetrations of this motor in the markets. In

term of efficiency, this motor enjoys much higher efficiency than the induction motor for the same power rating. Induction motors suffer from lower power factor; this is due to their inductive behavior, which in turn will be proportional to the losses. However, LSPMSM operates with higher power factor than the induction motor. This will increase the efficiency and reduce the total loss in term of the power and cost especially for higher rating motors. Regarding the motor torque, LSPMSM suffers from low starting torque due to braking torque coming from magnets in the rotor [1].

Motors are susceptible to many types of faults. A motor failure may become catastrophic, thus undetected motor faults may cascade into motor failure, which in turn may cause production shutdowns. Such shutdowns are costly in terms of lost production time, maintenance costs, and wasted raw materials.

1.3 Thesis Objectives

The main objective of this thesis is to develop a monitoring and diagnostic tool, to detect the demagnetization faults in line start permanent magnet synchronous motor (LSPMSM). Using one of the diagnostic and detection techniques, important features extracted from stator current signature, motor speed and motor torque will be studied and analyzed in order to determine precisely the characteristics of the demagnetization fault. The developed tool will provide an early warning of possible failures due to demagnetization, without need for human intervention. The thesis objectives can be summarized as follows:

1. Deriving a mathematical model for healthy LSPMSM incorporating the effect of the magnet parameters on the performance of the motor.

2. Building Finite Element Method (FEM) model for selected motor and make simulation of healthy and faulty (demagnetized) motor under different loading conditions.
3. Proposing accurate diagnostic tool for online early detection of LSPMSM under demagnetization conditions.

1.4 Thesis Organization

Besides the introduction, this thesis comprises another five chapters. Chapter two introduces a comprehensive literature review, which covers the faults in electrical motors and emphasizes the demagnetization fault and its diagnostic methods. The mathematical modeling of the LSPMS motor under healthy conditions is covered in chapter three. Chapter four depicts the analysis and simulation of the LSPMS motor using JMAG software. Chapter five details the proposed detection technique of partial and uniform demagnetization using ANN. Finally, chapter six presents the conclusions and recommendations regarding future works.

CHAPTER TWO

LITERATURE REVIEW

2.1 Configuration of LSPMSM

LSPMSMs are hybrid between PMSMs and IMs. The major difference between LSPMSMs, PMSMs and IMs is in the construction of the rotor. The stator design is similar in the three types of motors. However, the rotor of LSPMSM consists of permanent magnets (from the PMSM design) and cage bars (from IM design). Figure 2-1 shows the detailed construction of the LSPMSM.

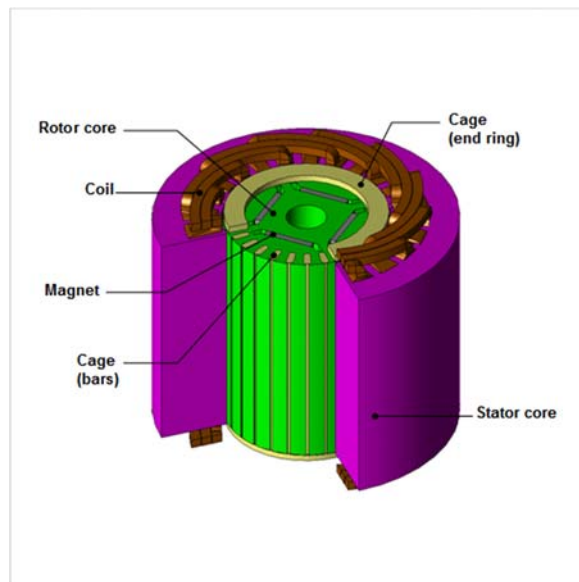


Figure 2-1 Construction of LSPMSM

[1]-[8] [13],[15] studied the detailed construction of LSPMSM and suggested several improvements, shapes and design parameters to achieve higher performance.

2.2 B-H Curve of Permanent Magnet in LSPMSM

PMSM and LSPMSM operates in the second quadrant of B-H curve of the permanent magnets [9][10]. Typical permanent magnet B-H curve is shown in figure 2-2.

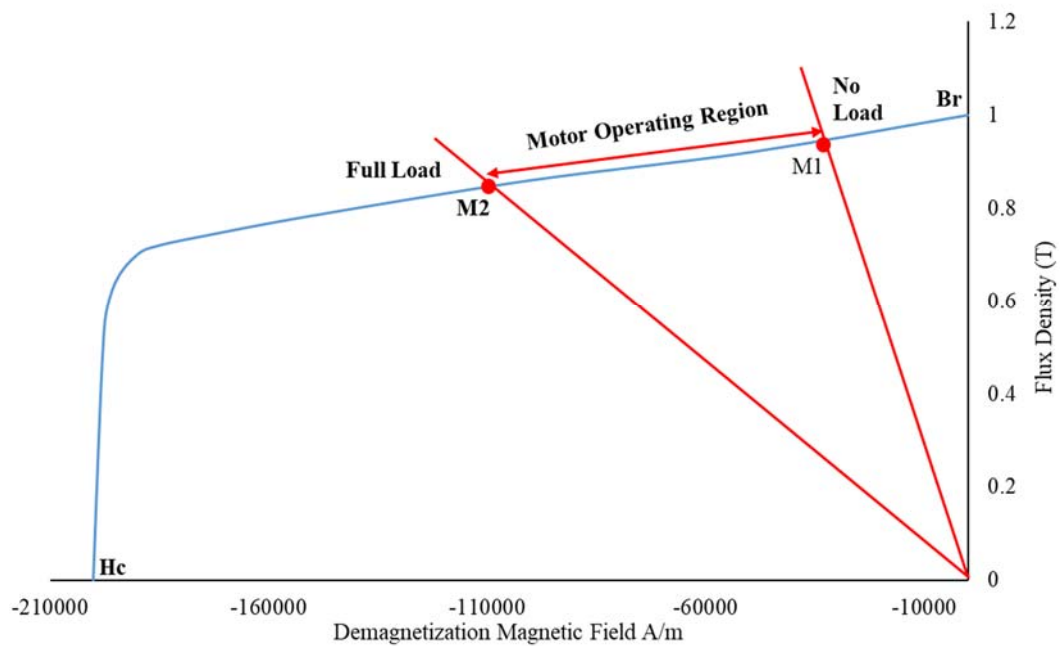


Figure 2-2 Typical BH curve for LSPMSM

The motor operates in healthy conditions between points M1 and M2. As the load increases, more current flows in the stator coils, which increases the demagnetizing magnetic field. Accordingly, the operating point will move to the left towards point M2.

A ferro magnetic material is usually characterized by its B-H curve, where B is the magnetic flux density and H is the magnetic field. The B-H curve describes how the magnetic flux density in a material varies with an externally applied magnetic field. Two important material properties can be extracted from the B-H curve; the remanence (Br) and the coercivity (Hc). After a material has been saturated by an external magnetic field, the remanence is the remaining magnetic flux density in the material after the external applied field is removed. The coercivity is a measure of how high external applied field is needed to reduce the internal magnetic flux density of the material to zero.

From an electrical machine's perspective, there are two types of magnetic material; first there is "hard magnetic material" which is characterized by high remanence and high coercivity. The second material type is characterized by low remanence and low

coercivity and is therefore called “soft magnetic”. A low coercivity enables the magnetic field to easily rotate inside the material, which is a good property for stator steel, in which the magnetic field rotates with the same frequency as the electrical frequency of the machine. When the field has completed one lap it has in the same time completed one lap on the B-H curve and has been subjected to a phenomena called hysteresis [11][12].

2.3 Permanent Magnet Material

Permanent magnets are generally hard magnetic, i.e. they have high coercivity (H_c) and high remanence (B_r). As mentioned above, the coercivity is a measure of how high an external magnetic field is needed to reduce the magnetic flux density inside the material to zero. However, this value does not necessarily mean that the magnetization of the material is reduced to zero. A good magnet grade will not lose any magnetization when the magnetic flux density is reduced to zero. The necessary field strength to reduce the magnetization to zero is denoted H_{ic} and called the intrinsic coercivity, an example figure of how the magnetic polarization ($J_m = \mu_0 M$) and the magnetic flux density is related to an external field is depicted in figure 2-2. All material have some property that change with temperature, magnetic materials are no exception. Generally, the temperature coefficient of the remanence is negative for all magnetic materials, meaning that the remanence decreases with increasing temperature. The temperature coefficient of coercivity depends on the material. Ferrites and Alnico have a positive coefficient, meaning that the coercivity increases with increasing temperature, whereas it is negative for other magnetic materials [11].

Table 2-1 lists some commonly used magnet types from high to low order of measures. [10].

Table 2-1 Ordering by measures useful in motor applications [10]

(BH)max	Br	Hc	Energy to magnetize	Max. service temp.	Temp. stability	Relative cost to stored energy
Nd-Fe-B	Alnico	SmCo	SmCo	Alnico	Alnico	SmCo
SmCo	Nd-Fe-B	Nd-Fe-B	Nd-Fe-B	SmCo	SmCo	Nd-Fe-B
Alnico	SmCo	Ba,Sr ferrites	Ba,Sr ferrites	Ba,Sr ferrites	Ba,Sr ferrites	Alnico
Ba,Sr ferrites	Ba,Sr ferrites	Alnico	Alnico	Nd-Fe-B	Nd-Fe-B	Ba,Sr ferrites

The choice of using the proper magnet is affected by the required motor's performance characteristics and the cost of the motor. Neodymium-iron-boron (Nd-Fe-B) has the highest maximum area under BH curve which stands for energy product. Alnico has the highest remanence, highest operating temperature and highest temperature stability. Samarian-cobalt (SmCo) has the highest coercivity, highest energy to magnetize the material but the highest cost over all magnets. Barium and strontium ferrites (Ba,Sr ferrites) has moderate characteristics and lowest magnet price.

2.4 LSPMSM Modelling Methods

There are three major modelling methods, which will be discussed in this section.

2.4.1 Two-axes Reference Frame Model

In the study of AC motors, mathematical transformations are often used to decouple variables, to facilitate the solution of difficult equations with time-varying coefficients or to relate all variables to a common reference frame. However, three-phase to two-phase transformation can be used to decouple the abc variables of the stator phases. Such transformation is called "Park's transformation." Another transformation type, known as "Poly-phase to two-phase transformation," is the generalization of Park's transformation. This transformation can be used to decouple the abc variables of the rotor equations in the case of the poly-phase rotor distribution [7]. However, all variables should be related to a common reference frame.

2.4.2 Equivalent circuit mathematical model

Equivalent circuit modelling of the AC machines, which is known as "coupled circuit approach" is necessary for facilitating real-time simulations. Modelling process begins with identifying the purpose of the model and its constraints, as well as the kinds of simplifying assumptions or omissions that can be made, along with defining the available computational facilities. However, this method is less time consuming and yields satisfactory accuracy if compared with other techniques such as the Finite Element Method (FEM)

2.4.3 Finite Element Method (FEM)

FEM is a powerful numerical technique, used to find approximate solution for partial differential equations or boundary value problems based on dividing a large problem into simple problems called "finite element". The use of FEM is helpful in the design of AC machines. A lot of softwares called FEM based softwares were developed based on the FEM concept. Well known examples of FEM based softwares are ANSYS Maxwell, COMSOL Multiphysics, ADINA, Opera and JMAG. The softwares varies in facilitating graphical interface, available material libraries, interface with other CAD softwares and file types, ease of creating geometries, speed of simulations, available machines ready models, built in functions and modules and interface with simulation softwares like Matlab.[23-27]

2.5 Faults in LSPMSM

Faults in motors generally happens either in the rotor or in the stator components. LSPMSM has common behavior with the IM and PMSM. LSPMSM starts as IM and the steady state will be PMSM. Accordingly, the faults of IM and PMSM are applicable to LSPMSM. Motor faults are generally categorized into stator faults and rotor faults.

The two categories will be discussed hereafter with concentration on the demagnetization faults in the rotor magnets of LSPMSM.

2.5.1 Stator Faults

The stator is the external group of coils which apply the electromagnetic force to the rotor and cause the rotation. The main parts of the stator are the; core, windings and the frame. These parts are subjected to unavoidable stress, whether mechanical or electrical. Bonnett and Soukup (1992) described these stresses well, and their contribution to premature failures in [37]. The mentioned stresses severely affect the stator condition, leading to faults. These faults are known as phase-to-ground faults, phase-to-phase faults, stator inter-turns faults, coil to coil faults, and also include an open circuit in one phase, and core damage [37-41]. Most stator abnormalities occurs in the winding end parts [42]. From the literature [43, 45] it has been reported that stator winding faults in induction machines represent around 36% of motor faults.

L.S. Maraaba in [14] developed mathematical model for asymmetrical stator winding in LSPMSM depending on stator current signature.

2.5.2 Rotor Faults

Rotor faults in LSPMSM can be categorized into three major parts: Broken Bars, Eccentricity and Magnet Demagnetization.

2.5.2.1 Broken Bars

Broken bars faults have been studied in IM and LSPMSM. Broken bars fault is the fault occurs on the squirrel-cages in the rotor. Squirrel-cage bars are responsible for the rotor rotation in IM and transient rotation in LSPMSM. Khalid L Barad'ieh in [46] has developed mathematical model for detecting the broken bars faults in LSPMSM depending on stator current signature. Summary of causes and effects leading to the broken rotor bars is tabulated in table 2-2.

Broken bar faults in LSPMSM will have effects during the transient stage of starting the motor. It heats up the rotor and leads to various problems like demagnetizing the permanent magnets in LSPMSM or cause the motor to vibrate in both IM and LSPMSM [46].

Table 2-2 Causes and effects of broken rotor bars [46]

No	Reason	Effect
1	Thermal stress	Imbalance, excessive losses, hot spots and sparking.
2	Magnetic stress	Imbalance, magnetic pull, electromagnetic forces, vibration and electromagnetic noise.
3	Dynamic stress	Cyclic stress, centrifugal forces and shaft torques.
4	Residual stress	Issues induced in the manufacturing process
5	Environmental stress	Contamination on the rotor material due to some chemical reactions.
6	Mechanical stress	Bearing failures and loss of lamination parts.

2.5.2.2 Eccentricity Faults

Eccentricity related faults are responsible for about 5% to 15 % of the total faults. This fault happens when there is a non-uniform distance between stator inner race and rotor outer race, which in turn will result in an unbalance magnetic field in the air gap. The unbalanced magnetic flux will lead to having a non-uniform flux linking both the stator and rotor circuits. This will affect mainly the motor inductances due to the non-uniform air gap distance. Moreover, the synchronization process and time variation of the stator current will be affected. There will be an injection of harmonics in the stator line current. There are three types of eccentricity that can occur in electrical motors: the first type is static eccentricity, and the second one is dynamic eccentricity. The combination of both static and dynamic eccentricities is called mixed eccentricity, which combines both static and dynamic faults.[47,48].

Ibrahim Mahmoud Hussein in [47] studied the eccentricity in LSPMSM and developed mathematical model for detecting the eccentricity faults through ANN.

2.5.2.3 Magnet Demagnetization Faults

Interior magnets are common between PMSM and LSPMSM. Demagnetization is defined as any reduction in magnetic flux density of the magnet. Demagnetization occurs partially on part of the magnets or uniformly on the full magnet area [49,51]. Demagnetization of rotor magnets have negative effects on the behavior of LSPMSM and PMSM. Demagnetization of magnets results in reduction of the residual magnetic flux density B_r , which will reduce the magnetic flux of the magnet and ultimately reduce the motor torque [49]. The steady state stator current will increase as demagnetization increases to compensate for the reduction in the magnetic flux. Deep demagnetization will prevent the motor from reaching the synchronism.

Demagnetization has been studied for both PMSM and LSPMSM as both of them utilizes the magnets in the rotor to replace the rotor coils and attain the synchronization in the steady state.

S.S Moosavi [51] studied demagnetization in PMSM and presented review of the state-of-the-art. He presented various methods and parameters used to detect the demagnetization faults in PMSM.

Sami Ruoho [52] presented hazardous situations causing risk of demagnetization in PMSM which is the same definition of the irreversible demagnetization. And he mentioned the effect of temperature rise on increasing the risk of demagnetization.

Mehmet Akar and Mustafa Eker [53] explained that demagnetization in PMSM may occur in high loading conditions due to armature reaction that occurs due to rapid change from permanent situation to static state. Demagnetization fault is caused by the additional sideband components of the motor current in FFT spectrum.

Symbolic identification algorithm for fault detection in PMSM has been presented in [54]. The algorithm was validated by experimental setup. The detection was extracted from the line current and voltage.

Min Zhu [55] studied the effect of demagnetization on the torque ripple in PMSM. He concluded that irreversible demagnetization causes the torque ripple to increase.

Guang-Jin Li in [56] studied the demagnetization on PMSM surface mounted magnets and explained the effect of adding flux gaps in the rotor and number of stator slots on the depth of demagnetization. Adding the flux gaps will reduce the risk of demagnetization but on the other hand will weaken the rotor structure. As the number of stator slots increases, the risk of demagnetization increases as well.

Another method presented in [57] by Juio-Cesar Urresty which is zero-sequence voltage component to detect the demagnetization faults in surface mounted PMSM. The proposed method provided preliminary data only and didn't provide exact details of demagnetization. However, the method is on-line detection which is plus compared with the other off-line methods.

T.H Akinaga in [58] presented FEA based method to estimate the demagnetization in PMSM. The method depends on the Back EMF to decide the demagnetization level. S. Saeid Moosavi also used FEA in [60] in detecting the demagnetization in PMSM.

Jin-Hyung Yoo presented continuous wavelet transform to detect the presence of demagnetization in PMSM [59]. The method didn't specify clearly the demagnetization level and was limit to detect magnetization existence only.

James D. McFarland studied the demagnetization faults in PMSM using FEA and insights into how the transient currents flowing in the PMSM after causing irreversible demagnetization [61].

Demagnetization in LSPMSM has been studied in [19] and [62, 63, 64, 65, 66].

Demagnetization conditions comparison for LSPMSM has been presented in [62]. We-fu Lu did simulations only to give indications about the demagnetization occurrence for cases of partial and deep demagnetization. According to [62] the most severe demagnetization happens at the heavy load starting cases. Also larger moment of inertia allows more probabilities for irreversible demagnetization. He also gave cases like internal three phase short circuit, reclosing on larger voltage switch and excess load all could cause severe demagnetization to the rotor magnets.

Sudden reversal of LSPMSM rotation has been studied by Xu Tang and found to cause irreversible demagnetization. Demagnetization percentage increase as the load torque increases. [63].

Jian-Xin Shen studied demagnetization in LSPMSM and suggested several rotor magnets configurations to reduce the risk of demagnetization. The study was based on FEA. He suggested to add magnetic barriers and bridges to the rotor. Also he suggested dual cages along with magnetic barriers to protect the magnets [64].

Demagnetization under out of step conditions in LSPMSM was studied by Xu Tang in [65]. Sudden change of load torque may result in out of step and supersynchronous faults. The stator current will increase considerably in both cases which leads to increase in the demagnetizing magnetic field and ultimately irreversible demagnetization in the magnets. [65]

Study and detection of demagnetization in LSPMSM using ANN presented in [66]. The paper studied only the full uniform demagnetization in the LSPMSM which is not the common demagnetization case. The paper didn't propose model for partial demagnetization and utilizes the dq mathematical model of the healthy case to expect the uniformly demagnetization [66].

Weiful Lu studied the influencing factors on the demagnetization of LSPMSM during starting process. He utilized the FEA in his study. The load factor and moment of inertia, initial rotor position and supply voltage amplitude were studied and the effect of each of them was presented in [19]. Demagnetization is proportional to the load factor and moment of inertia. Lower supply voltage amplitude results in more starting time and ultimately more risk of causing demagnetization.

Table 2-3 summarizes the causes of demagnetization faults in LSPMSM.

Table 2-3 Summary for causes of demagnetization faults

Sr#	Demagnetization Causes
1	Heavy Starting Load
2	Three Phase Short Circuit
3	Out of Step
4	Open Phase
5	Sudden Reversal
6	Reclosing

2.6 Summary of Literature Review

Based on the above literature survey, there exists no tool that can detect partial and uniform demagnetization effectively on-line while the motor is running. In addition, there exists no tool that can detect the depth of demagnetization without disturbing the motor operation. The ANN is not utilized effectively in the presented tools for detecting the demagnetization.

This study aims at developing a tool for detecting the type and percentage of demagnetization using ANN fed by features extracted from motor stator current, motor load and temperature of the motor. The tool will be tested on randomly selected cases of the motor under different loading conditions.

Table 2-4 lists the references into groups based on the concentration of each reference.

Table 2-4 Summary of Literature Review

Concept	References
Design and performance of LSPMSM	[1]-[11], [13],[15]-[18], [19]-[30], [77]
Motor Faults	[37]-[49]
Stator Motor Faults	[37]-[43]
Eccentricity Faults	[47],[48]
Broken Bar Faults	[46]
Demagnetization in PMSM	[49]-[61]
Demagnetization in LSPMSM	[19], [62]-[66]

CHAPTER THREE

MATHEMATICAL MODELLING AND PARAMETER DETERMINATION OF LSPMSM

3.1 Introduction

In the LSPMS motor, the stator consists of three phase windings, which are displaced by 120 electrical degrees with N_s equivalent winding turns and phase resistance r_s . The rotor is equipped with permanent magnets (PM) and rotor bars. The rotor bars are shortened on both ends by end rings. This configuration is called a squirrel-cage rotor. As discussed before, this motor will start like an induction motor due to the rotor cage, and attains the synchronous speed due to the embedded magnets in the rotor core.

The mathematical model of the LSPMS motor will be developed for the healthy condition.

3.2 Mathematical Model Description

The following assumptions will be considered throughout the derivation of the dynamic motor model of the LSPMS motor [13]:

1. The stator windings distribution is sinusoidal.
2. An equivalent three-phase windings distribution of the rotor circuit.
3. Eddy current and hysteresis losses are neglected.
4. The magnetic operating point is assumed to have a fixed value.

Figure 3.1 shows the LSPMS motor with three phase windings for the stator and the rotor, the rotor cage, and the magnets. Besides, the stator and rotor winding axis, as well as the quadrature and direct axis of the magnets are shown.

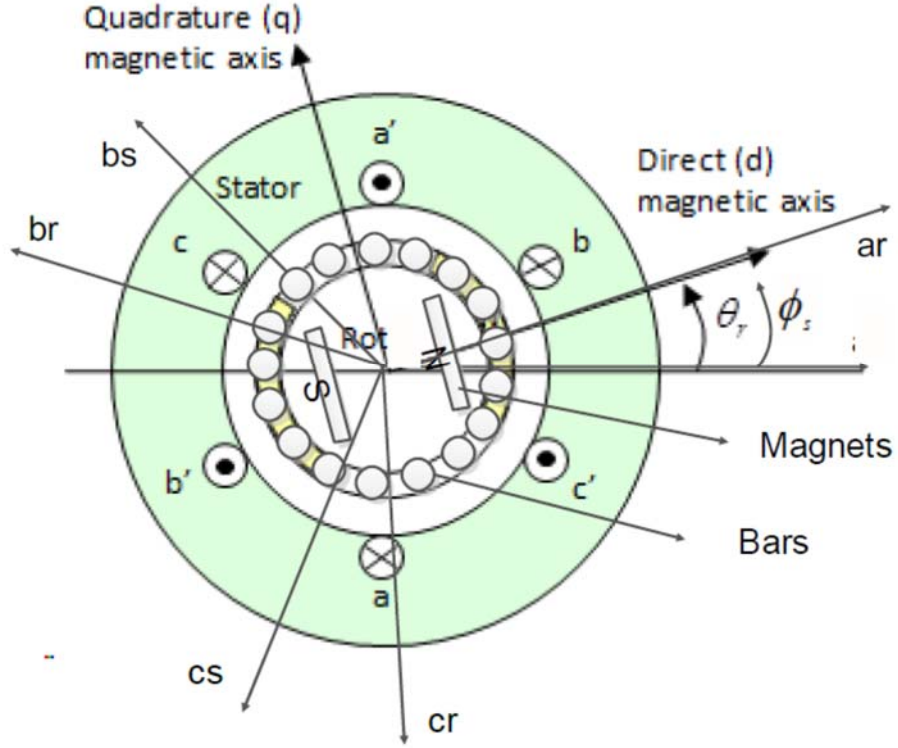


Figure 3-1 Stator and rotor circuits of LSPMS motor [47]

3.2.1 Stator and Rotor Voltage Equations

For the LSPMS motor shown in Figure 3.1, coupled magnetic circuit approach can be used to obtain the stator and rotor voltage equations:

$$\begin{bmatrix} V_{s,abc} \\ V_{r,abc} \end{bmatrix} = \begin{bmatrix} r_{s,abc} & \mathbf{0} \\ \mathbf{0} & r_{r,abc} \end{bmatrix} \begin{bmatrix} i_{s,abc} \\ i_{r,abc} \end{bmatrix} + \frac{d}{dt} \begin{bmatrix} \lambda_{s,abc} \\ \lambda_{r,abc} \end{bmatrix} \quad (3.1)$$

Where $V_{s,abc}$, $i_{s,abc}$, $r_{s,abc}$, $\lambda_{s,abc}$, $V_{r,abc}$, $i_{r,abc}$, $r_{r,abc}$, $\lambda_{r,abc}$ are the stator and rotor phase voltages, currents, resistances, and flux linkages, respectively. They can be defined as the following:

$$\begin{aligned} V_{s,abc} &= [V_{sa} \ V_{sb} \ V_{sc}]^T, & i_{s,abc} &= [i_{sa} \ i_{sb} \ i_{sc}]^T \\ V_{r,abc} &= [V_{ra} \ V_{rb} \ V_{rc}]^T, & i_{r,abc} &= [i_{ra} \ i_{rb} \ i_{rc}]^T \\ \lambda_{s,abc} &= [\lambda_{sa} \ \lambda_{sb} \ \lambda_{sc}]^T, & \lambda_{r,abc} &= [\lambda_{ra} \ \lambda_{rb} \ \lambda_{rc}]^T \end{aligned}$$

$$r_{s,abc} = \begin{bmatrix} r_s & 0 & 0 \\ 0 & r_s & 0 \\ 0 & 0 & r_s \end{bmatrix}, \quad r_{r,abc} = \begin{bmatrix} r_r & 0 & 0 \\ 0 & r_r & 0 \\ 0 & 0 & r_r \end{bmatrix}$$

The flux linkage equations for stator and rotor are given by:

$$\begin{bmatrix} \lambda_{s,abc} \\ \lambda_{r,abc} \end{bmatrix} = \begin{bmatrix} L_s & L_{sr} \\ L_{rs} & L_r \end{bmatrix} \begin{bmatrix} i_{s,abc} \\ i_{r,abc} \end{bmatrix} + \begin{bmatrix} \lambda_{s,pm} \\ \lambda_{r,pm} \end{bmatrix} \quad (3.2)$$

And,

$$\lambda_{pm} = \lambda_m \begin{bmatrix} \sin(\theta_r) \\ \sin(\theta_r - \frac{2\pi}{3}) \\ \sin(\theta_r + \frac{2\pi}{3}) \end{bmatrix} \quad (3.3)$$

Where L_s, L_r are the self-inductance of stator and rotor windings, L_{sr}, L_{rs} are the mutual inductance between stator and rotor, and rotor to stator, respectively. λ_{pm} are the permanent magnet flux components for stator $\lambda_{s,pm}$ and rotor $\lambda_{r,pm}$ with peak flux λ_m . θ_r as the angle of the permanent magnet flux with respect to the winding axis (as). This angle will be zero for the rotor components.

3.3 Transformation to qd0 Reference Frame

Dynamic qd0 modeling is used to study the motor during transient and steady state operation. In addition, this will result in time invariant inductance in equation (3.2). The Park's transformation is a well-known three-phase to qd0 transformation in synchronous machines [69]. The transformation equation is defined as:

$$S_{qd0} = K(\theta) S_{abc} \quad (3.4)$$

Where $S_{qd0}, K, S_{abc}, \theta$ are the output transformed variables, the transformation matrix, and the input variables, θ is the transformation angle. This transformation should be applied to transform the voltage and flux equations into the qd0 reference frame. The

transformation axis will be attached to the rotor with $\omega = \omega_r$ or $\theta = \theta_r$ as presented in figure 3-2.

The Park's transformation matrix K_s is given as:

$$K_s = \frac{2}{3} \begin{bmatrix} \cos(\theta_r) & \cos(\theta_r - \frac{2\pi}{3}) & \cos(\theta_r + \frac{2\pi}{3}) \\ \sin(\theta_r) & \sin(\theta_r - \frac{2\pi}{3}) & \sin(\theta_r + \frac{2\pi}{3}) \\ \frac{1}{2} & \frac{1}{2} & \frac{1}{2} \end{bmatrix} \quad (3.5)$$

The inverse of the transformation matrix can be obtained as:

$$(K_s)^{-1} = \begin{bmatrix} \cos(\theta_r) & \sin(\theta_r) & 1 \\ \cos(\theta_r - \frac{2\pi}{3}) & \sin(\theta_r - \frac{2\pi}{3}) & 1 \\ \cos(\theta_r + \frac{2\pi}{3}) & \sin(\theta_r + \frac{2\pi}{3}) & 1 \end{bmatrix} \quad (3.6)$$

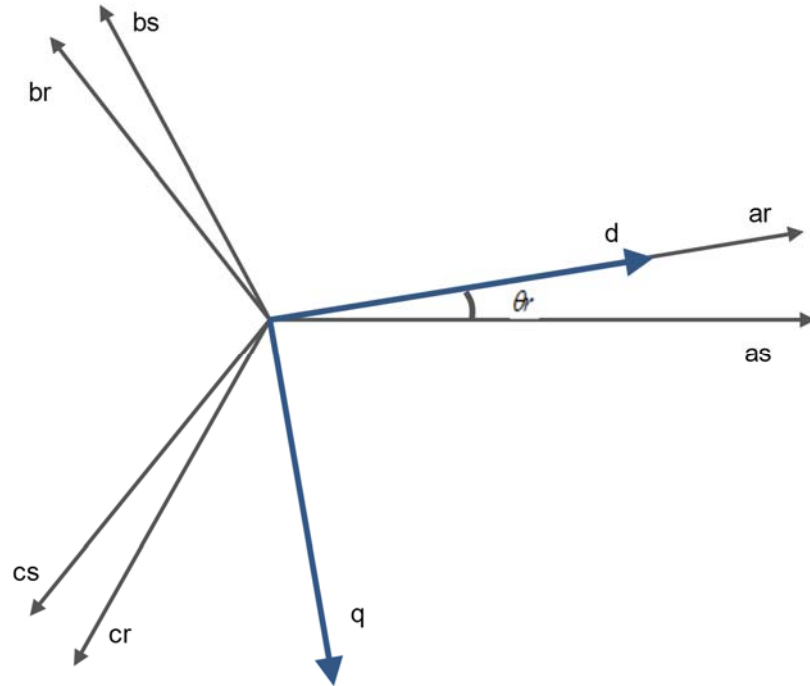


Figure 3-2 qd reference frame attached to rotor

Another important transformation, which can be used to transform the rotor variables to the qd0 reference frame, is Clark's transformation K_r . This transformation can be obtained by setting the transformation angle in equation (3.5) to zero [70].

3.3.1 Stator and Rotor Voltage Equations in qd0 Reference Frame

Following the last discussion in the previous section, the stator and rotor voltage equations will be transformed into a qd0 rotating reference. Performing the transformation to the stator voltage equations presented in equation (3.1) yields:

$$K_s V_s = K_s r_s i_s + K_s \frac{d}{dt} \lambda_{s,abc} \quad (3.7)$$

$$V_{s,qd0} = K_s r_s K_s^{-1} i_{s,qd0} + K_s \frac{d}{dt} \lambda_{s,abc}$$

The first term of the right-hand side can be written as:

$$K_s \frac{d}{dt} [(K_s^{-1} \lambda_{s,qd0})] = K_s \frac{d}{dt} [K_s^{-1}] \lambda_{s,qd0} + K_s K_s^{-1} \frac{d}{dt} \lambda_{s,qd0} \quad (3.8)$$

Where:

$$\frac{d}{dt} (K_s^{-1}) = \omega_r \begin{bmatrix} -\sin(\theta_r) & \cos(\theta_r) & 0 \\ -\sin\left(\theta_r - \frac{2\pi}{3}\right) & \cos\left(\theta_r - \frac{2\pi}{3}\right) & 0 \\ -\sin\left(\theta_r + \frac{2\pi}{3}\right) & \cos\left(\theta_r + \frac{2\pi}{3}\right) & 0 \end{bmatrix} \quad (3.9)$$

But

$$K_s \frac{d}{dt} K_s^{-1} = \omega_r \begin{bmatrix} 0 & 1 & 0 \\ -1 & 0 & 0 \\ 0 & 0 & 0 \end{bmatrix} \quad (3.10)$$

So

$$V_{s,qd0} = r_s i_{s,qd0} + \omega_r \begin{bmatrix} 0 & 1 & 0 \\ -1 & 0 & 0 \\ 0 & 0 & 0 \end{bmatrix} \lambda_{s,qd0} + \frac{d}{dt} \lambda_{s,qd0} \quad (3.11)$$

Where $V_{s,qd0}$ are the stator voltage equations transformed into qd0 reference frame. In the same way, the rotor voltage equations obtained in equation (3.1) can be transformed to the qd0 reference frame as:

$$K_r V_{r,abc} = K_r r_r i_{r,abc} + K_r \frac{d}{dt} \lambda_{r,abc} \quad (3.12)$$

$$V_{r,qd0} = K_r r_r K_r^{-1} i_{r,qd0} + K_r \frac{d}{dt} \lambda_{r,abc}$$

Again, for the first term of the right-hand side, it can be written as:

$$K_r \frac{d}{dt} [(K_r^{-1} \lambda_{r,qd0})] = K_r \frac{d}{dt} [K_r^{-1}] \lambda_{r,qd0} + K_r K_r^{-1} \frac{d}{dt} \lambda_{r,qd0} \quad (3.13)$$

But

$$\frac{d}{dt} (K_r^{-1}) = 0 \quad (3.14)$$

$$K_r K_r^{-1} = I$$

So,

$$V_{r,qd0} = 0 = r_r i_{r,qd0} + \frac{d}{dt} \lambda_{r,qd0} \quad (3.15)$$

3.3.2 Flux Linkage Equations in qd0 Reference Frame:

Recall that the flux linkage equations are given in equation (3.2). Applying the transformation to the rotating reference frame and substituting the values of the current in qd0 reference frame yields:

$$\begin{bmatrix} \lambda_{s,qd0} \\ \lambda_{r,qd0} \end{bmatrix} = \begin{bmatrix} K_s L_s K_s^{-1} & K_s L_{sr} K_r^{-1} \\ K_r L_{sr} K_s^{-1} & K_r L_r K_r^{-1} \end{bmatrix} \begin{bmatrix} i_{s,qd0} \\ i_{r,qd0} \end{bmatrix} + \begin{bmatrix} K_s \lambda_{s,pm} \\ K_r \lambda_{r,pm} \end{bmatrix} \quad (3.16)$$

The transformation of λ_{pm} to the rotor reference frame is considered by setting $\theta_m = \theta_r$ as the stator components and $\theta_m = 0$ as the rotor components, which yields:

$$\lambda_{s,m} = K_s \lambda_{s,pm} = \lambda_m \begin{bmatrix} 0 \\ 1 \\ 0 \end{bmatrix} \quad (3.17)$$

For the rotor components, the flux becomes:

$$\lambda_{r,m} = K_r \lambda_{r,pm} = \lambda_m \begin{bmatrix} 0 \\ 1 \\ 0 \end{bmatrix} \quad (3.18)$$

Which means that the permanent magnet flux components are shown only on the d-axis for both stator and rotor, which is donated by $\lambda_{s,m}$, and $\lambda_{r,m}$. The flux linkage equations become:

$$\begin{bmatrix} \lambda_{s,qd0} \\ \lambda_{r,qd0} \end{bmatrix} = \begin{bmatrix} K_s L_s K_s^{-1} & K_s L_{sr} K_r^{-1} \\ K_r L_{sr} K_s^{-1} & K_r L_r K_r^{-1} \end{bmatrix} \begin{bmatrix} i_{s,qd0} \\ i_{r,qd0} \end{bmatrix} + \begin{bmatrix} \lambda_{s,m} \\ \lambda_{r,m} \end{bmatrix} \quad (3.19)$$

The detailed calculation of the inductance terms shown in equation (3.19) are based on the MWFM,[47] and it will lead to the following inductance expressions:

$$L_{s,qd0} = K_s L_s K_s^{-1} = \begin{bmatrix} L_{ls} + \frac{3}{2} L_{ss,q} & 0 & 0 \\ 0 & L_{ls} + \frac{3}{2} L_{ss,d} & 0 \\ 0 & 0 & L_{ls} \end{bmatrix} \quad (3.20)$$

$$L_{sr,qd0} = K_s L_{sr} K_r^{-1} = \begin{bmatrix} \frac{3}{2} L_{sr,q} & 0 & 0 \\ 0 & \frac{3}{2} L_{sr,d} & 0 \\ 0 & 0 & 0 \end{bmatrix} \quad (3.21)$$

$$L_{rs,qd0} = L_{sr,qd0}^T \quad (3.22)$$

$$L_{r,qd0} = K_r L_r K_r^{-1} = \begin{bmatrix} L_{lr} + \frac{3}{2} L_{rr,q} & 0 & 0 \\ 0 & L_{lr} + \frac{3}{2} L_{rr,d} & 0 \\ 0 & 0 & L_{lr} \end{bmatrix} \quad (3.23)$$

Where $L_{ss,q}, L_{ss,d}, L_{rr,q}, L_{rr,d}, L_{sr,q}, L_{sr,d}$ are the self-inductance of stator and rotor windings, and the mutual inductance between stator and rotor in the direction of quadrature and direct axis, respectively. L_{ls}, L_{lr} are the per phase leakage inductance of stator and rotor windings. Defining the following magnetizing inductances for a symmetric winding distribution and by referring the inductances to the stator side, yields:

$$\begin{aligned}
L_{mq} &= \frac{3}{2} L_{ss,q} = \frac{3}{2} \frac{N_s}{N_r} L_{rr,q} = \frac{3}{2} \frac{N_s}{N_r} L_{sr,q} \\
L_{md} &= \frac{3}{2} L_{ss,d} = \frac{3}{2} \frac{N_s}{N_r} L_{rr,d} = \frac{3}{2} \frac{N_s}{N_r} L_{sr,d}
\end{aligned} \tag{3.24}$$

Where N_s, N_r are the number of stator and rotor turns, respectively. The complete flux linkage equations of stator and rotor can be written in compact form as:

$$\begin{bmatrix} \lambda_{sq} \\ \lambda_{sd} \\ \lambda_{s0} \\ \lambda_{rq} \\ \lambda_{rd} \\ \lambda_{r0} \end{bmatrix} = \begin{bmatrix} L_{ls} + L_{mq} & 0 & 0 & L_{mq} & 0 & 0 \\ 0 & L_{ls} + L_{md} & 0 & 0 & L_{md} & 0 \\ 0 & 0 & L_{ls} & 0 & 0 & 0 \\ L_{mq} & 0 & 0 & L_{lr} + L_{mq} & 0 & 0 \\ 0 & L_{md} & 0 & 0 & L_{lr} + L_{md} & 0 \\ 0 & 0 & 0 & 0 & 0 & L_{lr} \end{bmatrix} \begin{bmatrix} i_{sq} \\ i_{sd} \\ i_{s0} \\ i_{rq} \\ i_{rd} \\ i_{r0} \end{bmatrix} + \begin{bmatrix} 0 \\ \lambda_m \\ 0 \\ 0 \\ \lambda_m \\ 0 \end{bmatrix} \tag{25}$$

Where $\lambda_m = i_m L_{md}$ which is the magnetization current multiplied with the mutual d-axis inductance.

3.3.3 Equation of Motion and Electromagnetic Torque

The electromechanical torque developed by the motor can be obtained from the input power being transferred into the airgap [7, 30,], which is given by:

$$T_{em} = \frac{3}{2} \frac{P}{2} (\lambda_d i_q - \lambda_q i_d) \tag{3.26}$$

In addition, the rotor motion equation is governed by:

$$\omega_r(t) = \frac{P}{2J} \int (T_{em} + T_{mech} - T_{damp}) dt \tag{3.27}$$

Where P is the number of poles, J is the motor inertia, T_{mech} is the input mechanical load, T_{damp} is the damping torque, and ω_r is the rotor angular velocity.

3.3.4 Healthy Model Summary

The summary of the healthy model equations is introduced in the synchronous reference frame for stator and rotor voltage and flux equations. In the following equations, the prime notation indicates rotor variables being referred to the stator side by a proper turn ratio which can be defined as:

$$\lambda'_{rqd} = \frac{N_s}{N_r} \lambda_{rqd} \quad (3.28)$$

$$i'_{rqd} = \frac{N_r}{N_s} i_{rqd} \quad (3.29)$$

$$l'_{lr} = \left[\frac{N_s}{N_r} \right]^2 l_{lr} \quad (3.30)$$

The voltage and flux equations becomes:

$$V_{s,qd0} = r_s i_{s,qd0} + \omega_r \begin{bmatrix} 0 & 1 & 0 \\ -1 & 0 & 0 \\ 0 & 0 & 0 \end{bmatrix} \lambda_{s,qd0} + \frac{d}{dt} \lambda_{s,qd0} \quad (3.31)$$

$$V'_{r,qd0} = 0 = r'_r i'_{r,qd0} + \frac{d}{dt} \lambda'_{r,qd0} \quad (3.32)$$

$$\begin{bmatrix} \lambda_{sq} \\ \lambda_{sd} \\ \lambda_{s0} \\ \lambda'_{rq} \\ \lambda'_{rd} \\ \lambda'_{r0} \end{bmatrix} = \begin{bmatrix} L_{ls} + L_{mq} & 0 & 0 & L_{mq} & 0 & 0 \\ 0 & L_{ls} + L_{md} & 0 & 0 & L_{md} & 0 \\ 0 & 0 & L_{ls} & 0 & 0 & 0 \\ L_{mq} & 0 & 0 & L'_{lr} + L_{mq} & 0 & 0 \\ 0 & L_{md} & 0 & 0 & L'_{lr} + L_{md} & 0 \\ 0 & 0 & 0 & 0 & 0 & L'_{lr} \end{bmatrix} \begin{bmatrix} i_{sq} \\ i_{sd} \\ i_{s0} \\ i'_{rq} \\ i'_{rd} \\ i'_{r0} \end{bmatrix} + \begin{bmatrix} 0 \\ \lambda_m \\ 0 \\ 0 \\ \lambda'_m \\ 0 \end{bmatrix} \quad (3.33)$$

The above equations can be easily translated into Matlab Simulink and the behavior of the motor can be studied accordingly in the healthy conditions. The Matlab code is shown in appendix C.

3.4 Parameter Determination of LSPMSM

In order to simulate the behavior of LSPMSM, the required parameters have to be determined accurately. Parameters can be classified into geometry and measurable parameters. Geometry can be directly measured by de-assembling the motor or by getting the related drawings from the manufacturers. However, the other parameters need to be measured accurately. Ref. [13] summarized the required tests by which the required motor parameters can be determined. Table 3-1 shows the summary of the tests.

Table 3-1 Summary of parameter tests

#	Parameter Description		Test Name
1	stator resistance	r_s	DC Test
2	PM flux linkage	$\lambda_{0'}$	Open Circuit Test
3	d - and q -axis synchronous inductances	L_{ds}, L_{qs}	Synchronous Speed Loading Test
4	rotor leakage inductance and rotor bar resistance	$X_{br} \text{ } (\Omega)$ $R_{br}(\Omega)$	Blocked Rotor Test
5	leakage inductances	$L_{ls}, L'_{lkd},$ L'_{lkq}	Single-phase AC Test

A brief description about each test is presented in the next lines which is taken from [13].

3.4.1 DC Test

The stator resistance r_s can be determined through DC Test as presented in [13]. DC voltage is applied to the stator windings of the test machines and the voltage across the windings and the current through the windings are measured. Because the current is not alternating, the induced voltage is zero and there is no voltage drop across the inductances. The rotor resistance can be calculated as per 3.34.

$$r_s = \frac{V_{DC}}{2 * I_{DC}} \quad (3.34)$$

Several readings have to be taken and the final result will be the average of all readings.

The value of r_s is not completely accurate with DC test, because it neglects the skin effect that occurs when an AC voltage is applied to the windings.

3.4.2 Open Circuit Test

The flux linkage created by the PMs referred to the stator side, can be measured using a setup which is similar to that used to obtain open-circuit characteristics for synchronous machines [13]. The test machine, with its stator terminals kept open, the rotor is coupled with a DC motor as a prime mover. An induced voltage will be generated in the stator of the test machine and the electrical frequency of the stator is equal to the electrical velocity of the rotor, i.e. $\omega_s = \omega_r$. The d- and q-axis voltage under this condition is:

$$\begin{aligned} v_{ds} &= 0 \\ v_{qs} &= \omega_r \lambda_0' \end{aligned} \quad (3.35)$$

Therefore, the flux linkage of PMs referred to the stator side is:

$$\lambda_0' = \frac{60}{P \pi n_m} \frac{V_{ab}}{\sqrt{3}} \quad (3.36)$$

where n_m is the mechanical speed of the rotor in r/min and V_{ab} is the peak value of the line voltage.

3.4.3 Synchronous Speed Loading Test

In order to measure the d- and q-axis synchronous inductances (L_{ds} and L_{qs}), the rotor position has to be measured to get information of the operating torque angle (δ). More details presented in [13] section 2.3.3.

Since at steady state, the test machines rotate at synchronous speed, there is no current in the rotor and therefore can be considered to operate as salient pole synchronous machines. A conventional phasor diagram of a salient pole synchronous machine shown in Figure 3-5 is employed to determine the d- and q-axis synchronous reactances (X_{ds} and X_{qs}). E , V_t and I_{ph} denote the rms value of the per phase induced voltage, terminal

voltage and phase current. According to Figure 3-3(a), under the condition that the machine operates at lagging power factor and $\theta > \delta$, the stator current and voltage components can be expressed as:

$$\left. \begin{aligned} I_{ds} &= I_{ph} \sin(\theta - \delta) \\ I_{qs} &= I_{ph} \cos(\theta - \delta) \\ V_{qs} &= V_t \cos \delta \\ &= E + I_{ph} r_s \cos(\theta - \delta) + I_{ph} X_{ds} \sin(\theta - \delta) \\ &= E + I_{qs} r_s + I_{ds} X_{ds} \\ V_{ds} &= V_t \sin \delta \\ &= I_{ph} X_{qs} \cos(\theta - \delta) - I_{ph} r_s \sin(\theta - \delta) \\ &= I_{qs} X_{qs} - I_{ds} r_s \end{aligned} \right\} \quad (3.37)$$

Under the condition of lagging power factor and $\theta < \delta$ as shown in Figure 3-3(b), the expressions are:

$$\left. \begin{aligned} I_{ds} &= I_{ph} \sin(\delta - \theta), \quad I_{qs} = I_{ph} \cos(\delta - \theta) \\ V_{qs} &= V_t \cos \delta \\ &= E + I_{ph} r_s \cos(\delta - \theta) - I_{ph} X_{ds} \sin(\delta - \theta) \\ &= E + I_{qs} r_s - I_{ds} X_{ds} \\ V_{ds} &= V_t \sin \delta \\ &= I_{ph} X_{qs} \cos(\delta - \theta) + I_{ph} r_s \sin(\delta - \theta) \\ &= I_{qs} X_{qs} + I_{ds} r_s \end{aligned} \right\} \quad (3.38)$$

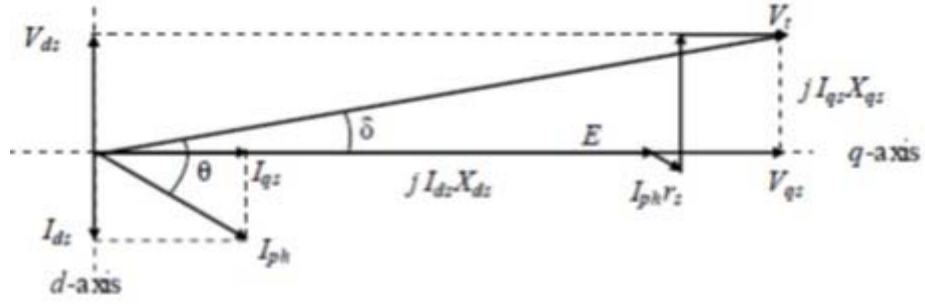
Figure 3-3(c) represents the phasor diagram for a leading power factor

$$\left. \begin{aligned}
 I_{ds} &= I_{ph} \sin(\delta + \theta), I_{qs} = I_{ph} \cos(\delta + \theta) \\
 V_{qs} &= V_t \cos \delta \\
 &= E + I_{ph} r_s \cos(\delta + \theta) - I_{ph} X_{ds} \sin(\delta + \theta) \\
 &= E + I_{qs} r_s - I_{ds} X_{ds} \\
 V_{ds} &= V_t \sin \delta \\
 &= I_{ph} X_{qs} \cos(\delta + \theta) + I_{ph} r_s \sin(\delta + \theta) \\
 &= I_{qs} X_{qs} + I_{ds} r_s
 \end{aligned} \right\} \quad (3.39)$$

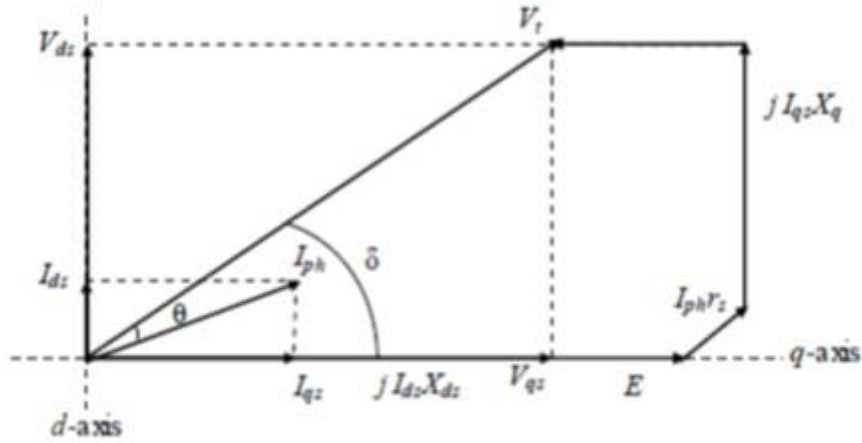
:

Incorporating the above conditions, leading power factor angle, θ is taken as positive and lagging power factor angle is taken as negative, the synchronous reactances can be solved as:

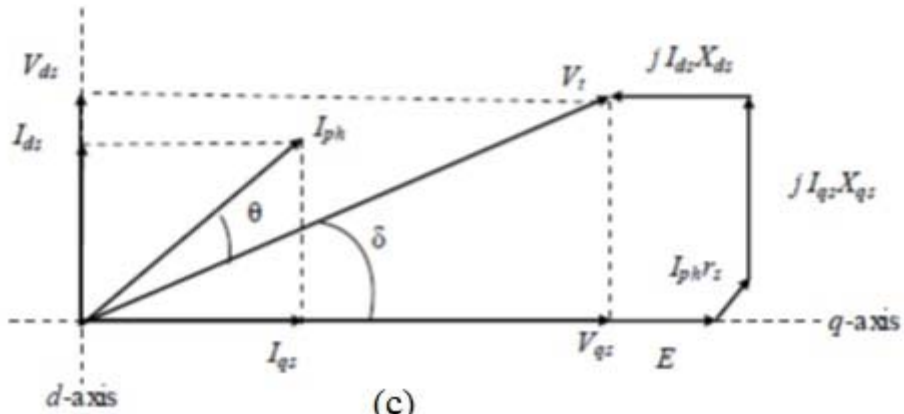
$$\left. \begin{aligned}
 X_{ds} &= \frac{E + I_{qs} r_s - V_{qs}}{I_{ds}} \\
 X_{qs} &= \frac{V_{ds} - I_{ds} r_s}{I_{qs}} \\
 E &= \omega_r \lambda_0' \\
 V_{ds} &= V_t \sin(\delta) \\
 V_{qs} &= V_t \cos(\delta) \\
 I_{ds} &= I_{ph} \sin(\delta - \theta) \\
 I_{qs} &= I_{ph} \cos(\delta - \theta)
 \end{aligned} \right\} \quad (3.40)$$



(a)



(b)



(c)

Figure 3-3 Phasor diagram of a salient pole PMSM. (a) Lagging power factor $\theta > \delta$. (b) Lagging power factor $\theta < \delta$. (c) Leading power factor [13].

3.4.4 Blocked Rotor Test

In order to obtain rotor leakage inductance and damper resistance, a blocked rotor test has to be performed on the LSPMSM for a set of low three-phase voltages [13]. Under a blocked rotor condition ($\omega_r = 0$), in the equivalent circuits of Figure 3-4, each

dependent voltage source in the stator branch is considered as shorted. Also, as the operating voltage to establish rated current flow under a blocked rotor condition is much lower than its rated value, the flux in the machine is extremely low and hence the magnetizing branches of L_{md} and L_{mq} in Figure 3-4 can be treated as open circuited. Therefore, each of the d and q equivalent circuits reduces to a series network consisting of two resistances (stator and cage) and two leakage inductances (stator and cage). The total resistance and total leakage reactance, R_{br} and X_{br} respectively, represent the input resistance and reactance, viewed from the stator side, under blocked conditions and are computed from the blocked rotor test results using (2.38) and (2.39).

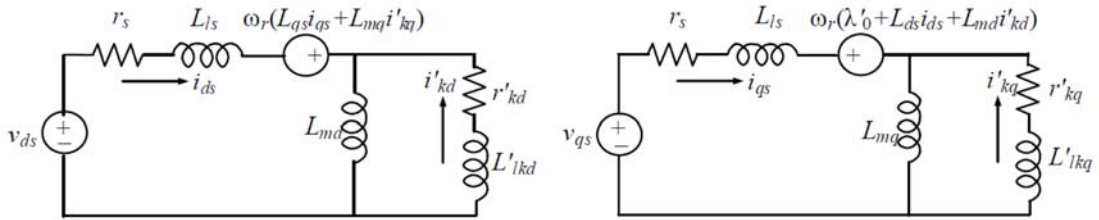


Figure 3-4 dq-axis equivalent circuit model of a LSPMSM in the rotor reference frame. (a) d-axis. (b) q-axis

$$R_{br} = \frac{V_{pk}}{I_{pk}} \cos(\theta) = r_s + r'_{kd(kq)} \quad (3.41)$$

$$X_{br} = \frac{V_{pk}}{I_{pk}} \sin(\theta) = X_{ls} + X'_{kd(kq)} \quad (3.42)$$

3.4.5 Single-phase AC Test

A blocked rotor test is valid under the condition that the inductances of the magnetizing branches L_{md} and L_{mq} are higher than the leakage inductances of the damper L'_{lkd} and L'_{lkq} . Moreover, the rotor structure needs to be known in order to determine the machine class, to be able to determine L_{ls} , L'_{lkd} and L'_{lkq} from X_{br} . A single-phase AC test was proposed based on the fundamental magnetic circuit properties of the machine [13].

3.5 Behavior of LSPMSM

In order to simulate the motor behavior under different loading conditions, motor parameters has been obtained utilizing the motor data sheets, the tests mentioned in the previous section and summarized in Table 3-2.

Figure 3-5 shows analysis for the torque components mentioned in equation 3-27. Curve “1” represents the torque generated by the squirrel cages, curve “2” represents the breaking torque from the permanent magnets and curve “3” represents the average torque during starting process. It is clear that the motor starting time is inversely proportional to the magnet strength as the breaking torque is proportional with magnet strength. Demagnetization faults which weaken the magnet and ultimately the breaking torque, will enhance the starting characteristics of the LSPMSM. However, steady state characteristics will be affected negatively.

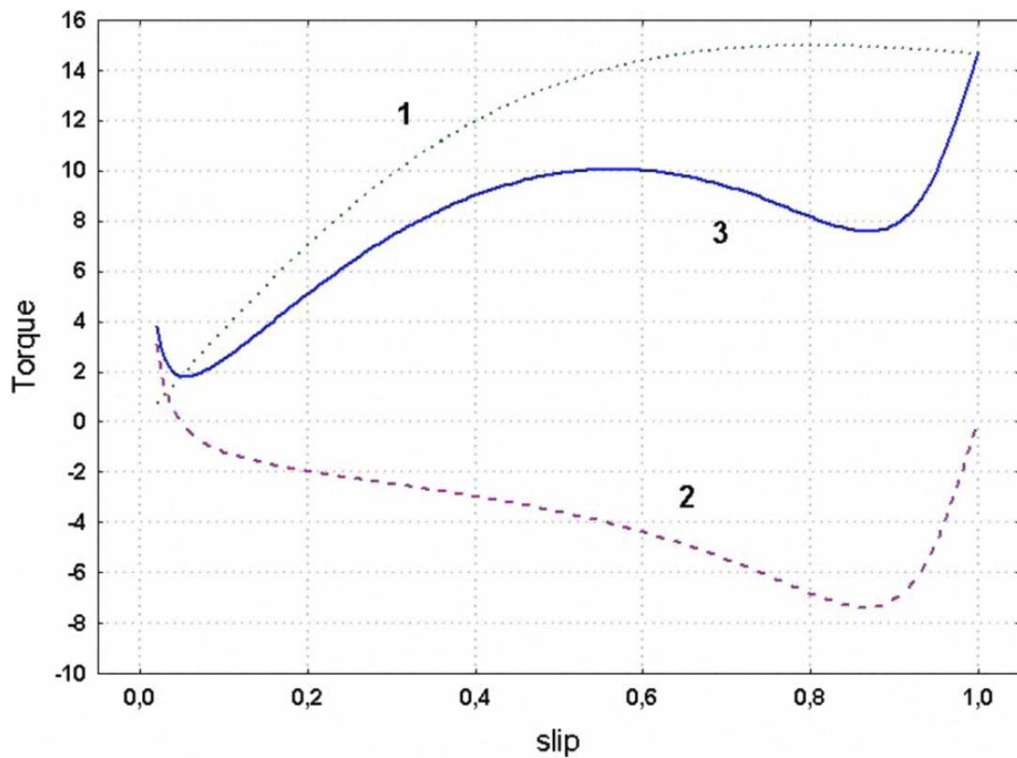


Figure 3-5 Analysis for starting torque in LSPMSM

Table 3-2: LSPMS motor specifications

Parameter	Value
Rated power (W)	750
Rated Voltage (V)	400
Stator phase resistance (Ohm)	10
Stator leakage inductance (mH)	0.001
Number of poles	4
Frequency (Hz)	60
Air-gap length (mm)	0.3
Outer/inner stator diameter (m m)	120/75
Number of stator/rotor slots	24/20
Axial length of stator core (mm)	72
Number of turns per slot	86
Height of stator yoke (mm)	45
Height of stator/rotor slots (mm)	13/9.5
Remanent of magnet (T)	1.02
PM Linkage flux	0.591287
Equivalent rotor resistance (ohm)	1.3295e-3
Inertia in equation of motion (kg/m ²)	0.00146

The simulation of the healthy LSPMSM using MATLAB™ shows that the maximum starting torque capability of the motor whose parameters are listed in table 3-2 is 3.98 N.m. Figure 3-6 to 3-8 show the stator current, torque and motor rotational speed for different loading conditions.

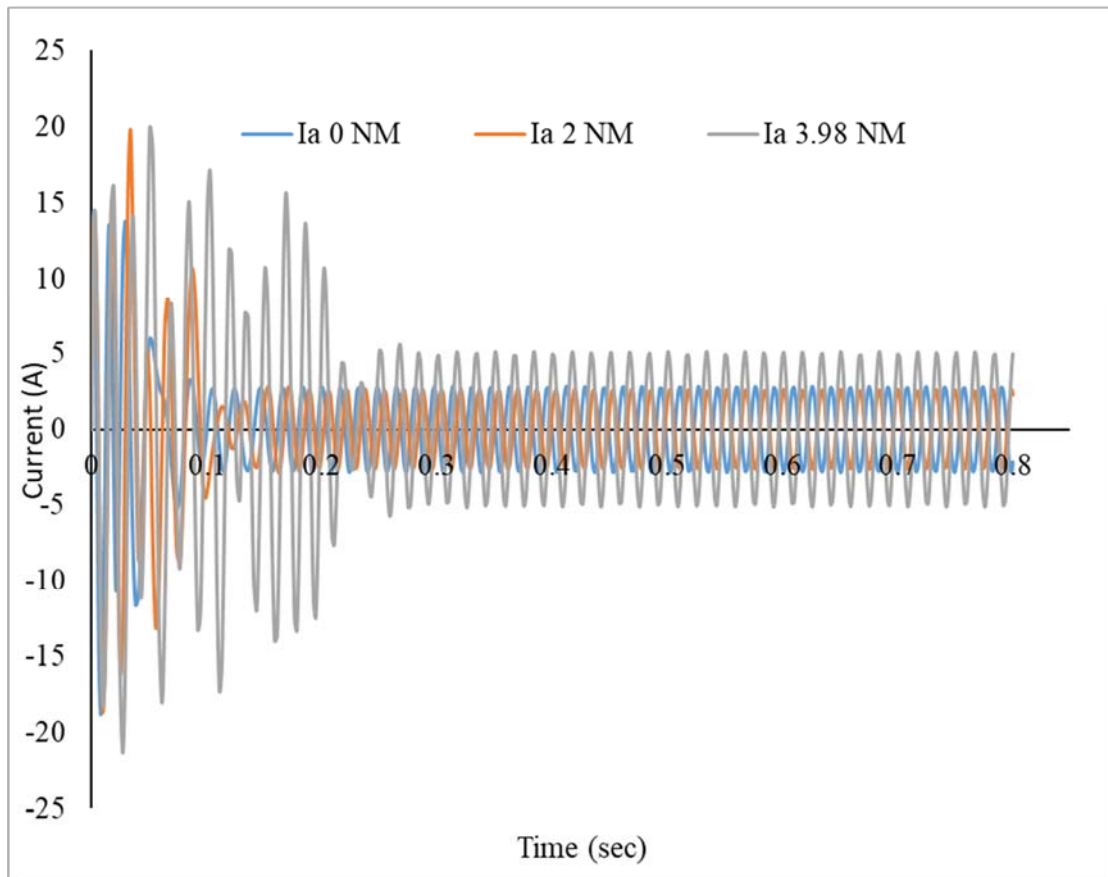


Figure 3-6: Stator current under different loading conditions

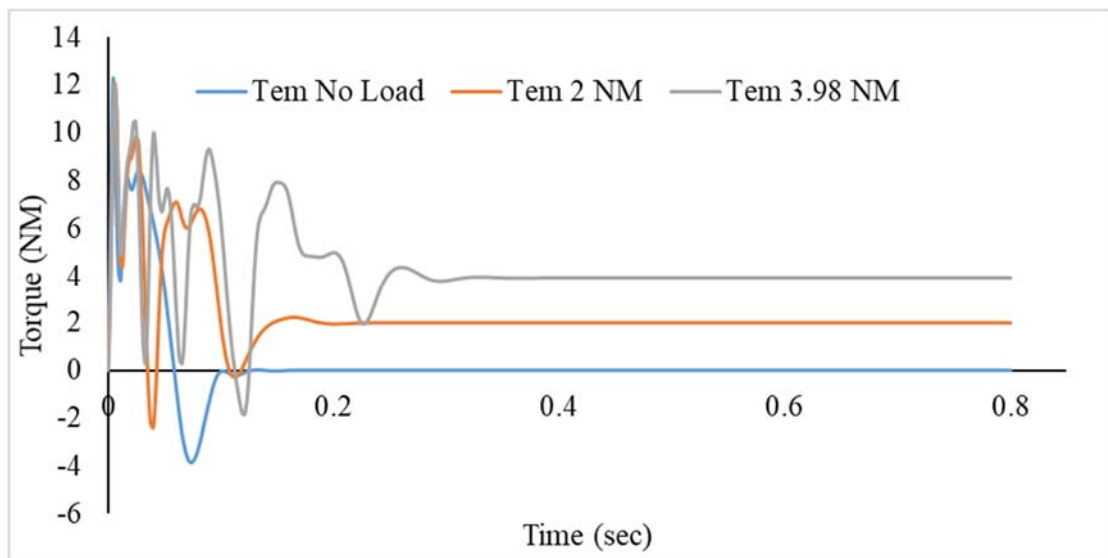


Figure 3-7: Electromagnetic torque under different loading conditions

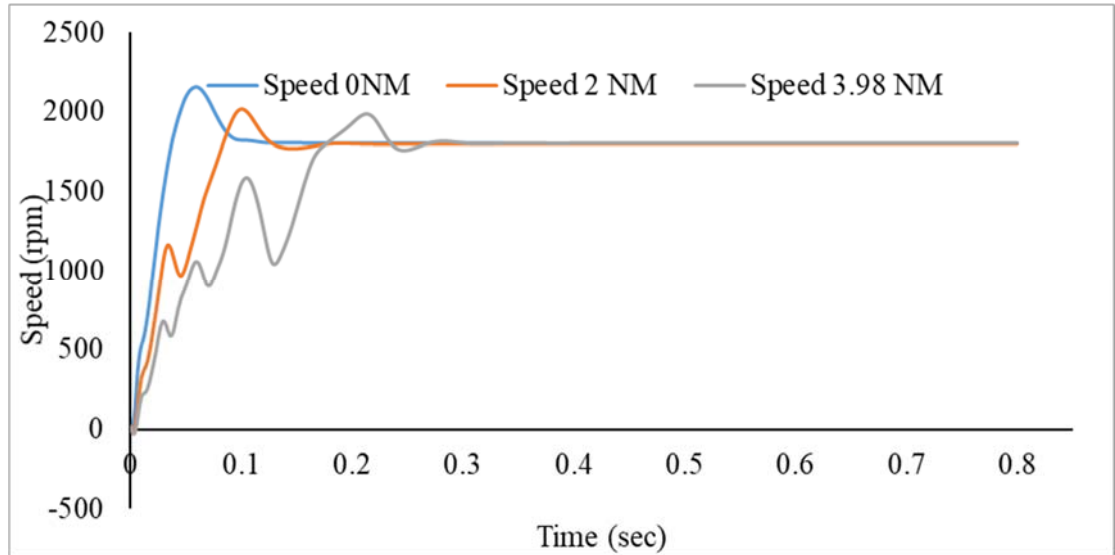


Figure 3-8 Motor speed under different loading conditions

It is clear that the motor synchronization time significantly increases as motor loading increases. Furthermore, if the load value is increased to more than 3.98 N.m, the motor will not reach to the synchronous speed, see figure 3-9.

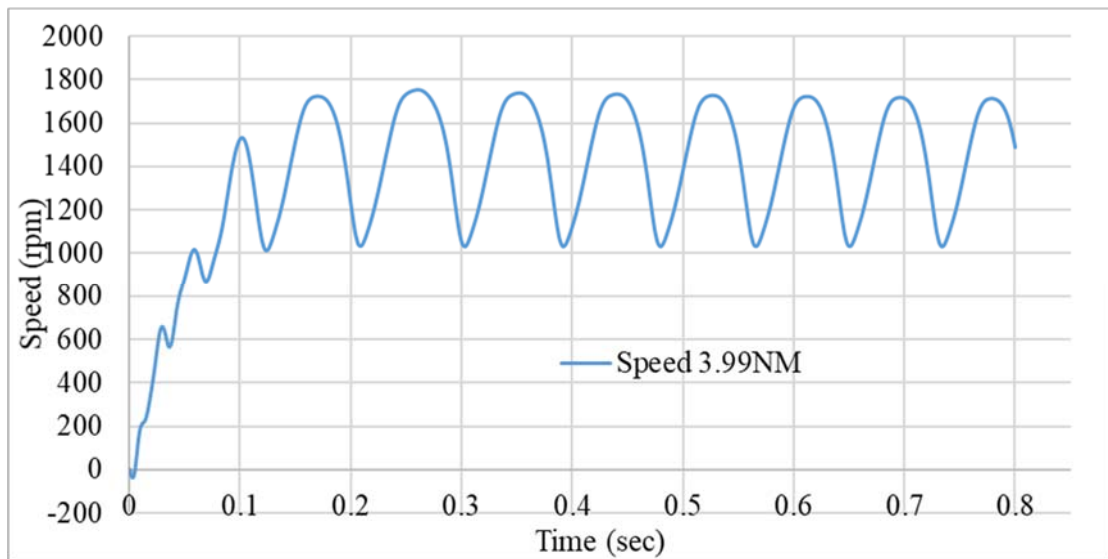


Figure 3-9 Motor speed under 3.99 NM load

Figures 3-10 to 3-12 show the behavior of the motor with 50% and 10% value of the permeant magnet flux respectively.

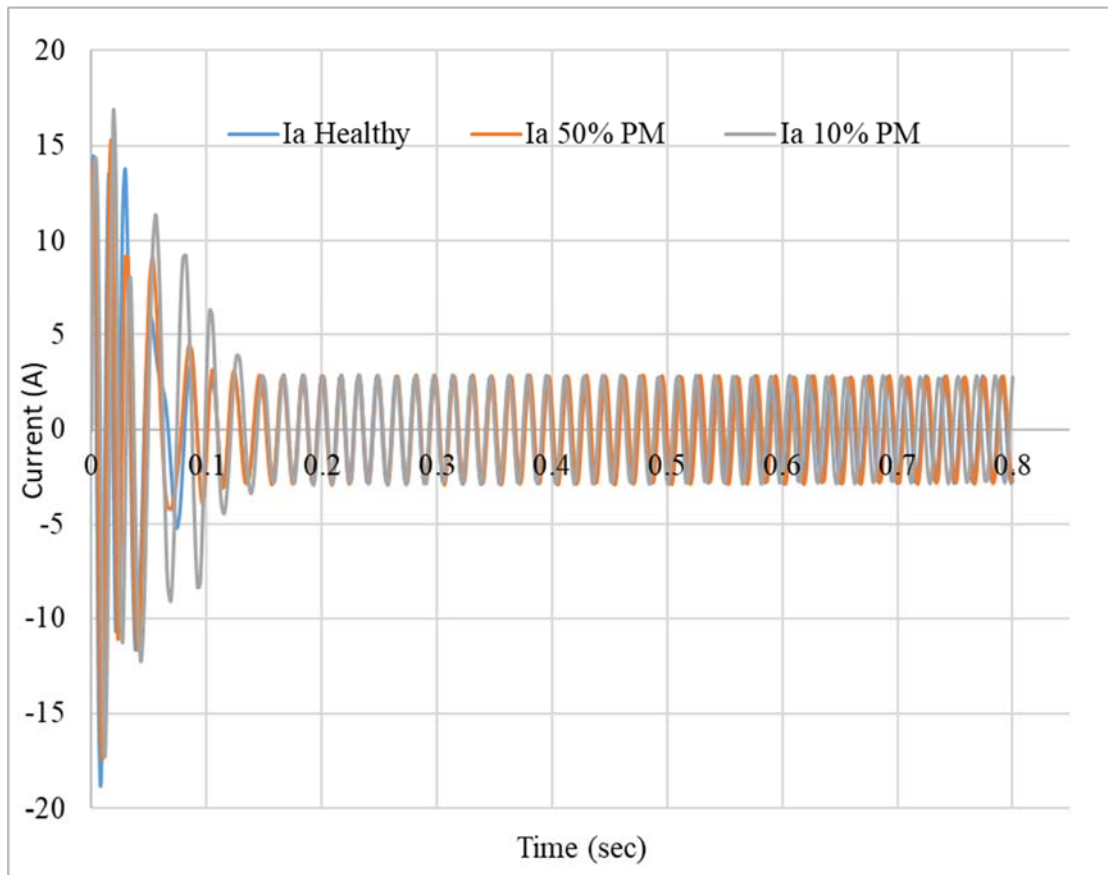


Figure 3-10 Motor current with 50% and 10% value of the magnet flux

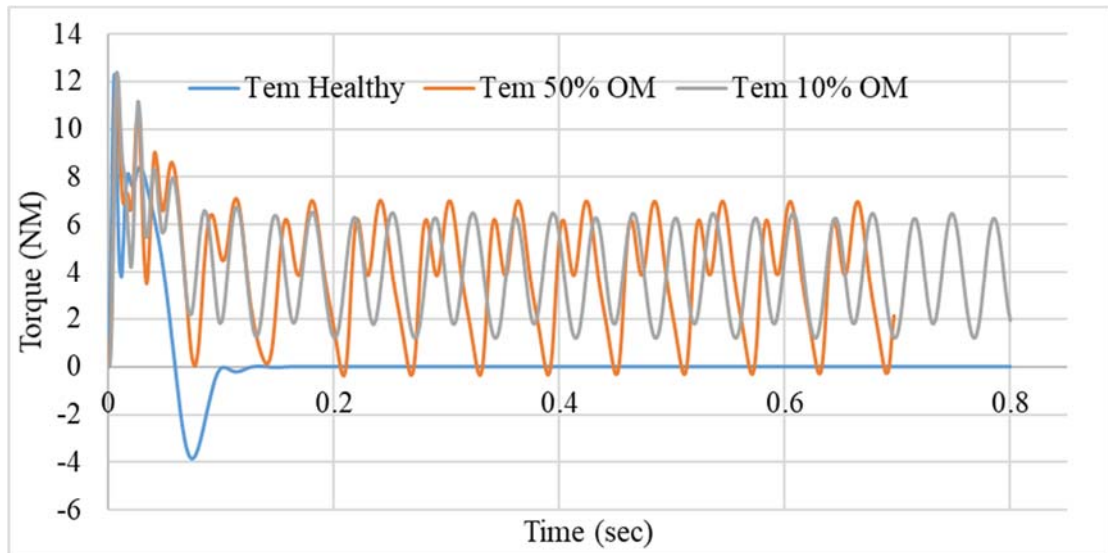


Figure 3-11 Motor torque with 50% and 10% value of the magnet flux

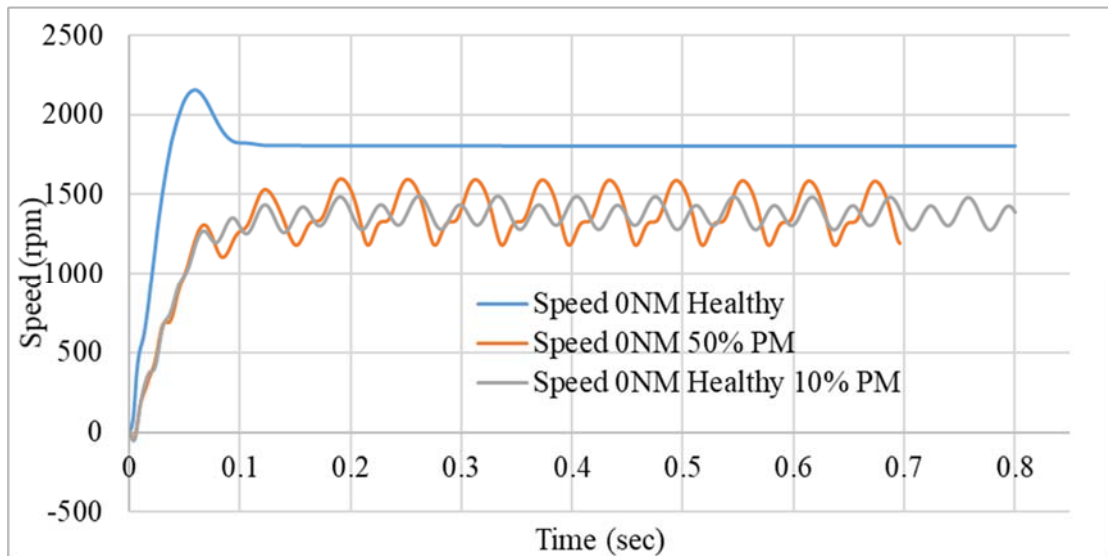


Figure 3-12 Motor speed with 50% and 10% value of the magnet flux

Figures 3-12 shows that a uniform reduction of 50% and 90% of the magnet flux linkage under heavy load, will prevent the motor from reaching the synchronous speed. The motor will keep working in transient period, which leads to heating up the rotor due to the current flowing in the cage bars.

Moreover, figure 3-11 shows that the torque experiences ripple due to the reluctance torque generated by the permanent magnet because the motor is not reaching the steady state.

CHAPTER FOUR

MODELLING OF LSPMSM USING JMAG

(FEM BASED SOFTWARE)

4.1 Introduction

The finite element method is a numerical technique handling problems involving complex geometries and inhomogeneous media. FEM introduced by Courant in 1943, the method was not applied to electromagnetic (EM) problems until 1968. Since that date FEM has been employed in diverse areas such as wave-guided problems, electric machines, semiconductor devices, microstrips, and absorption of EM radiation by biological bodies. [78].

The finite element analysis of any problem involves basically four steps [78]:

- 1- Discretizing the solution region into a finite number of sub-regions or elements.
- 2- Deriving governing equations for typical element.
- 3- Assembling of all elements in the solution region.
- 4- Solving the resulted system of equations.

A lot of softwares were developed based on the above steps which are called FEM based softwares. Well known examples of FEM based softwares are ANSYS Maxwell, COMSOL Multiphysics, ADINA, Opera and JMAG. The softwares varies in facilitating graphical interface, available material libraries, interface with other CAD softwares and file types, ease of creating geometries, speed of simulations, available

machines ready models, built in functions and modules and interface with simulation softwares like Matlab.

Design, optimization and testing of rotating machines can be accurately done using FEM softwares. Motor geometry, characteristics and parameters such as current, torque, speed, flux density, inductances, losses and efficiency can be easily calculated and optimized using FEM softwares.

JMAG is an electromagnetic simulation program developed by JSOL corporation. JMAG provide a 2D/3D platform to construct the motor model. Material properties can be assigned to each part in the model. JMAG consists of material library based on commercial and industrial materials. Material properties and names are depicted from the manufacturers data sheets and brochures. Additional materials can be easily added with complete mechanical, electrical and magnetic properties. Also the available material can be customized based on the application.

JMAG software includes JMAG-EXPRESS, JMAG-DESIGNER, and JMAG-RT. The level of problem complexity decides the software package to be used. JMAG EXPRESS contains some common motor templates which can be used to generate basic characteristics. JMAG DESIGNER is considered to be the core program in the JMAG software environment and will be used in this thesis. It allows a 2D and 3D electromechanical finite element analysis and design with numerous analysis tools such as parametric analysis, optimization, and scripting.

JMAG software package supports users in developing and designing electronic and electric equipment such as motors, actuators, circuit components, and antennae. JMAG performs the following analytic functions:

Magnetic field analysis, Thermal analysis, Structural analysis, Electric field analysis
AND Thermal stress analysis.

JMAG also perform the coupled analyses listed below by combining the above functions:

Magnetic field and thermal analyses, Magnetic field and structural analyses, Magnetic field and thermal stress analyses, Thermal and electric field analyses, Thermal and structural analyses.

The analysis process in JMAG runs through the flow chart in figure 4-1.



Figure 4-1 JMAG Work Process Flowchart

Details about each process can be found in appendix B.

4.2 Modeling Demagnetization Fault

Rare earth magnets has characteristics of large energy product, but decrease when using in an area exceeding a knee point causing irreversible demagnetization. For motors, the possibility of thermal demagnetization through thermal stress may occur when the magnet temperature rises due to iron loss or copper loss during rotation. Demagnetization of magnets in a motor, is one of the causes of decrease in motor performance, where whether or not performance has decreased, demagnetization needs to be predicted. The magnetic field analysis simulation can handle magnetic fields or temperature generated in an internal magnet, which can evaluate demagnetization in the magnet accurately.

This section includes the final JMAG model of healthy conditions, explanation about demagnetization mechanism, demagnetization indexing scheme, and simulation for sudden rotational speed reversal and sudden increase in coils current.

4.2.1 Healthy Model

Figure 4-2 and table 4-1 show the final JMAG model of the LSPMSM being tested and summary of motor parameters respectively.

Table 4-2 summarizes the study parameters for the model shown in figure 4-2.

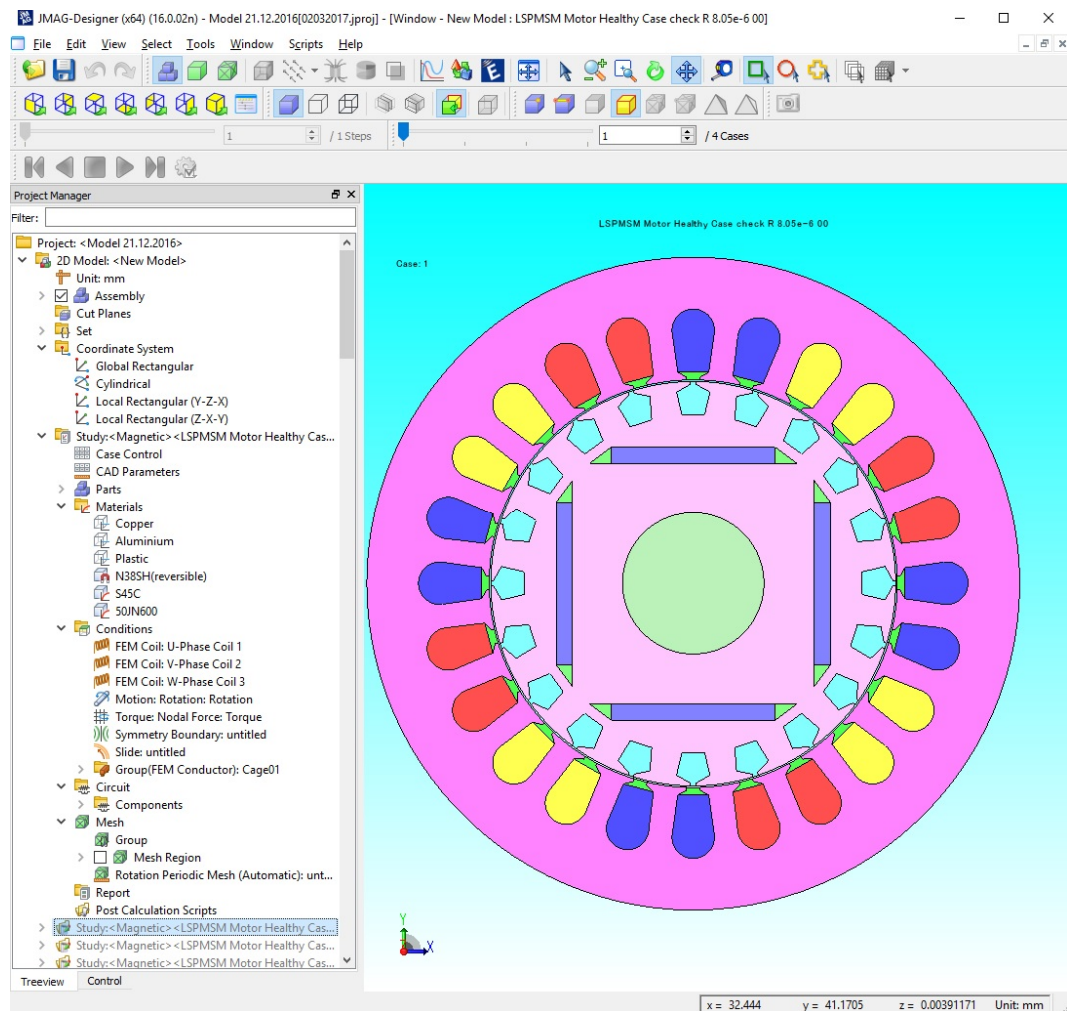


Figure 4-2 Final LSPMSM Model

Table 4-1 Summary for motor parameter

Sr#	Parameter	Value	Unit
1	Shaft diameter	26	mm
2	Rotor diameter	74.4	mm
3	Air gap	0.3	mm
4	Stator internal diameter	75	mm
5	Stator external diameter	120	mm
6	Number of magnets	4	
7	Length of magnet	80	mm
8	Width of magnet	30	mm
9	Thickness of magnet	3	mm
10	Number of rotor bars	20	
11	Number of coils	24	
12	Material of shaft	S45C	
13	Material of rotor core	50JN600	
14	Material of coils	Copper	
15	Material of rotor bars	Aluminium	
16	Material for magnet barriers	Plastic	
17	Material of magnets	N38SH	
18	Number of coils per phase	4	
19	Number of turns per coil	86	
20	Phase coil resistance	10.36	Ohm
21	End ring resistance	8.05e-06	Ohm
22	Mesh model scale factor	1.2	
23	Mesh Part length	1	mm
24	Supply voltage	326	VpLL
25	Supply frequency	60	Hz
26	Temperature	60	Degree C

Table 4-2 Summary of study properties

Sr#	Parameter	Value
1	Calculation method	FEM
2	Number of steps	301
3	Type	Regular interval
4	Unit	S
5	End time	0.048
6	Divisions	48
7	Stack length	80 mm
8	Maximum non-linear iterations	400
9	Convergence tolerance	0.0001
10	Relaxation factor	2

The motor is simulated on Loads [0,1,2,3,4] NM and the results of rotational speed, torque and phase A current is shown in figures 4-3, 4-4 and 4-5 respectively.

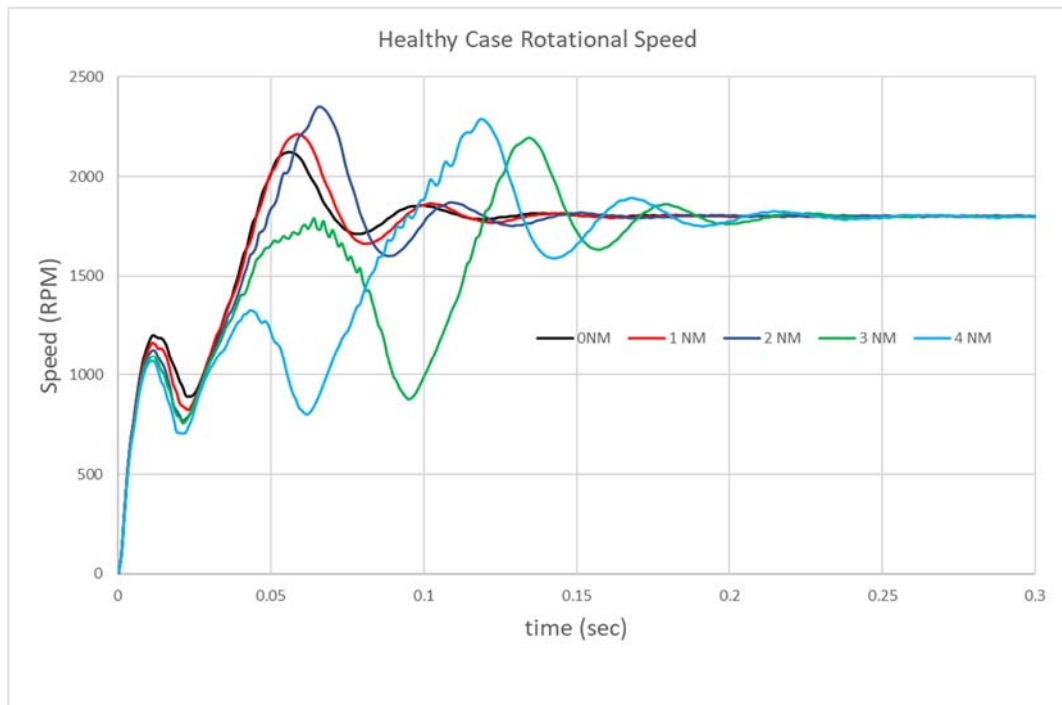


Figure 4-3 Rotational speed for healthy case

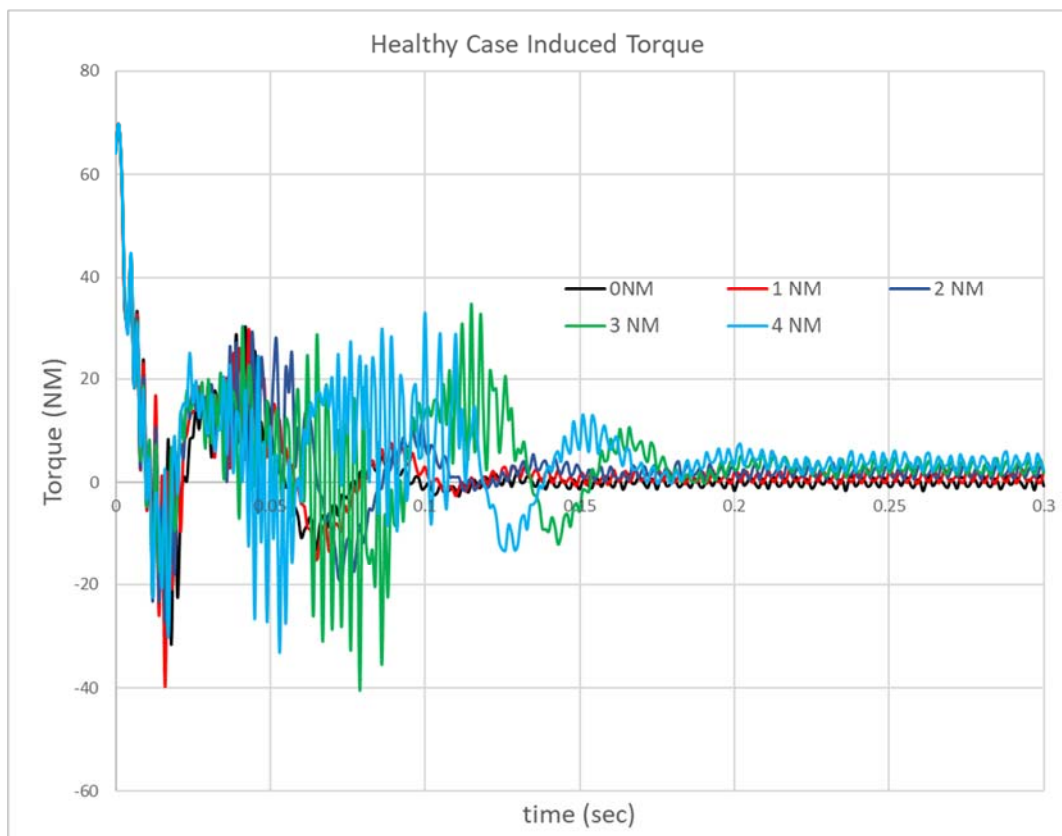


Figure 4-4 Induced torque for healthy case

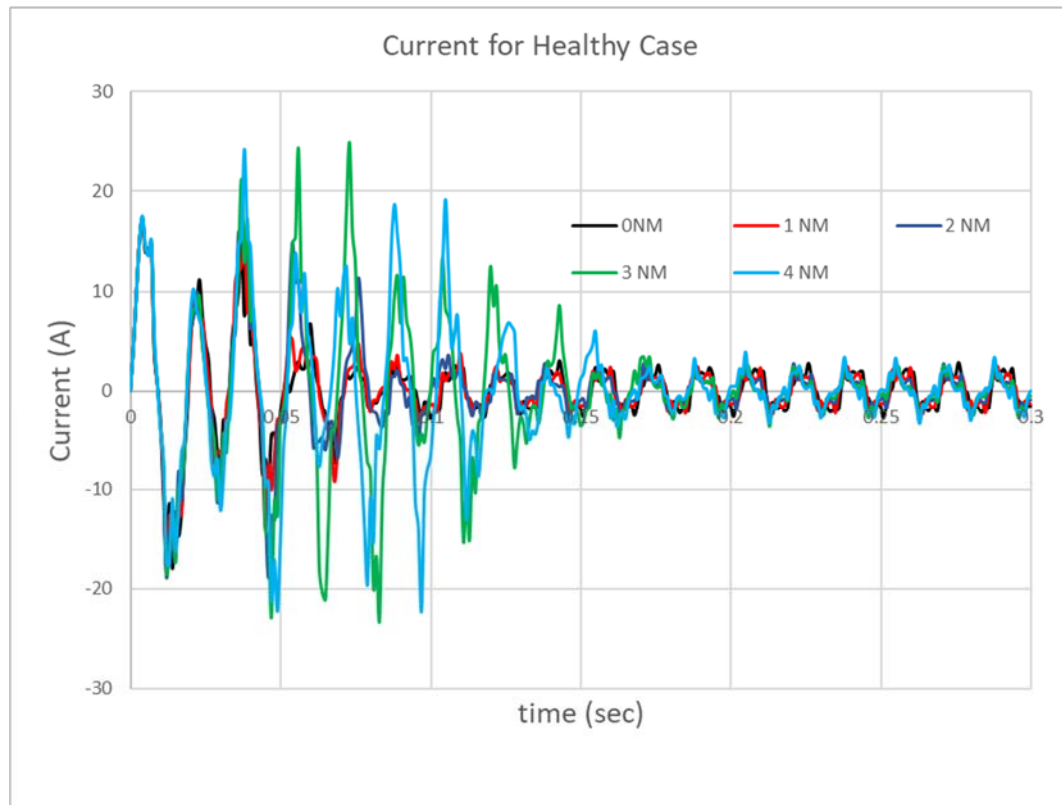


Figure 4-5 Phase A current for healthy case

As shown in figure 4-3, as the load increases, the synchronizing time increases, and the phase current peak value increases as well as shown in figure 4-5.

Figures 4-6 to 4-8 show the simulation results of the motor speed, current and torque respectively for JMAG and the mathematical model at full load. The figures show very good agreement in the final results.

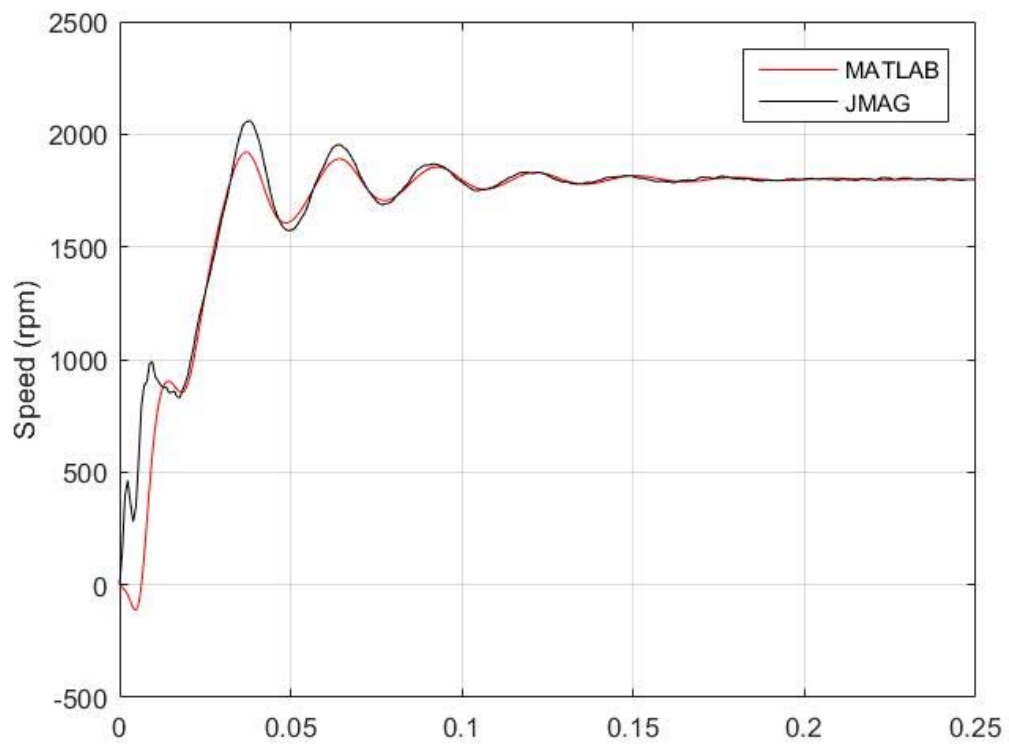


Figure 4-6 Comparison of motor speed at full load between Jmag and Matlab models

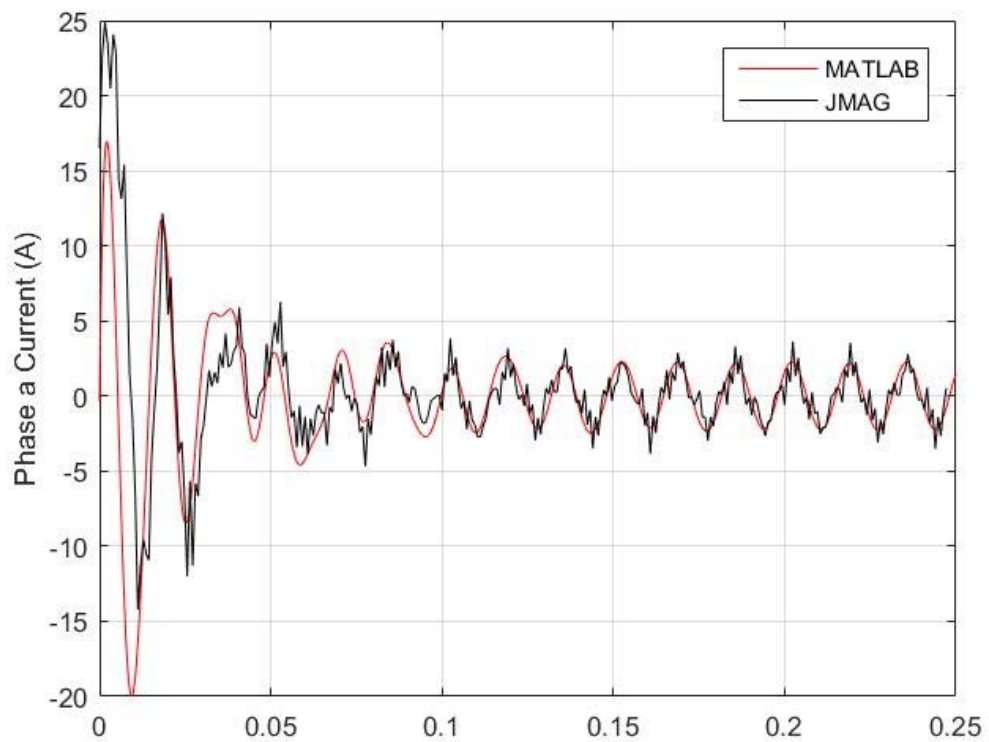


Figure 4-7 Comparison of motor current at full load between Jmag and Matlab models

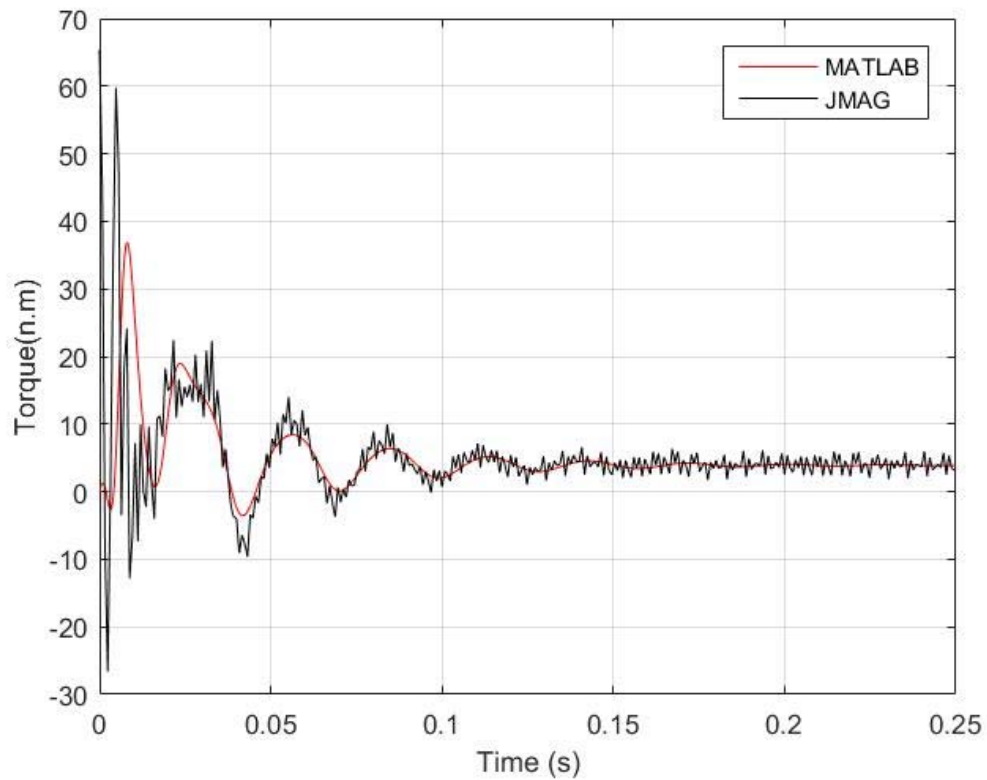


Figure 4-8 Comparison of motor torque at full load between Jmag and Matlab models

4.2.2 Demagnetization Mechanism in LSPMSM

As detailed in section 2.2 and 2.5.2.3 about the characteristics of BH curve and demagnetization fault in LSPMS respectively, the irreversible demagnetization occurs when the operating point of the motor exceeds the knee point at the BH curve. Once the operating points exceeds the knee point, new recoil curve may be formulated where all operating points on the new recoil curve will have lower values than the original curve. Figure 4-9 shows the BH curve of the magnets in LSPMSM with four operating points “M1”, “M2”, “M3” and “M4”. The point “M3” is the knee point voltage of the BH curve. As long as the motor operates above point “M3”, reversible demagnetization

occurs and motor operates normally. Once the motor operates lower than point "M3" say point "M4", then there is a big risk of irreversible demagnetization to occur.

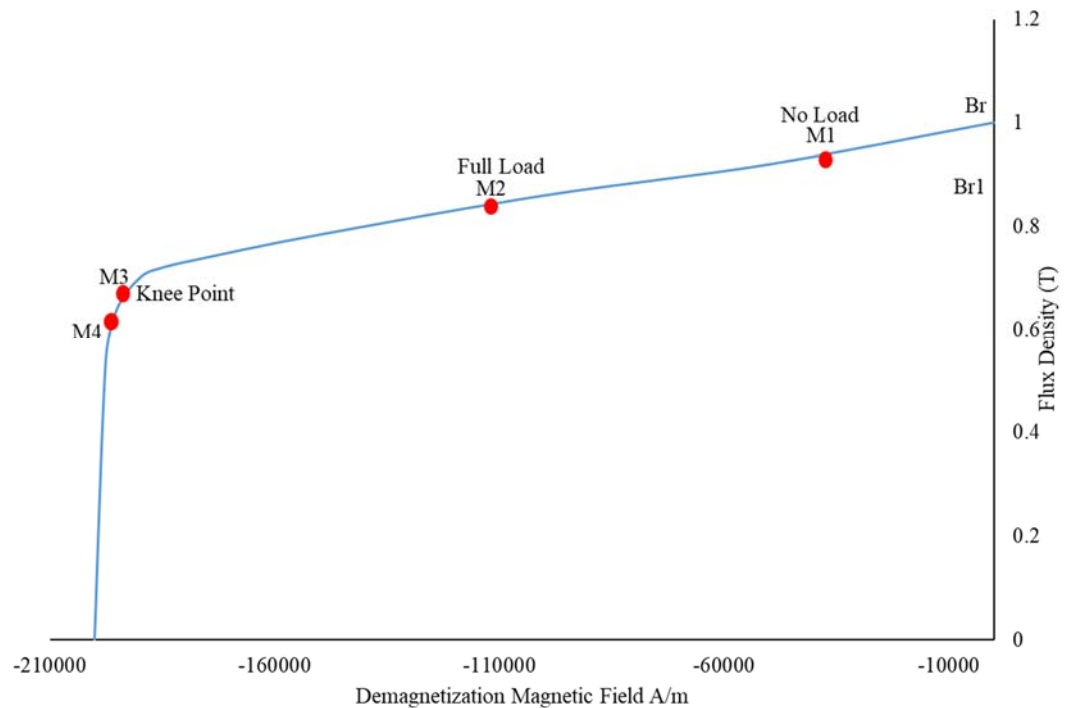


Figure 4-9 Demagnetization curve and recoil line of LSPMSM

In order for the risk of demagnetization to happen, the motor to be operated under magnetic stress and high temperature while magnetic stress alone or high temperature alone is not likely to cause irreversible demagnetization.

Based on the details given in section 2.5.2.3 about the major causes of demagnetization faults; demagnetization can be simulated in JMAG-Designer through several ways such as passing a considerable high current in the winding while the motor is rotating, or starting the motor on high starting load, or sudden reversal of rotation direction.

After any demagnetization process, the magnets data can be stored and imported in another model to simulate the motor behavior using the demagnetized magnets. The demagnetization level depends on the severity of demagnetization process.

Sections 4.2.4, 4.2.5 and 4.2.6 explain the demagnetization process caused by large amount of currents flows in the windings, sudden rotational speed direction reversal and sudden increase in the supply voltage respectively.

Upon completing the simulation process of demagnetization, the magnets conditions are studied and analyzed for the existence, percentage and type of demagnetization.

It is clear from the simulation cases done on the motor under test, that the demagnetization occurs evenly on the four magnets with the same percentage for all simulated demagnetization cases.

After completing the simulation process, the operating point is measured at selected locations and BH curve is plotted accordingly. Figure 4-10 shows the location of two selected points in one of the magnets.

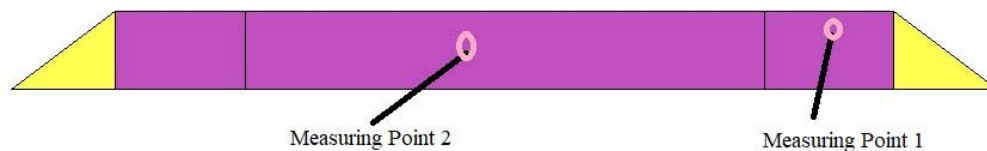


Figure 4-10 Measurement Location of Operating Point in the magnet

The values of the operating points at the two locations are shown in figure 4-11.

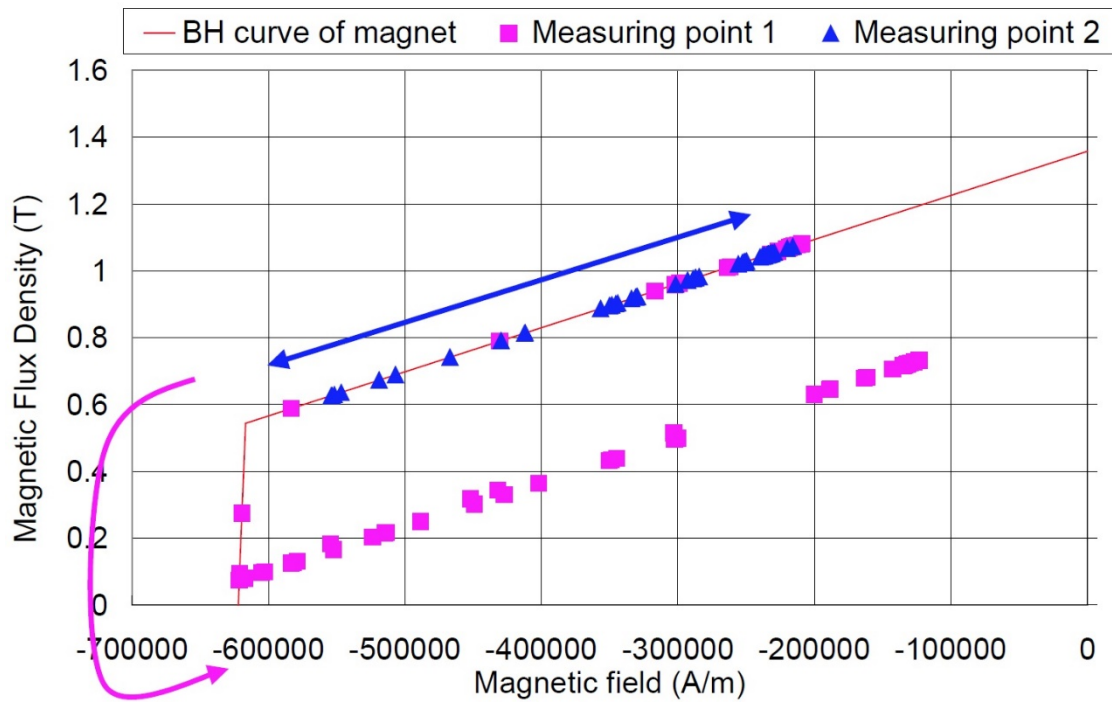


Figure 4-11 Values of operating points 1 and 2

It is clear from figure 4-11 that point 2 is working on the normal BH curve of the magnet; while point no.1 followed new recoil line lower than the BH curve of the magnet. The magnet has experienced irreversible demagnetization at point number 1 while a reversible demagnetization occurred at point number 2. In this case, we call a **partial** demagnetization occurred in the magnet. In case the two points follows the new recoil curve, then **uniform** demagnetization occurs.

4.2.3 Indexing of Demagnetization

Demagnetization faults are the most general faults in PMSM and LSPMSM. Related to the permanent magnets. An early indication about the healthiness of the permanent magnets of the rotor, will help in avoiding sudden disturbances to the motor operation. Two mechanisms have to be identified in order to decide about the conditions of the permanent magnet:

- 1- Detection technique, this topic is covered in chapter 5.
- 2- Index for healthiness or degree of magnet failure.

Jawad Faiz and H. Nedjadi in Ref. [68] delivered a comprehensive literature review in indexing the faults of PMSM magnets. Figure 4-12 shows tree for the various categories of indexes taken from Ref. [68]. The indexes based on the current is not considered in this study, as they are not directly related with the permanent magnets properties.

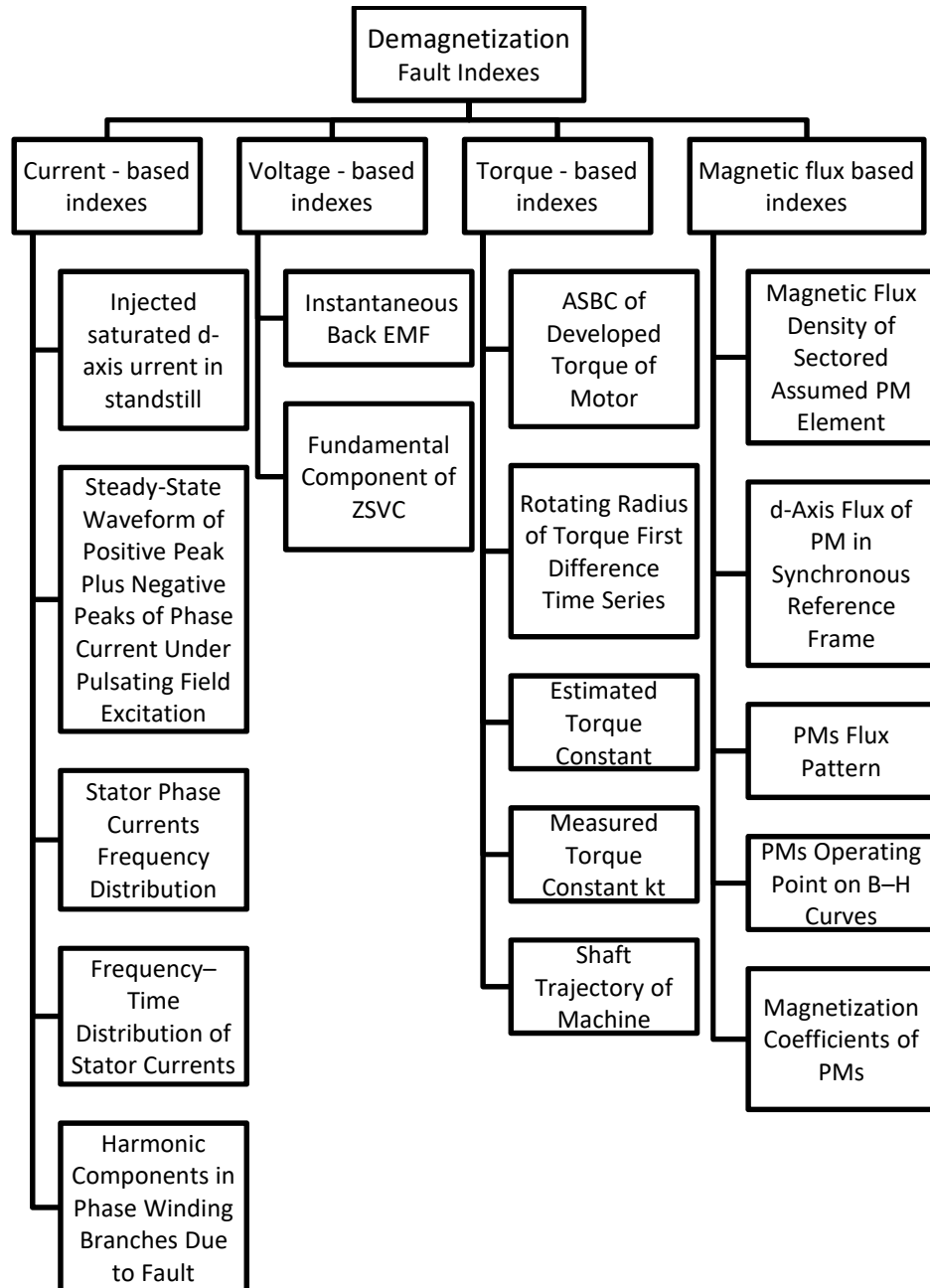


Figure 4-12 Summary of demagnetization indexes

On the other hand, among the magnetic flux based indexes, permanent magnet operating point on the B-H curve was attractive and accordingly utilized.

Since this study utilizes FEM analysis to simulate the demagnetization, it is found that the permanent magnet operating point at standstill condition can be easily reflected in the software and the values can be clearly extracted from the simulation results. PMSM and LPMSM operates in the second quarter of the B-H curve [09, 52] as shown in figure 4-13.

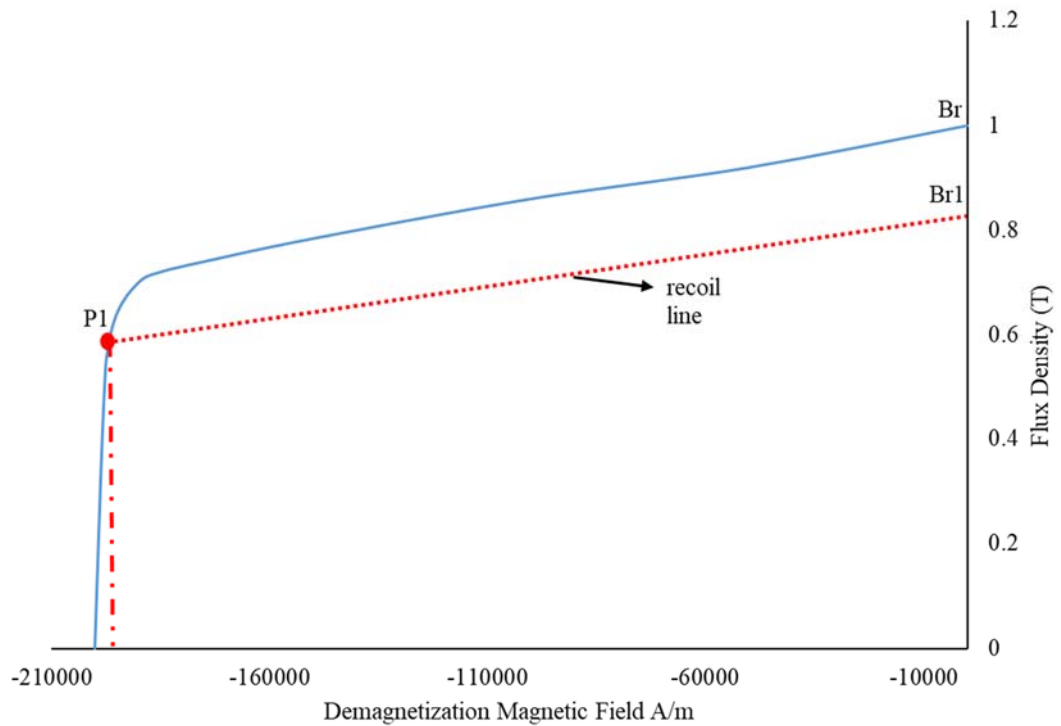


Figure 4-13 B-H curve for LSPMSM

When the motor is not rotating and the supply voltage is disconnected, the demagnetizing magnetic field is zero, the remanence is maximum, and crossing y-axis at point Br. Br is the point where demagnetization percentage is 0% for the BH curve shown in figure 4-13. In case the motor operated at point P1 which is lower than the knee point voltage, then the magnets will operate on the new recoil line due to demagnetization and new point Br1 formulated at the same conditions (power supply

is off and motor is not rotating). The value of remanence at point Br1 is smaller than the remnance at point Br, hence, irreversible demagnetization occurred and the demagnetization percentage is calculated according to equation 4.1.

$$\text{Demagnetization \%} = 1 - \frac{Br1}{B_r} \quad (4.1)$$

For the calculation to be accurate, the operating point has to be measured on several places in the magnet. In this study, six points where considered to be measured on each part of the magnet shown in figure 4-15 and the demagnetization percentage is calculated for each part based on the average of the six points.

As getting precise demagnetization percentage is not easy, this study suggests ranges for demagnetization which are categorized in table 4-3.

Table 4-3 Categories of Demagnetization

Sr#	Demagnetization Percentage	Demagnetization Class
1	less than 10%	A
2	from 10% and less than 30%	B
3	from 30% and less than 50%	C
4	from 50% and less than 70%	D
5	70% and more	E

These categorizes are valid for both uniform and partial demagnetization. Different demagnetization details are shown in the next three sections. In the case of uniform demagnetization, the average point will be taken for the full magnet length. While for the partial demagnetization, this study consider the average operating point on the first one-third length of the permanent magnet.

4.2.4 Demagnetization Through Three Phase Currents

Demagnetization can be done in JMAG by injecting three phase currents while the motor is rotating through external prime mover. The demagnetization percentage is proportional to the current amplitude and duration of current. After demagnetization process, the magnets data is stored and loaded in new model and motor behavior is studied accordingly. Figure 4-14 shows the circuit for this model. Figures 4-15 shows the magnet residual magnetic flux density before demagnetization, with partial demagnetization and with uniform demagnetization.

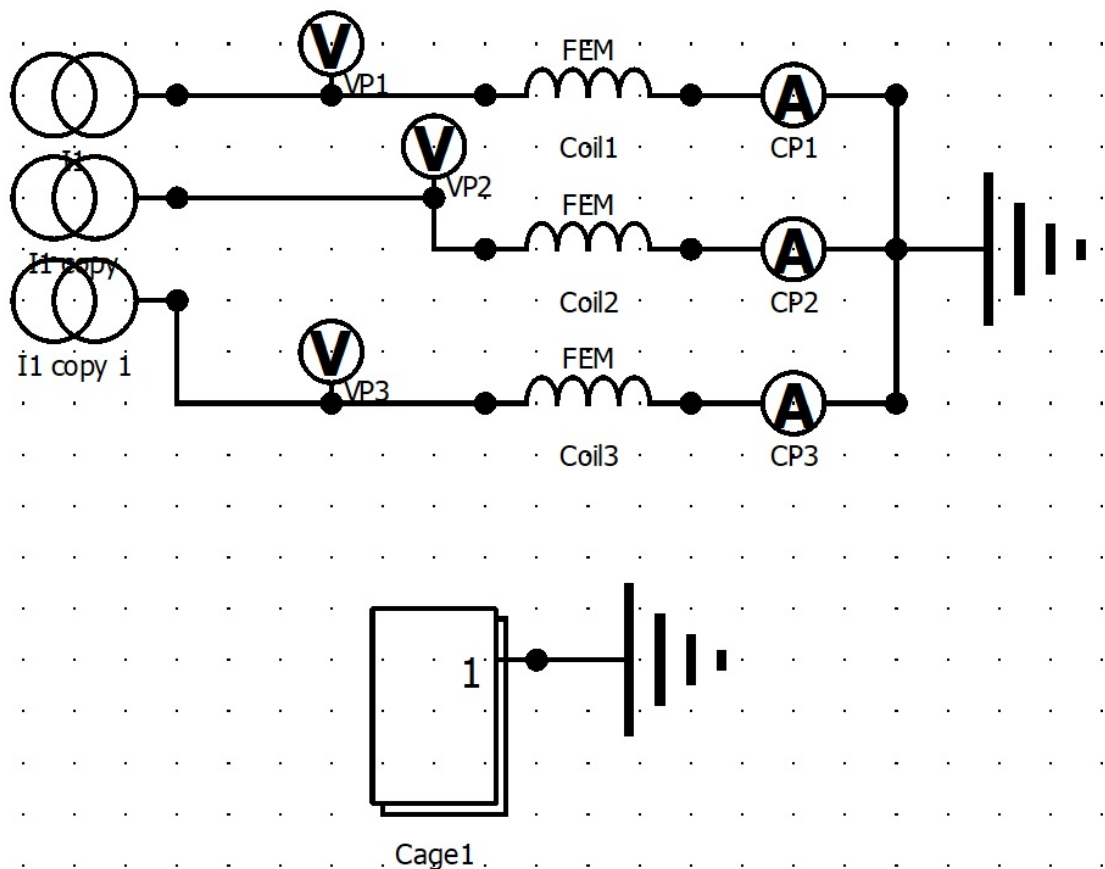


Figure 4-14 Circuit for Demagnetization by current

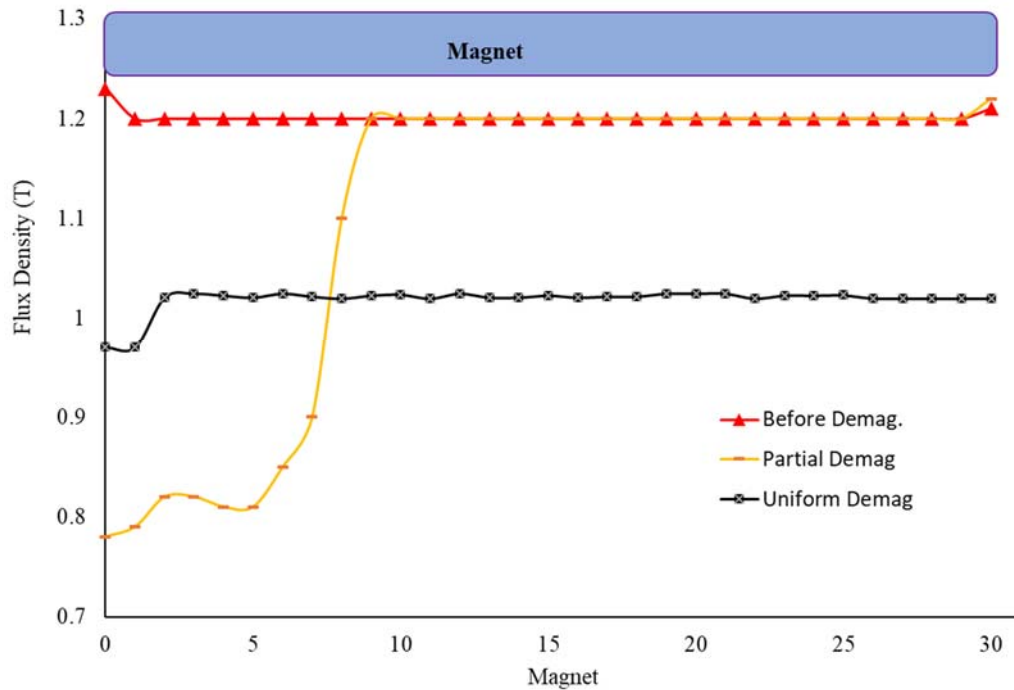


Figure 4-15 Residual magnetic flux density (T)

4.2.5 Sudden Rotation Reversal Model

Sudden rotation reversal can be simulated by reversing two phases connection with the supply after reaching the steady state rotation speed. Figure 4-16 shows the circuit for this model. The phasing reversal in the circuit is controlled through switches timely operated.

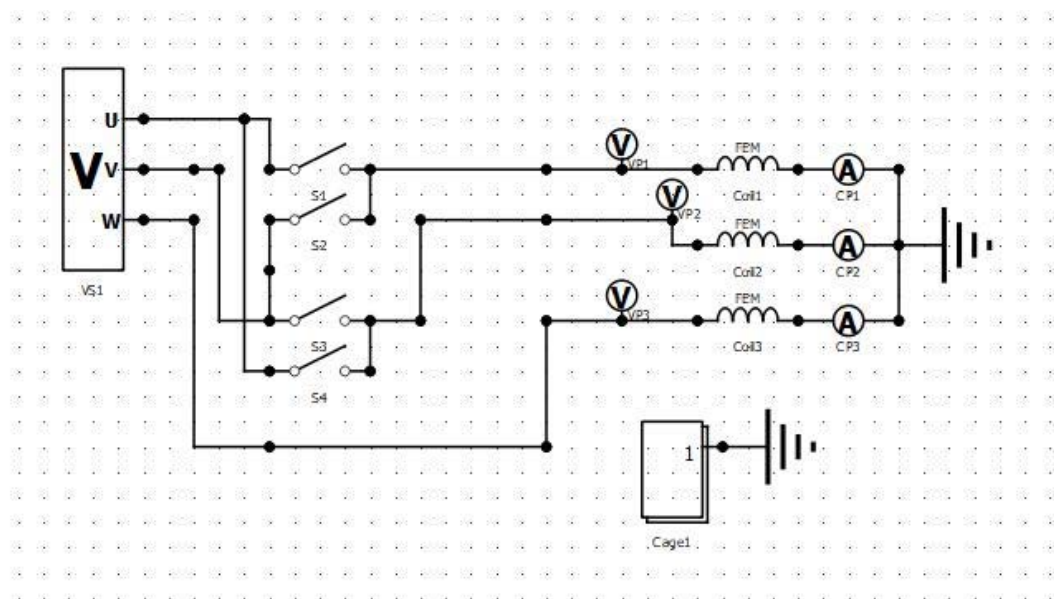


Figure 4-16 Circuit for rotation reverse

Figure 4-17 shows the rotation speed before and after reversing u,v phases. The reversal process occurred at 0.3 second from starting the motor.

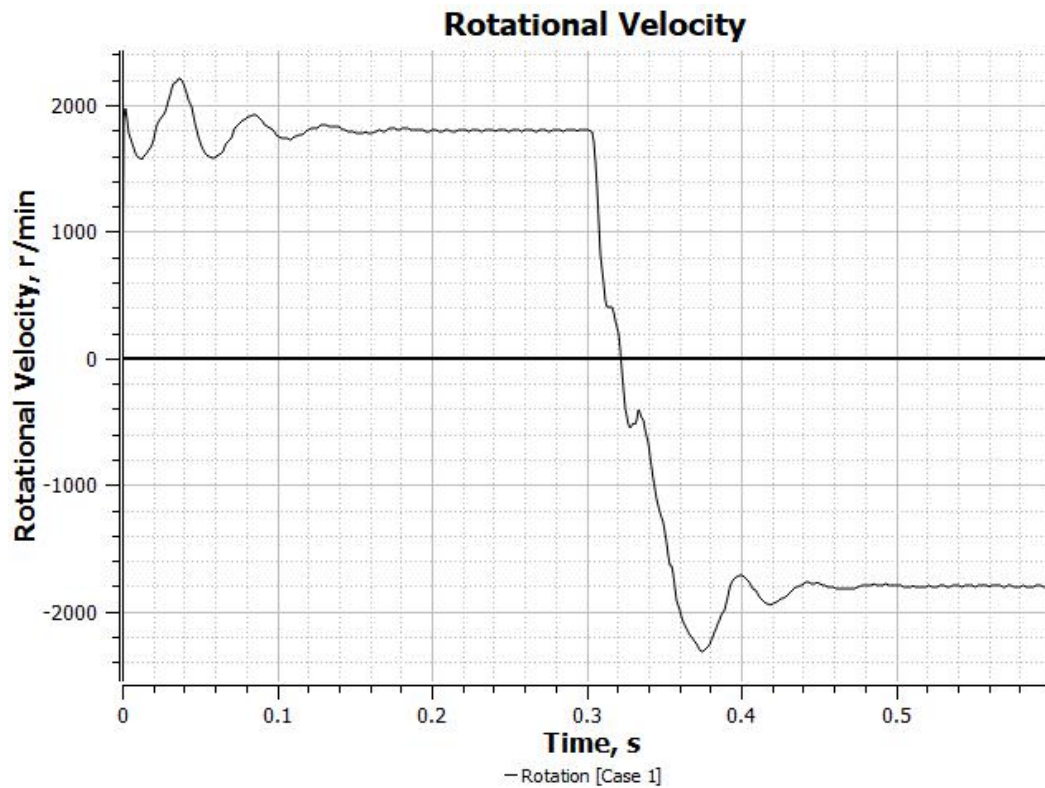


Figure 4-17 Rotational speed during phase reversal

The impact of reversal on demagnetization is proportional with the temperature and motor load. After reversal process, the magnets data is stored and loaded in new model and behavior is studied accordingly. Figures 4-18 and 4-19 show the impact of the magnetic field on the rotor magnets before and during the fault respectively.

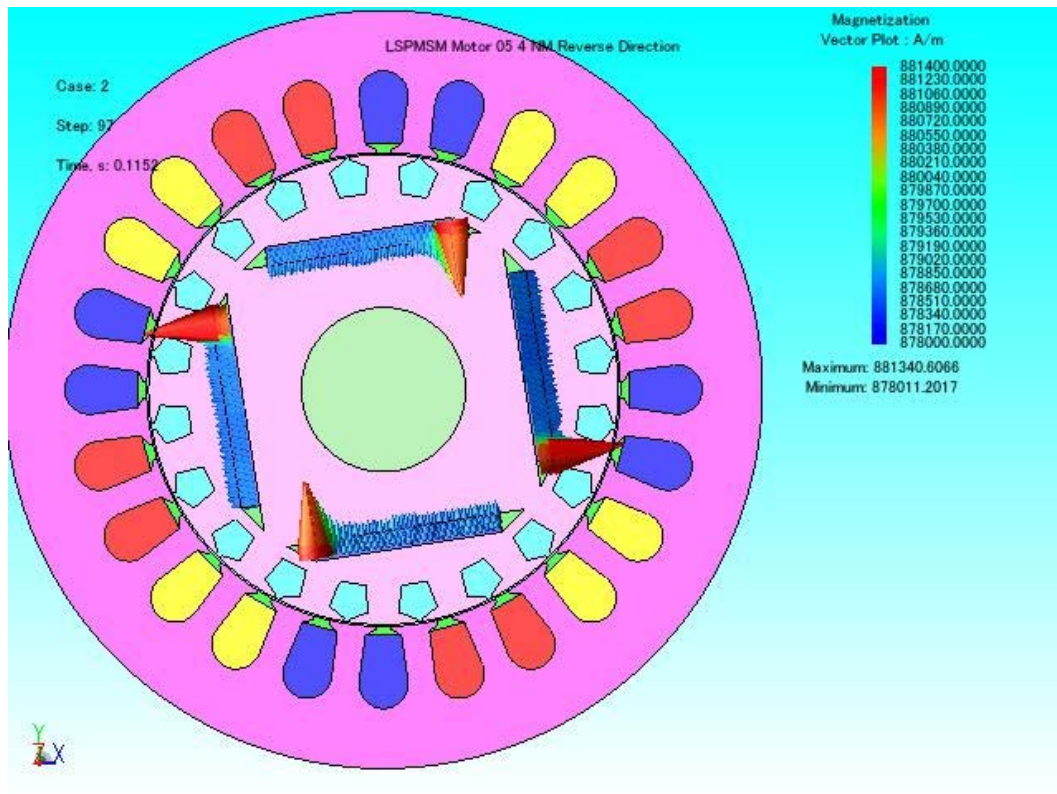


Figure 4-18 Rotor magnets before rotation reversal

As shown in figure 4-19, the stress is distributed on the whole area of the magnet uniformly. We expect a uniform demagnetization may results from the sudden rotation reversal cases.

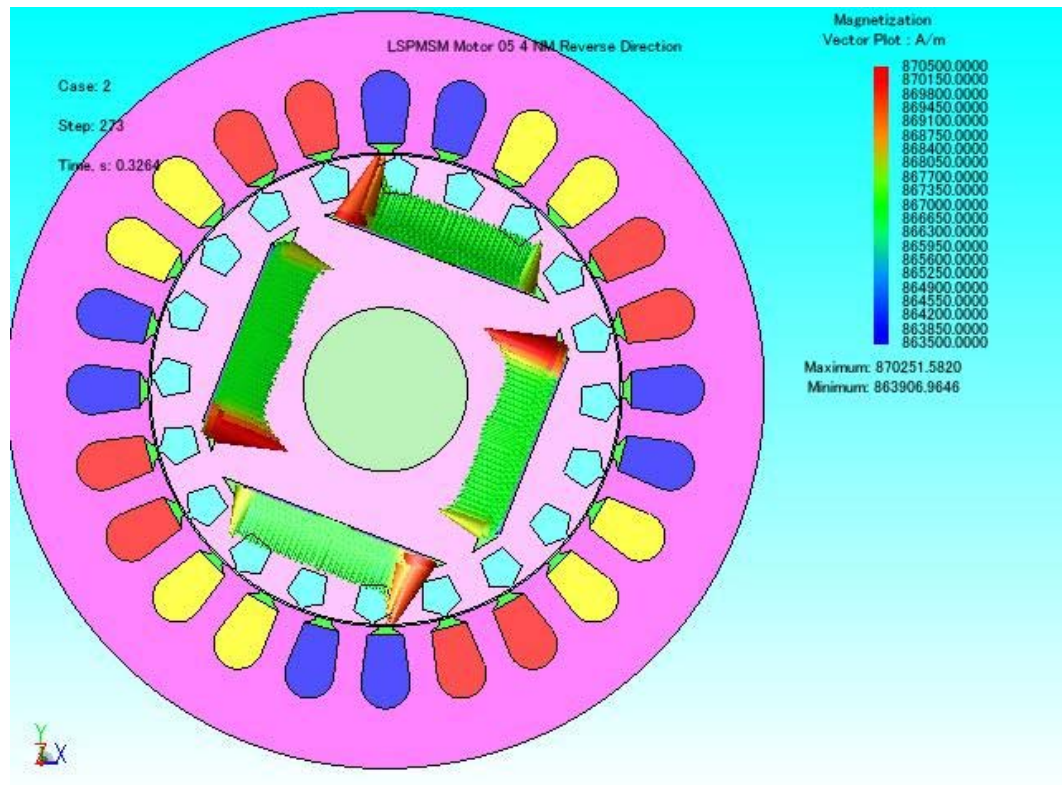


Figure 4-19 Rotor magnets during rotation reversal

4.2.6 Sudden increase in supply voltage Model

Current in the coils may increase due to short circuits in the windings or increase in the supply voltage. Figure 4-20 shows the circuit of the sudden voltage increase. VS2 voltage is larger than VS1 voltage. For voltage increase duration of 50ms, figure 4-21 shows the motor rotational speed behavior under 4NM load.

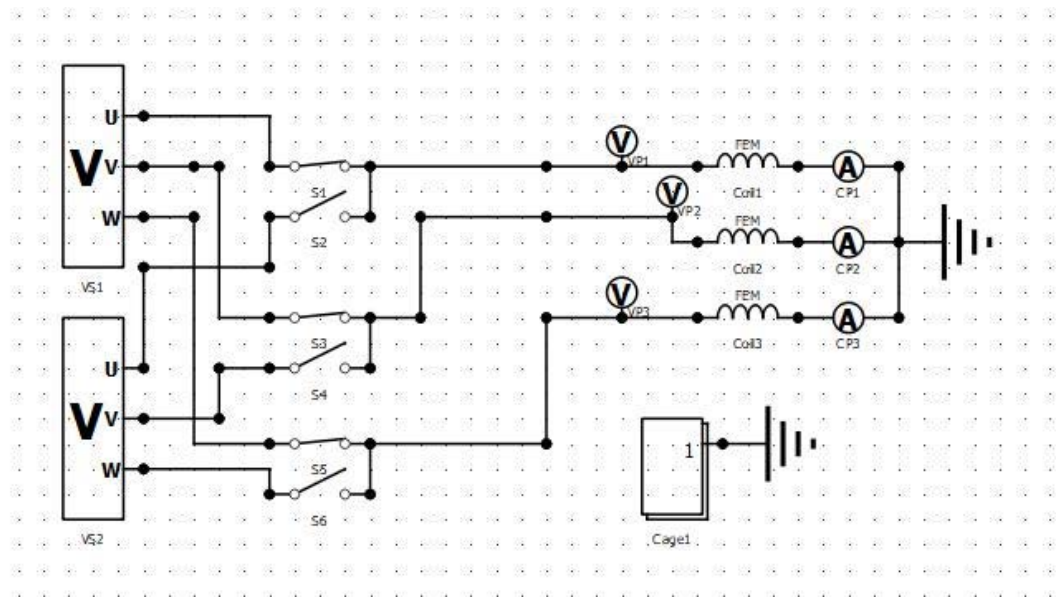


Figure 4-20 Circuit for supply voltage sudden increase

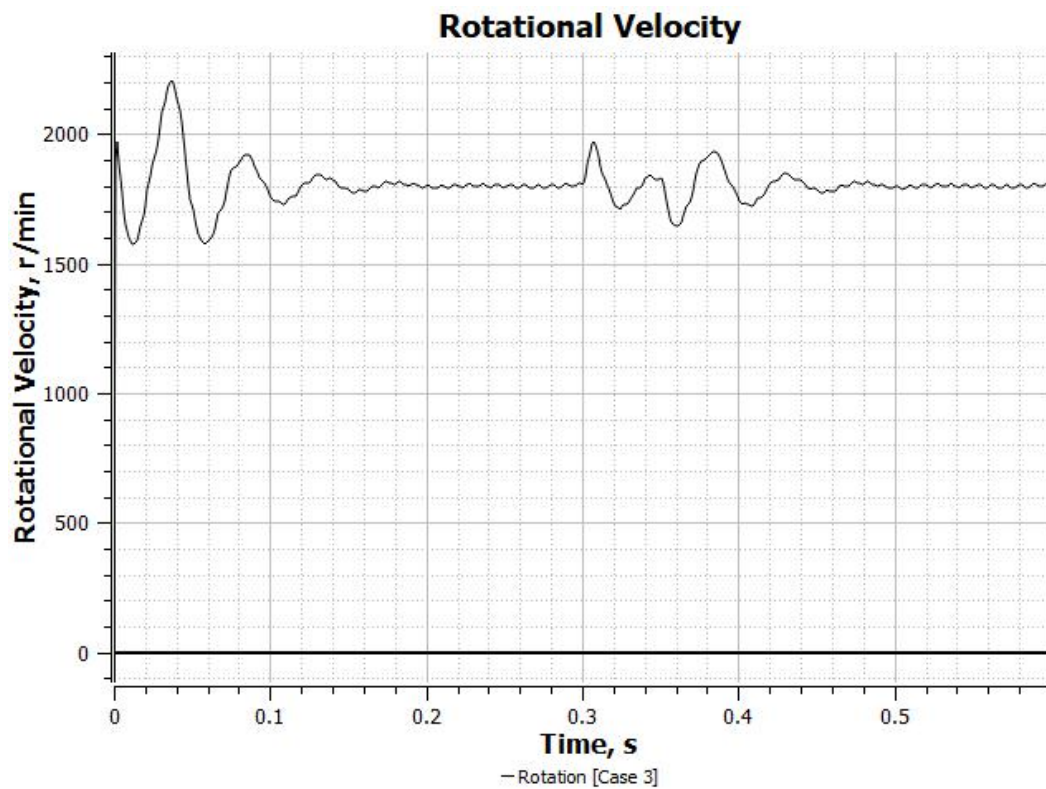


Figure 4-21 Rotational speed during supply voltage increase

Figures 4-22 and 4-23 show the rotor magnets in the normal conditions and during the supply voltage increase period respectively. As clearly shown in figure 4-23, the stress is partially applied on the magnets, hence we expect partial demagnetization may occur on the magnets.

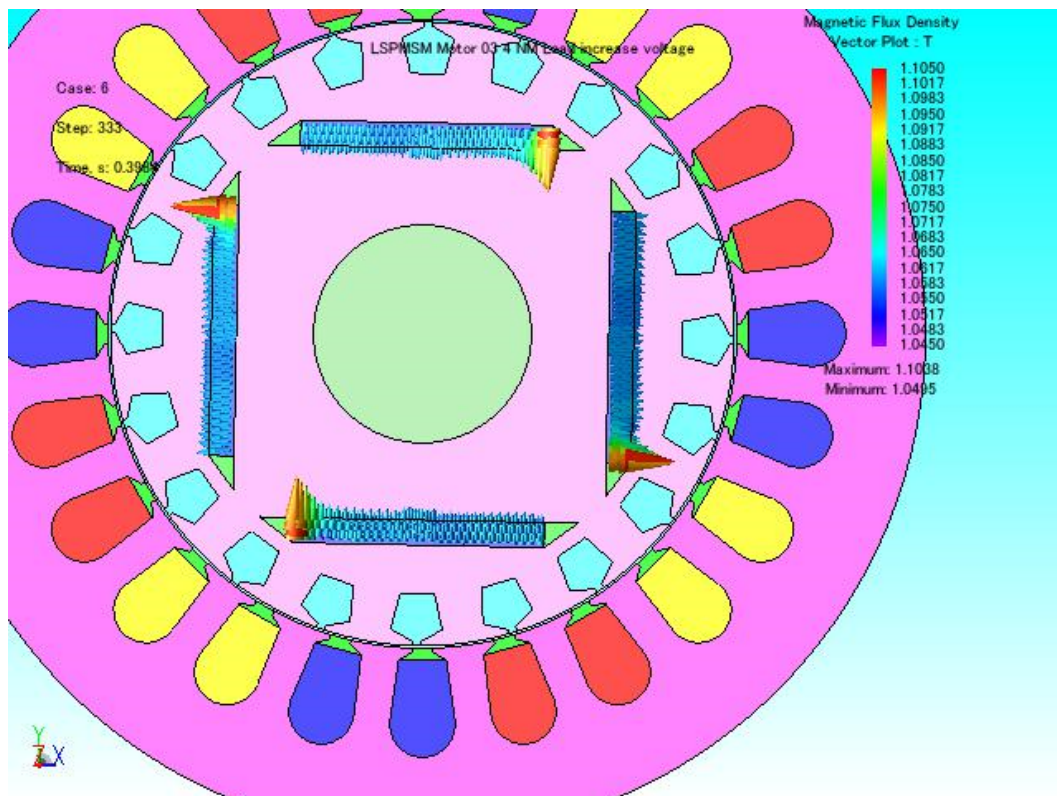


Figure 4-22 Rotor magnets during normal operation

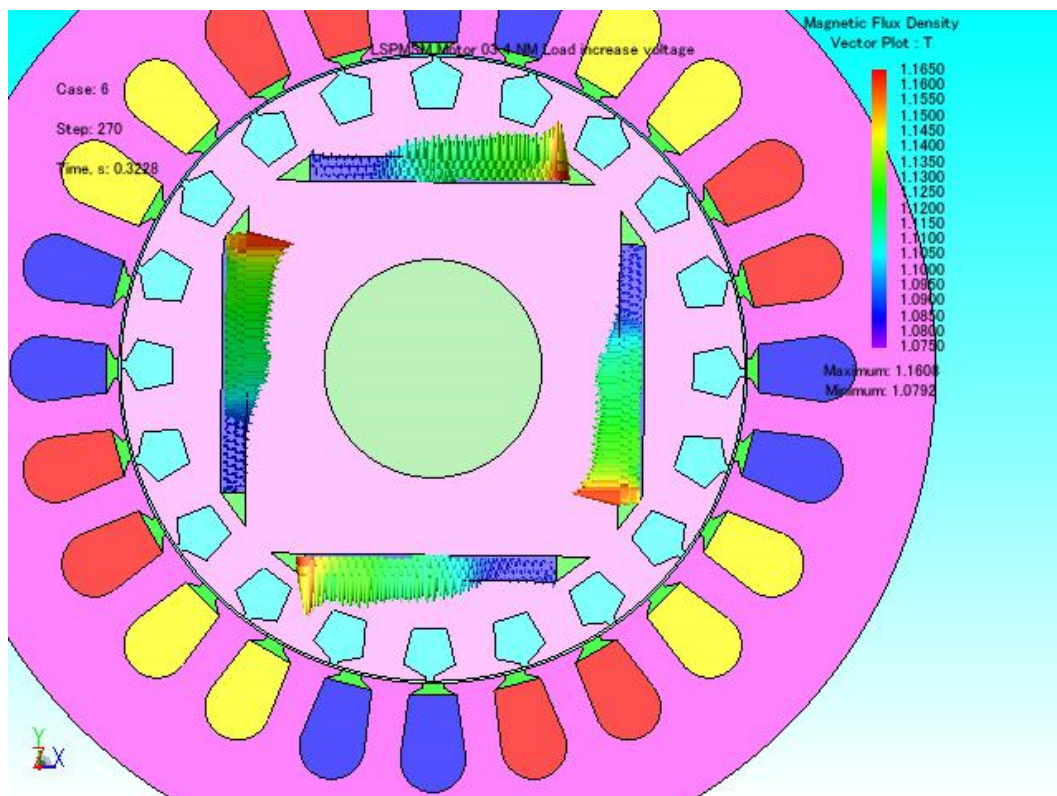


Figure 4-23 Rotor magnets during voltage increase

CHAPTER FIVE

PROPOSED DIAGNOSTICS TECHNIQUE FOR DEMAGNETIZATION FAULTS IN LSPMSM

5.1 Introduction

This chapter presents the diagnostic technique adopted to reach the tool, which will detect and identify the existence of irreversible demagnetization in the LSPMSM. The detection output will be the “type” and the “class” of demagnetization. Uniform and Partial demagnetization are studied and required to be identified. In each type, the percentage of demagnetization is divided into five classes as per Table 5-1 (discussed in section 4.4.3).

Table 5-1 Demagnetization Percentage Classification

Sr#	Demagnetization Percentage	Demagnetization Class
1	less than 10%	A
2	from 10% and less than 30%	B
3	from 30% and less than 50%	C
4	from 50% and less than 70%	D
5	more than 70%	E

Throughout this chapter, several features will be studied on the way to find the most suitable feature that helps in getting high efficient detection performance through ANN.

5.2 Artificial Neural Network (ANN)

Artificial Neural networks (ANNs) are inspired based on biological networks in the human body. The development of this method came from the desire of producing artificial systems which perform intelligent functions in the same way as a human brain. A neural network differs from computational analysis, as computers have some sort of learning algorithms and training rules, with a capability of extending results beyond the

trained data. In addition, there is no need for an explicit description of the problem being processed. In the training process, the neural network adapts itself to map the desired output to the input data. This method has a lot of applications, which include mainly classification and function approximation problems [74].

The biological neuron consists of terminal buttons which are connected to a huge number of other neurons across a gap called a synapse. The neuron has many dendritic trees; each tree will sum the weighted information being received from other neurons.

Mathematically, the neuron is implemented with simple algebraic equations [74]. Figure 5.1 represents an elementary neuron with input vector X and output Y . Each input is weighted by an appropriate weight w . In addition, a bias B will be added to the total sum, while an activation function F is used to generate the output.

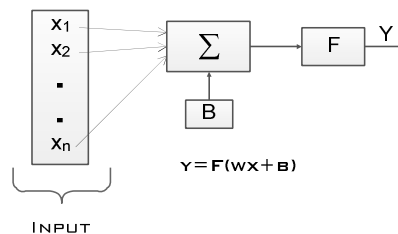


Figure 5-1: Basic structure of neuron.

Consequently, a series of N neurons will create a single layer in the network. Figure 5.2 presents the detailed layer topology and its equivalent notation.

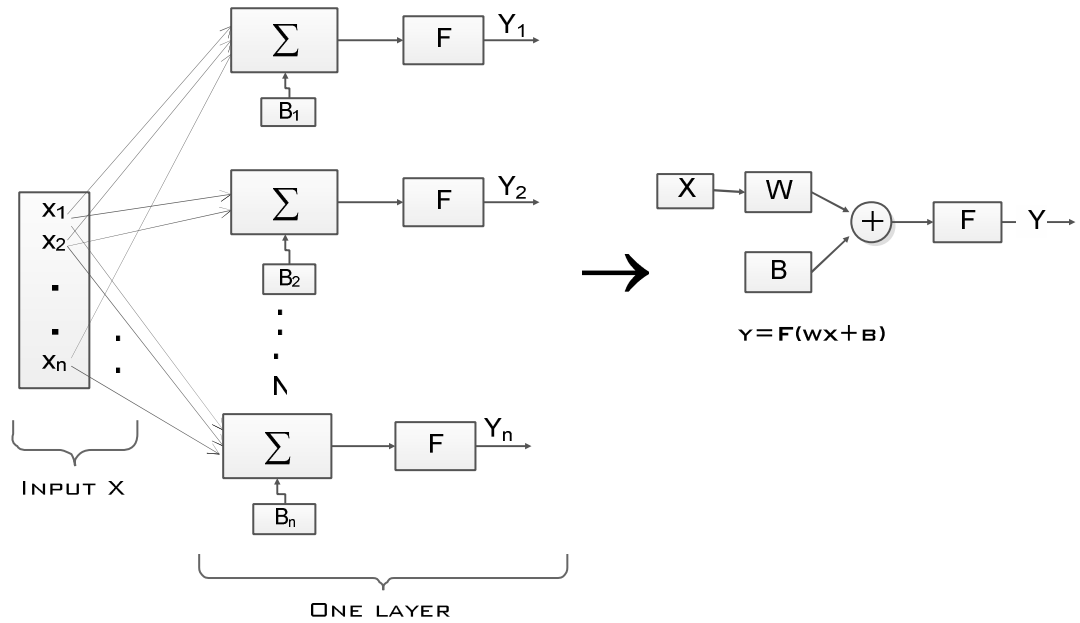


Figure 5-2: A single layer in neural networks.

This study uses multilayer feedforward ANN.

5.3 Fault Detection

ANN is capable to learn different type of complicated linear and nonlinear functions. Therefore, it can learn different types of motor faults, which result in an accurate prediction of fault occurrence and severity. This type of detection scheme is inexpensive and noninvasive. This thesis aims to develop ANN detection scheme which overcomes cost, complexity, and speed problems. In conventional detection schemes, a detailed mathematical model is required, and many features are needed to be extracted, which results in a costly instrument for measurement purposes [79].

However, the method used in this thesis will use the captured stator current and supply voltage data to extract the most important features. If these features are selected as the inputs to the ANN, then the detection of the demagnetization fault conditions can be implemented. Moreover, this scheme will be simple, economical and reliable. Figure

5-3 shows the detection scheme of demagnetization using ANN. Stator current and supply voltage are captured using a proper data acquisition system. In this thesis, the stator current is captured at a sampling rate of 1 kHz for a total time duration of 500 ms. Next, some important statistical parameters are calculated. This process is called feature extraction. For the selected features, the ANN is initialized with small weights to calculate the resultant error, as explained in Figure 5-3. The calculated error will propagate backward into the network to update the weights and reduce the output error process is repeated. This until reaching a specified global minimum of error. The neural network should be trained and tested carefully in a healthy and faulty state, under different loading conditions.

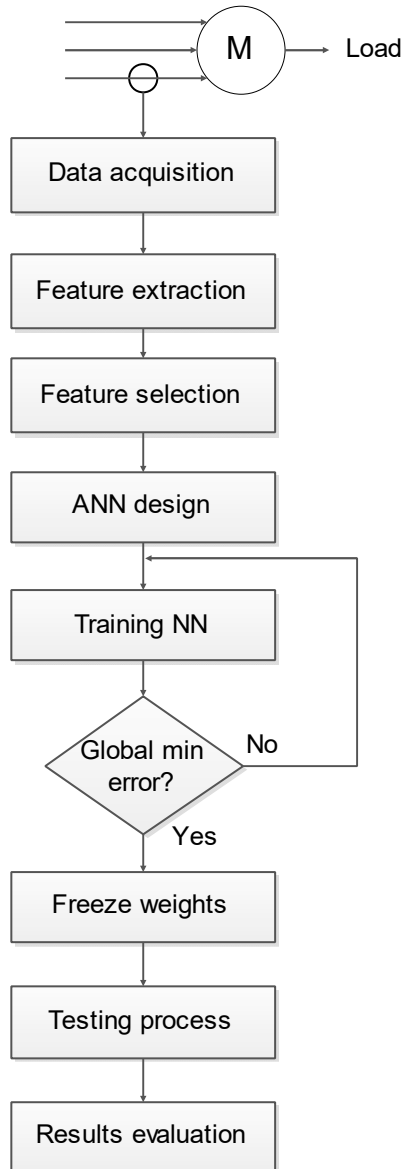


Figure 5-3: Detection scheme using ANN.

5.3.1 Features Extraction

In the process of fault detection using ANNs, two problems are faced: the selection of neural network inputs, and specifying the network parameters. The aim of this study is to provide an effective detection capability based on easy measurable inputs. The concentration will be on the stator current, supply voltage and torque measurements. Many features can be extracted from these variables like root mean square value, mean value, energy value, and harmonic analysis for the spectrum of the signal.

5.3.2 Features Selection

The features selection algorithms determine the most superior input variable, which maximizes the performance of the detection process. The suitable predictor variable depends on the relationship between the input data. The selection process is not straightforward due to [76]:

1. Large set of the available input variables.
2. Correlation between input variables which create redundancy.
3. Input variables which have no predictive power.

Modelers of ANNs realize that the input variable selection (IVS) algorithms should be utilized to maximize the network performance. The key considerations of IVS can be summarized as [76]:

1. Relevance: The input variables should be informative, which covers the behavior of the operating conditions.
2. Computational efforts: Small number of input variables will increase the speed of training process and decrease the network size.
3. Training difficulty: The difficulty in training increases as the number of redundant and irrelative input variables increases. Inputs that are more redundant result in more local minima under the training process. This may lead to convergence to local minima with poor generalization. In addition, the relationship between redundant variables and performance error is hard to map.
4. Input dimensions: This problem can be handled through the preprocessing of data to minimize the number of network inputs.

The last discussion suggests that the desired input variables should be informative, , with predictive ability, less redundant, and independent or dissimilar.

5.4 Possible Inputs

There are many variables that can be measured, and can directly or indirectly describe the behavior and the healthiness of the motor. The factors involved in considering such variables in detecting the faults in this study are: **ease of measurement, operation disturbance** and **requirement for special transducers/tools**. Table 5-2 shows different variables and the notes against each of them.

Table 5-2 Motor Variables

Sr#	Variable	Ease of Measurement	Tool	Operation Disturbance	Remarks
1	Supply voltage	Easy	Voltage Transducer	No	Cheap transducer
2	Stator Current	Easy	Current Transducer	No	Cheap transducer
3	Rotational Speed	Easy	Speedometer	No	Cheap transducer
4	Torque	Easy	Torque meter	No. if no transducer installed then yes.	
5	Magnetic Flux	Not Easy	Flux meter	Yes	Expensive device
6	Rotor Current	Very difficult	Can't be measured easily	Yes	
7	Back EMF	Easy	Voltage Transducer	Yes	Need external prime mover

It is clear from the above table, that relying on stator current, supply voltage, rotational speed and torque is the easiest, less expensive and less operational disturbance choices for monitoring the motor conditions.

Supply voltage is an external variable, which depends on the supply but not on the motor. However, voltage fluctuation or quality will directly affect the motor behavior. The rotational speed (N) of the motor depends on the frequency (f) of the supply and the number of motor poles (P) according to equation (5.1):

$$N = \frac{120 f}{P} \quad (5.1)$$

The supply voltage can be measured using voltage transducer, which will take instantaneous data based on certain sampling frequency.

Stator current can be easily measured through transducer connected to the supply lines through clamp meter or ring type current transformer.

Back EMF is the most variable that is strongly affected by any change in the permanent magnets. However, back EMF can't be measured unless the motor is removed from operation and an external prime mover is connected to the motor, which is against our goal to reduce the shutdown time.

5.5 Feature Selection

5.5.1 Transient Versus. Steady State

Depending on several simulation results under various loading conditions for LSPMSM, it is found that the behavior of the motor varies considerably with the following conditions:

- 1- Initial rotor angle.
- 2- Initial voltage angle.

Figures 5-4 and 5-5 show the rotational speed and phase current under different initial rotor positions. The figures shows that the transient period depends strongly on the initial conditions while the steady state is independent of the initial conditions.

In order to make field testing easier and more efficient, utilizing the information from steady state period will be the best choice. Moreover, the motor is not required to be taken out of service or out of work place system. Accordingly, features can be extracted from the steady state current, speed and torque.

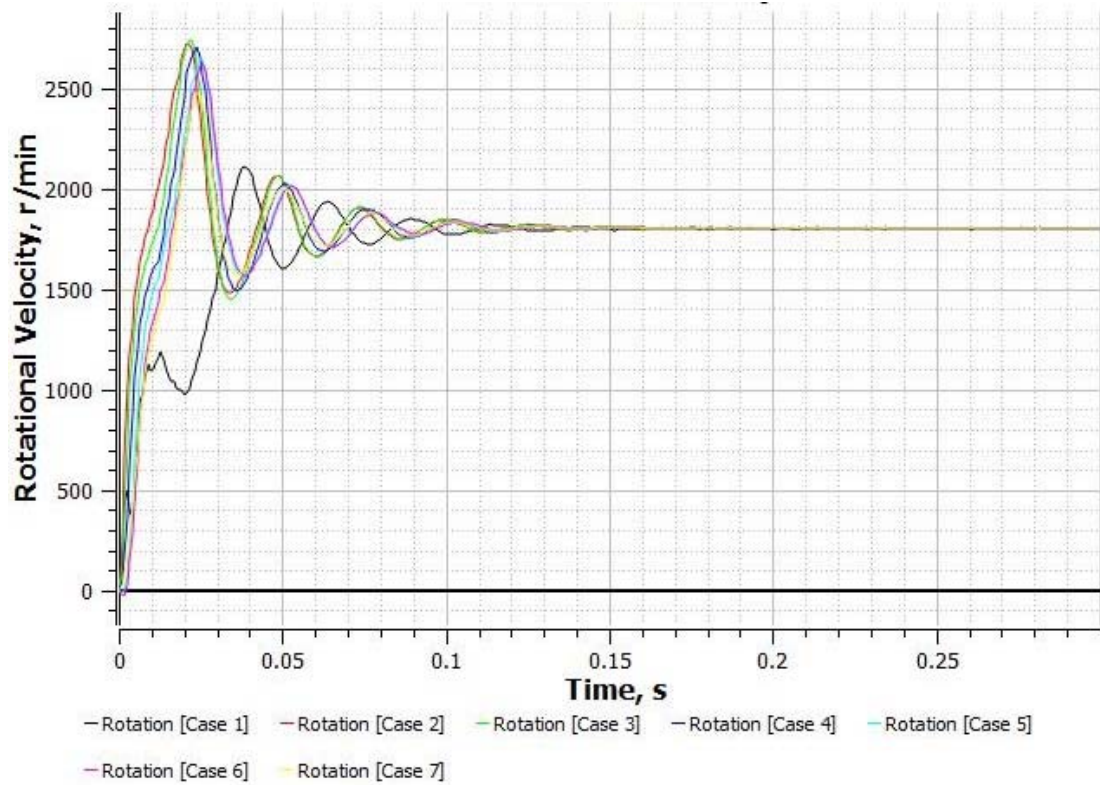


Figure 5-4 Rotational speed under various rotor initial position

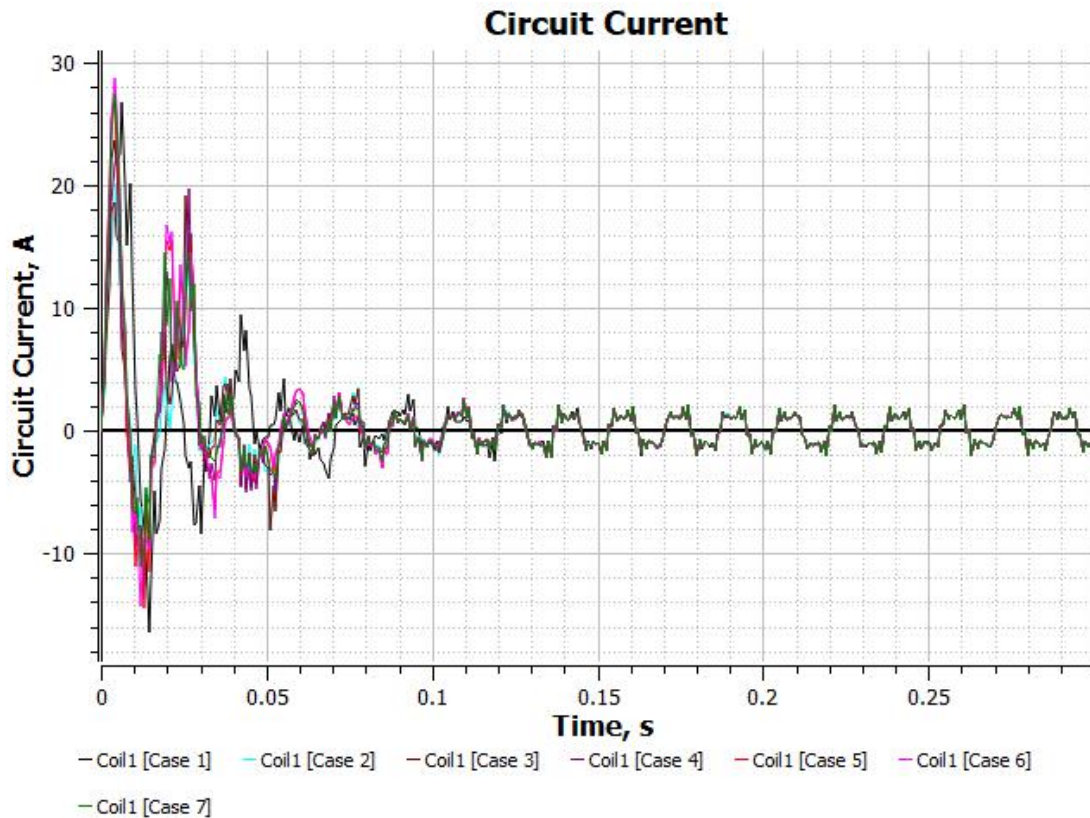


Figure 5-5 Phase current for various rotor initial positions

5.5.2 Stator Current Behavior

The stator current has been recorded from several simulations under healthy and demagnetized cases. It is noted that the stator no load RMS current is large compared with the loaded cases. The power factor is also very low at no load and light load cases. Hence, taking current as leading input to the neural network will not give the required results. Figure 5-6 shows the rms line current with the load variation.

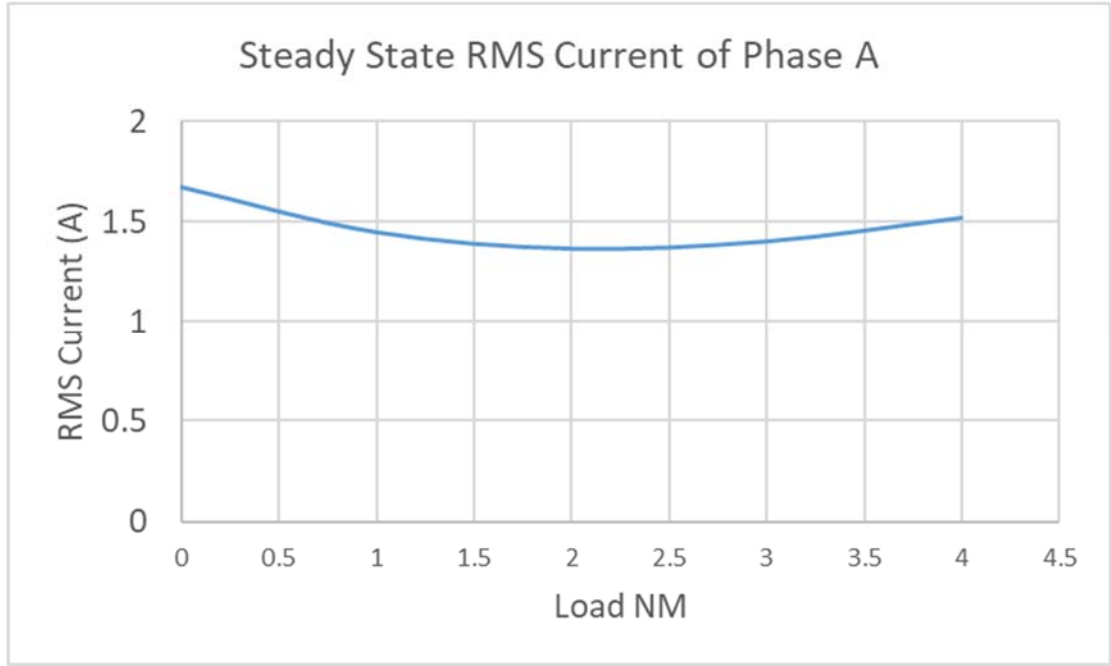


Figure 5-6 RMS stator phase current with load

5.5.3 Input Power

Because of the above behavior of the stator current, and after examining all possible features of the stator line current such as root mean square value, mean value, harmonics content, peak values, continuous wavelet analysis and singular value decomposition, it is found that utilizing these features alone will not give the required detection performance.

Then, instantaneous power has been studied and found to be efficient in comparing the demagnetization conditions and levels. extensive work in finding feature that is linearly related with the demagnetization levels, loading conditions and motor temperature, the instantaneous apparent power signal which is shown in figure 5-7 and the Fourier Transform of that signal which is shown in figure 5-8 gave sufficient information that could be utilized in the ANN. The difference between the fundamental harmonic (120Hz) and the dc component of the Fourier Transform gives linear relation under different loading conditions. Figures 5-9 to 5-14 show the relationship between the

selected feature and the demagnetization levels for different loading conditions for different motor temperatures.

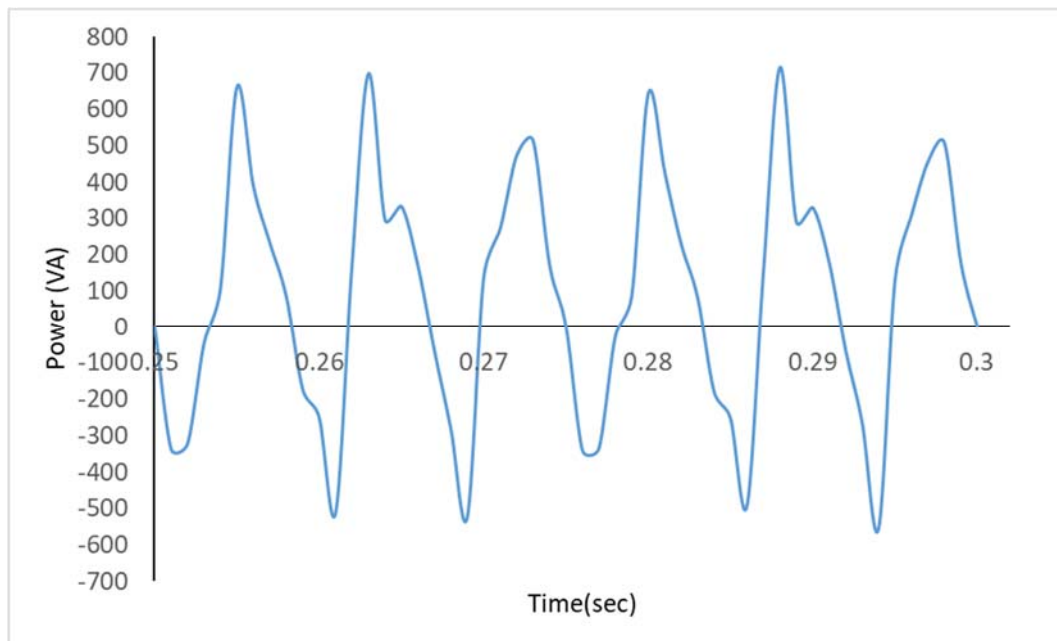


Figure 5-7 Instantaneous apparent power

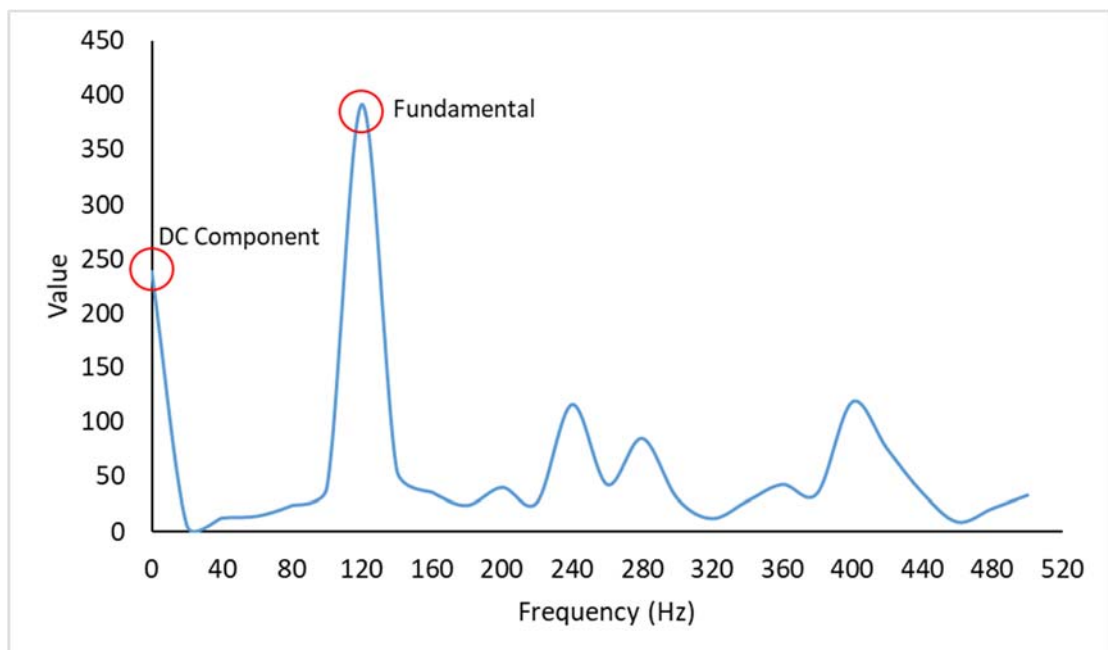


Figure 5-8 Instantaneous apparent power FFT

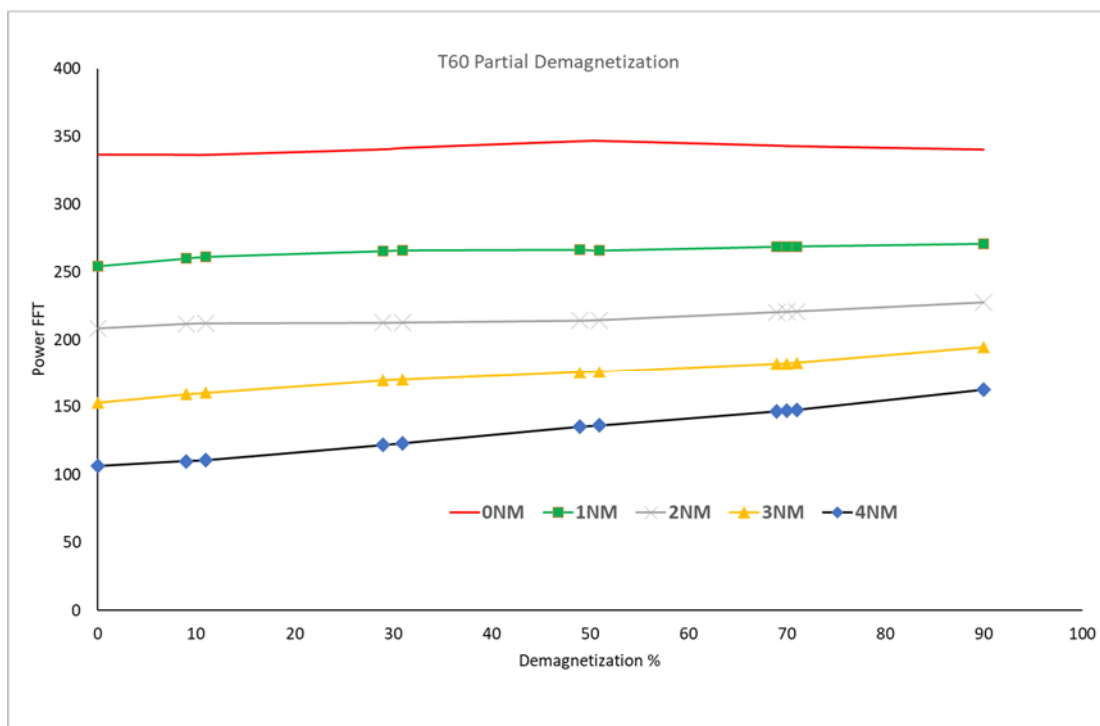


Figure 5-9 Partial Demagnetization for 60°C

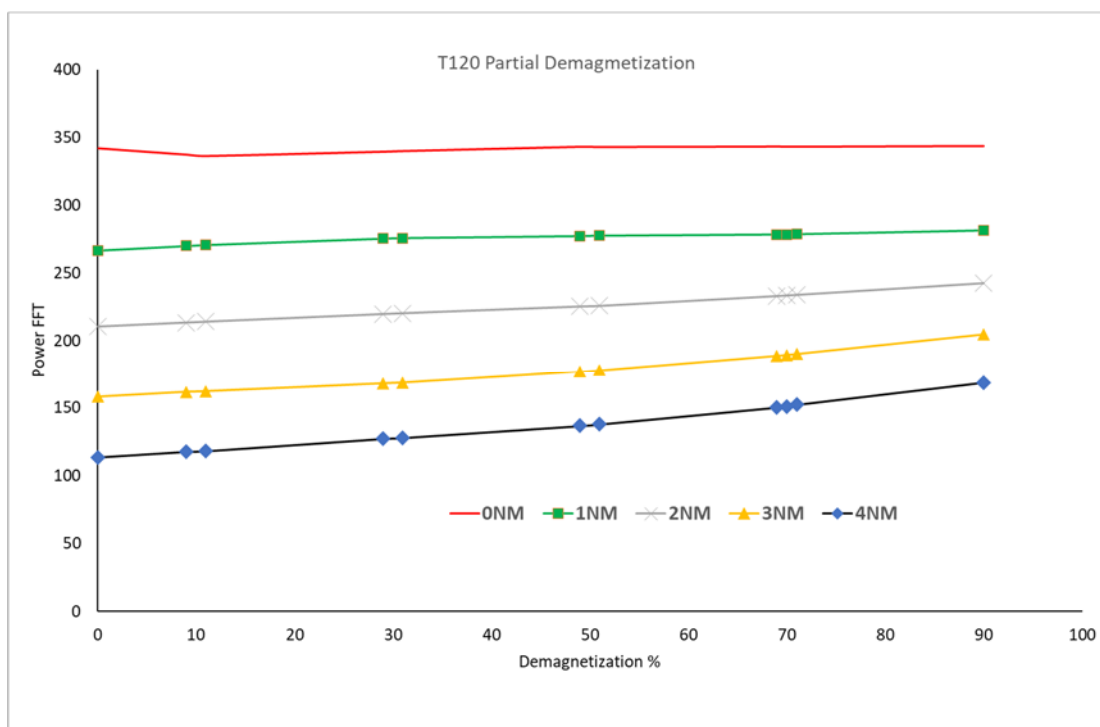


Figure 5-10 Partial Demagnetization for 120 °C

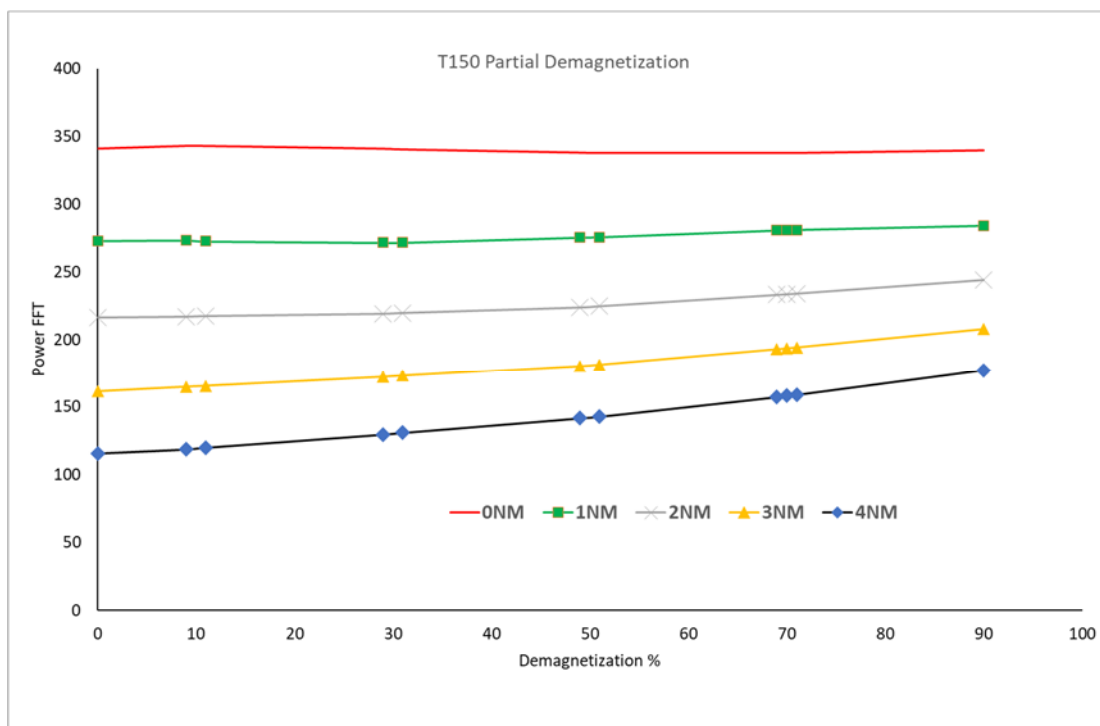


Figure 5-11 Partial Demagnetization for 150 °C

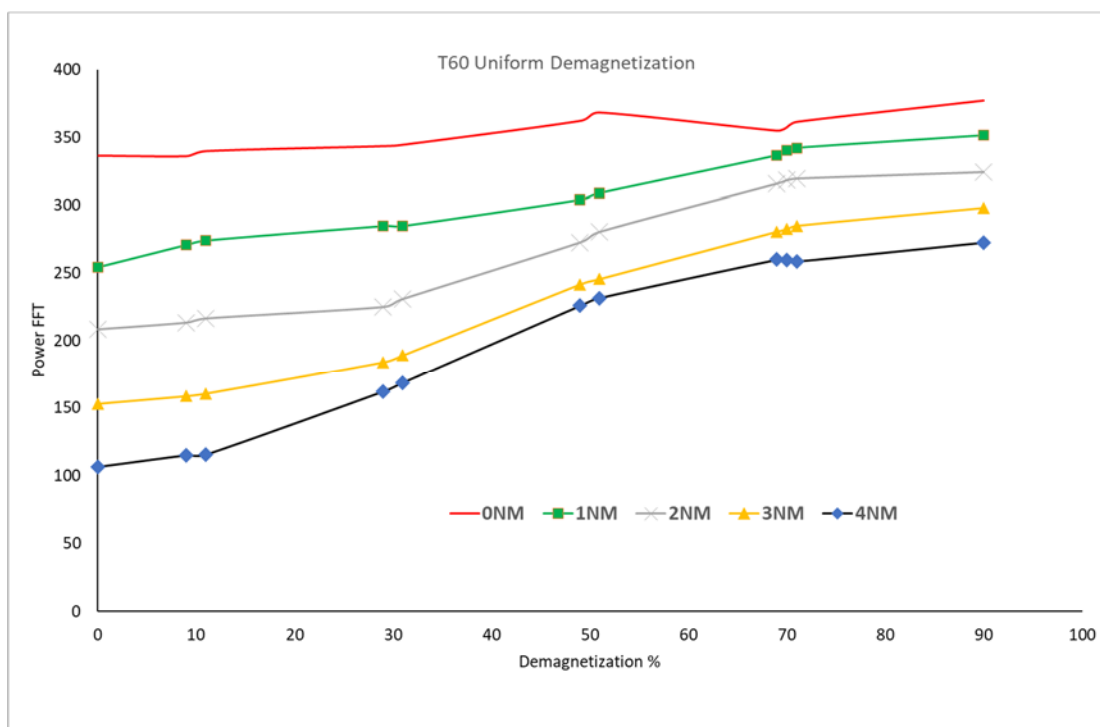


Figure 5-12 Uniform Demagnetization for 60 °C



Figure 5-13 Uniform Demagnetization for 120 °C



Figure 5-14 Uniform Demagnetization for 150 °C

5.6 Simulation of ANN

5.6.1 ANN Configuration and Selected Parameters

The performance of the ANN depends on the selected parameters for the number of hidden layers, number of neurons.

Two configurations have been tested in this study. The first is to use one neural network with four inputs (Temperature, Load, Extracted power feature and rms stator phase current) and two outputs (Demagnetization type and Class). Figure 5-15 shows the first neural network configuration.

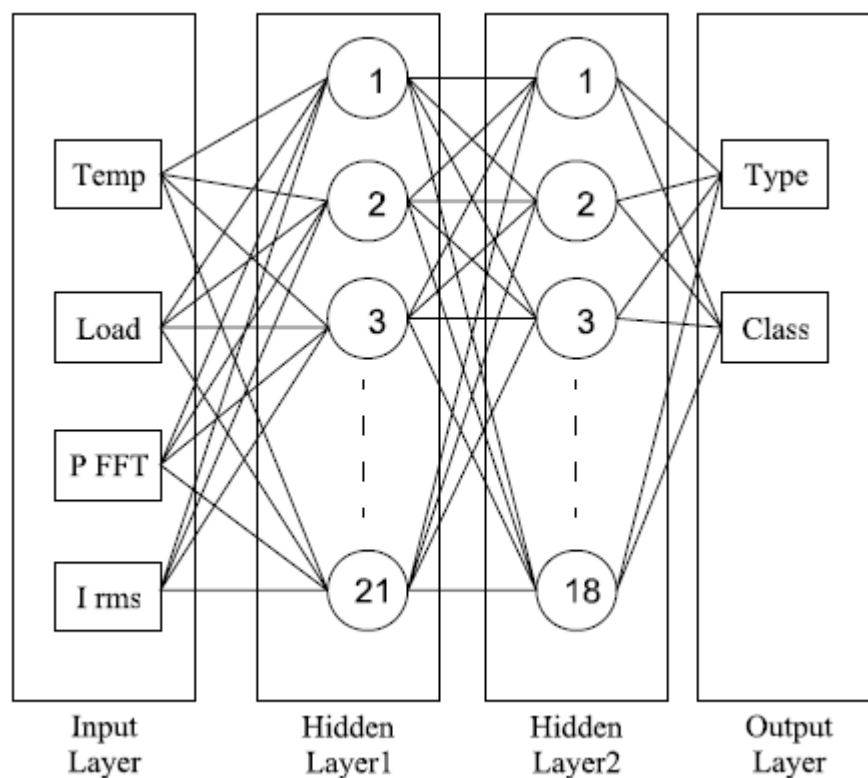


Figure 5-15 Configuration no.1 for ANN

The performance of the above configuration didn't exceed 83% with a lot of trials to change the number of neurons.

Since the complete ANN neural setup didn't give an acceptable performance, this study suggested to build separate ANN for each output. To enhance the overall detection performance. Figure 5-16 presents the flow chart for the detection process.

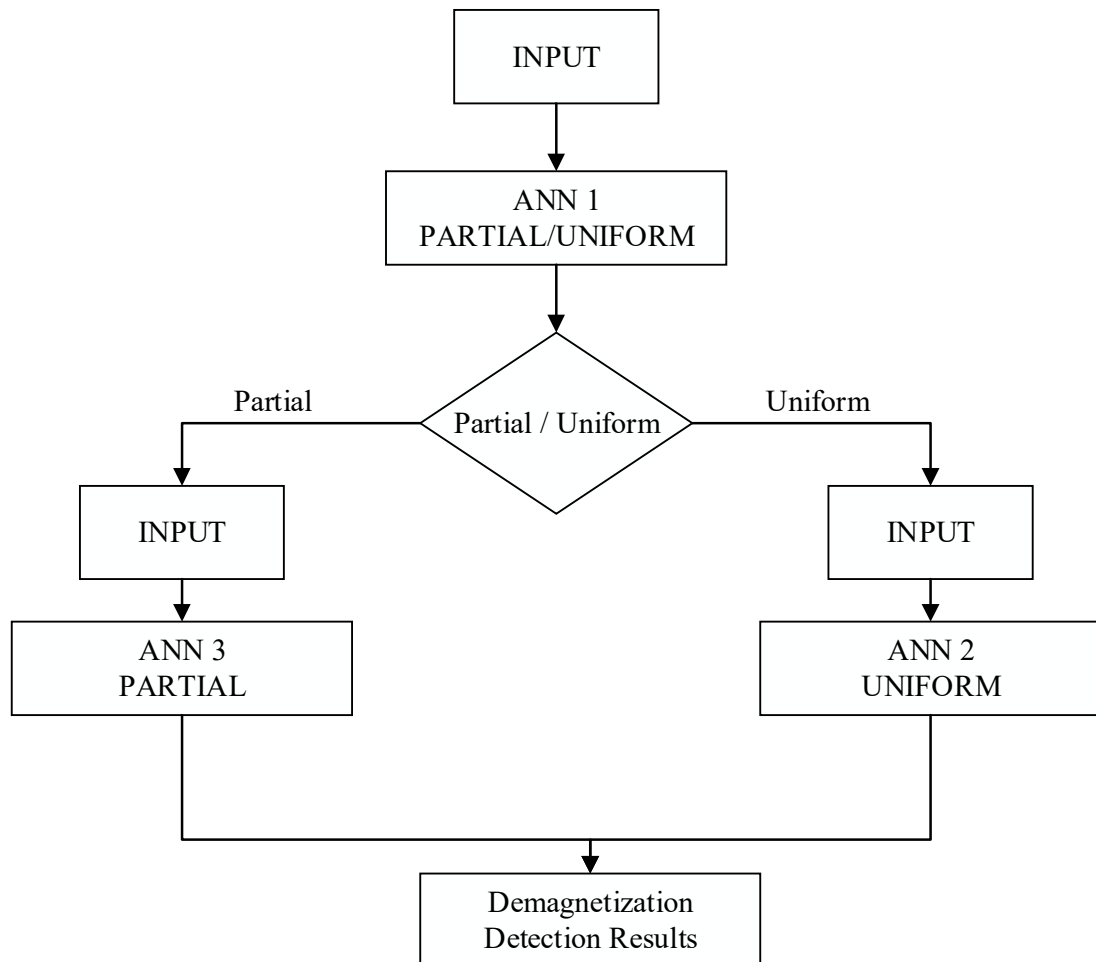


Figure 5-16 Flow chart for ANN Detection

The configuration of each of the three ANN is shown in table 5-3

Table 5-3 Configuration of ANN

ANN#	Inputs	No. of hidden layers	No. of neurons for 1 st layer	No. of neurons for 2 nd layer
ANN1	Temperature, Load,	2	10	5
ANN2	Power FFT	2	18	15
ANN3	RMS Current	2	18	15

Figure 5-17 shows the Matlab simulation of one of the ANN.

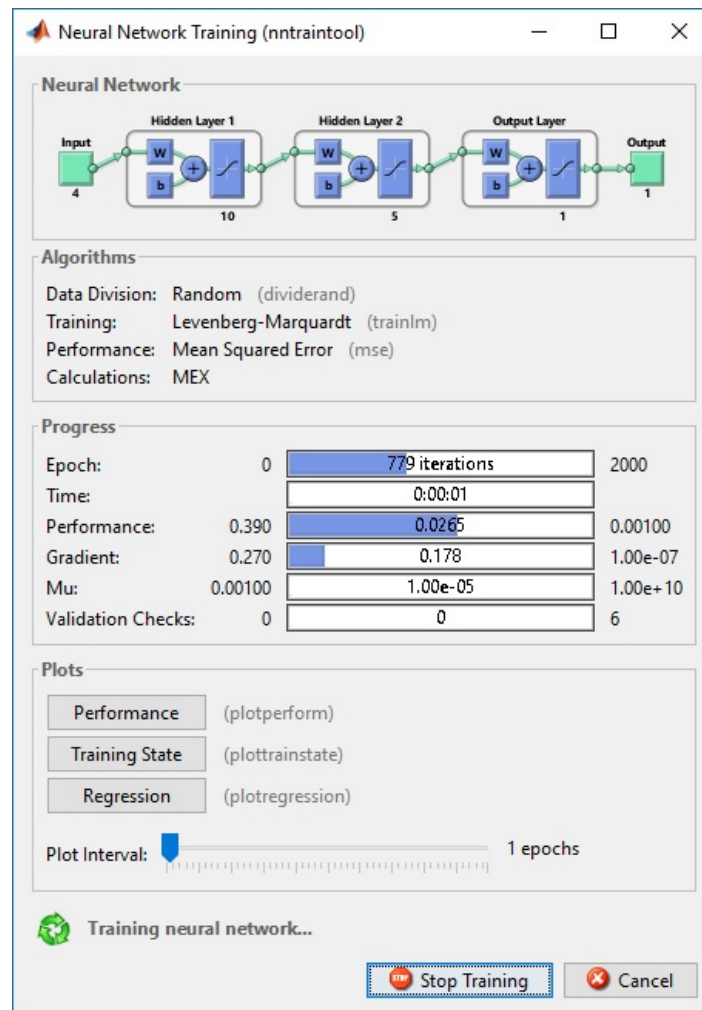


Figure 5-17 Matlab training process of ANN

5.6.2 Input / Output Training Lists

Based on the above feature selection and discussion, the selected inputs are Temperature, Load, Power FFT value for fundamental harmonic value minus DC component and RMS phase current. While the output is the type of demagnetization and the demagnetization class. Sample of the training cases are listed in table 5-4. Complete set of training list is shown in appendix D.

Table 5-4 Sample of training Cases

Temp	Load	Power FFT	Current rms(A)	Demag Type	Class
60	0	344.2194	1.681026	Partial	A
60	0	287.45514	1.683203	Partial	A
60	4	283.41734	1.696317	Partial	E
60	4	259.01379	1.755086	Partial	E
120	0	267.8159	1.766687	Partial	C
120	0	231.75222	1.766535	Partial	D
120	0	253.56735	1.76759	Partial	D
120	0	336.07752	1.767529	Partial	E
150	2	337.65363	1.525131	Partial	B
150	2	219.96627	1.529808	Partial	C
150	2	274.06299	1.574156	Partial	C
150	2	285.53546	1.579712	Partial	D
150	4	239.21472	1.67767	Partial	B
60	1	263.0631	1.818995	Uniform	C
60	1	338.83105	1.823967	Uniform	D
60	1	340.93853	1.94282	Uniform	D
60	1	230.02244	1.949894	Uniform	E
60	3	219.72608	2.452807	Uniform	E
60	4	235.34222	1.522571	Uniform	A
120	3	192.22128	2.308807	Uniform	E
120	3	206.80336	2.308989	Uniform	E
150	4	209.54737	2.022682	Uniform	B
150	4	209.802	2.044389	Uniform	C
150	4	179.75211	2.287844	Uniform	C
150	4	168.33452	2.31908	Uniform	D
150	4	209.54737	2.542732	Uniform	D

5.6.3 Test Cases:

Randomly selected 75 cases for different loads and demagnetization percentage were tested. Sample of the test cases is listed in table 5-5. The complete set of testing cases is listed in appendix F.

Table 5-5 Sample of Testing Cases

Temperature	Load	Power FFT	Current rms	Demag (F/P)	Demag. Class
60	3	152.90397	1.40369	Partial	A
60	3.7	122.02431	1.45999	Uniform	A
60	0	336.07752	1.68849	Partial	B
60	0	337.65363	1.74706	Uniform	B
120	2	219.96627	1.59103	Uniform	B
120	1	274.06299	1.54479	Partial	B
120	0	341.96672	1.76548	Partial	C
120	0	352.49964	1.85259	Uniform	C
150	1.5	257.06016	1.60381	Partial	D
150	1.3	316.12852	1.91608	Uniform	D
150	4	148.00372	1.80338	Partial	D
150	3	195.45628	1.70009	Partial	E
150	3	287.27188	2.3324	Uniform	E
60	0	341.44766	1.73533	Partial	E
60	0	363.00439	1.96709	Uniform	E

5.6.4 Results of Testing the ANN

The test cases have been investigated using the trained ANN and the results are shown in table 5-6.

Table 5-6 Result of ANN Test Cases

#	TEMP	Load	Power FFT	Current rms	Actual Type	Predicted Type	Actual Class	Predicted Class	Result
1	60	3	152.904	1.40368	Partial	Partial	A	A	Ok
2	60	3	152.903	1.40368	Uniform	Uniform	A	A	Ok
3	60	3.3	141.073	1.42214	Uniform	Partial	A	A	Ok
4	60	3.5	132.193	1.43888	Partial	Partial	A	A	Ok
5	60	3.7	122.024	1.45999	Uniform	Partial	A	A	Ok
6	60	3.8	116.336	1.47525	Partial	Partial	A	A	Ok

7	60	4	106.007	1.52257	Partial	Partial	A	A	Ok
8	60	4	106.006	1.52262	Uniform	Uniform	A	A	Ok
9	60	2	209.547	1.37353	Partial	Partial	A	A	Ok
10	60	2	209.802	1.39556	Uniform	Uniform	A	A	Ok
11	60	2.5	179.752	1.37377	Partial	Partial	A	B	Fail
12	60	2.8	168.334	1.41437	Uniform	Uniform	A	A	Ok
13	60	0	336.386	1.68144	Partial	Partial	A	A	Ok
14	60	0	344.219	1.72637	Uniform	Partial	A	C	Fail
15	60	0.5	287.455	1.57274	Partial	Partial	A	A	Ok
16	60	0.7	283.417	1.55199	Uniform	Uniform	A	A	Ok
17	60	1	259.013	1.46466	Partial	Partial	A	A	Ok
18	60	1	267.815 9	1.51673 1	Uniform	Uniform	A	A	Ok
19	60	1.3	253.567 4	1.48359 5	Uniform	Uniform	A	A	Ok
20	60	1.5	231.752 2	1.40309 7	Partial	Partial	A	A	Ok
21	60	0	336.077 5	1.68848 7	Partial	Partial	B	B	Ok
22	60	0	337.653 6	1.74706 3	Uniform	Uniform	B	B	Ok
23	120	2	219.966 3	1.59102 8	Uniform	Uniform	B	B	Ok
24	120	1	274.063	1.54479	Partial	Partial	B	B	Ok
25	120	1	285.535 5	1.71051 1	Uniform	Uniform	B	B	Ok
26	120	1.3	263.063 1	1.69109 6	Uniform	Uniform	B	B	Ok
27	120	1.5	239.214 7	1.49111 2	Partial	Partial	B	B	Ok
28	60	0	338.831 1	1.70483 5	Partial	Partial	B	B	Ok
29	60	0	340.938 5	1.74343 4	Uniform	Partial	B	E	Fail
30	120	2	230.022 4	1.71292 6	Uniform	Uniform	B	B	Ok
31	120	2	219.726 1	1.49348 9	Partial	Partial	B	B	Ok
32	120	2	235.342 2	1.74178 5	Uniform	Uniform	B	B	Ok
33	120	2.5	192.221 3	1.49769 2	Partial	Partial	B	B	Ok
34	120	2.8	206.803 4	1.80359 4	Uniform	Uniform	B	B	Ok

35	120	0	341.966 7	1.76547 9	Partial	Partial	C	E	Fail
36	120	0	352.499 6	1.85259 4	Uniform	Uniform	C	C	Ok
37	120	0.5	302.821	1.63104 2	Partial	Partial	C	C	Ok
38	120	0.7	308.679 1	1.78492 7	Uniform	Uniform	C	C	Ok
39	120	3.7	217.582 5	2.09664 4	Uniform	Uniform	C	C	Ok
40	120	3.8	141.14	1.66882 4	Partial	Partial	C	C	Ok
41	120	4	132.693 4	1.70369 3	Partial	Partial	C	C	Ok
42	120	4	213.513	2.16662 8	Uniform	Uniform	C	C	Ok
43	60	0	345.965 7	1.73408 1	Partial	Partial	C	C	Ok
44	60	0	352.241 5	1.85462 4	Uniform	Uniform	C	C	Ok
45	120	2	224.365 4	1.52396 6	Partial	Partial	C	C	Ok
46	120	3	174.500 8	1.57700 1	Partial	Partial	C	C	Ok
47	120	3	241.402 4	2.00011 6	Uniform	Uniform	C	C	Ok
48	120	3.3	233.391 7	2.06005 6	Uniform	Uniform	C	C	Ok
49	120	3.5	155.054 7	1.63210 1	Partial	Partial	C	C	Ok
50	150	1	276.918 9	1.63224 2	Partial	Partial	D	D	Ok
51	150	1	326.822 8	1.88555 6	Uniform	Uniform	D	D	Ok
52	150	1.3	316.128 5	1.91608 2	Uniform	Uniform	D	D	Ok
53	150	1.5	257.060 2	1.60381 2	Partial	Partial	D	D	Ok
54	150	3.7	259.541	2.31472 6	Uniform	Uniform	D	D	Ok
55	150	3.8	153.462 3	1.76826 2	Partial	Partial	D	D	Ok
56	150	4	148.003 7	1.80338 1	Partial	Partial	D	D	Ok
57	150	4	250.301 9	2.40615 3	Uniform	Uniform	D	D	Ok
58	60	0	345.099	1.73668 7	Partial	Partial	D	D	Ok
59	60	0	365.012	1.90457 8	Uniform	Uniform	D	D	Ok

60	150	2	229.071	1.60587 2	Partial	Partial	D	D	Ok
61	150	2	230.839 5	1.61756 6	Partial	Partial	D	D	Ok
62	150	2	312.938 3	2.07180 8	Uniform	Uniform	D	D	Ok
63	150	2.5	210.349	1.63888	Partial	Partial	D	D	Ok
64	150	2.8	287.972 4	2.18766	Uniform	Uniform	D	D	Ok
65	150	3	195.456	1.70008	Partial	Partial	E	E	Ok
66	150	3	287.271 9	2.3324	Uniform	Uniform	E	E	Ok
67	150	3.3	279.136 4	2.41639 9	Uniform	Uniform	E	E	Ok
68	150	3.5	173.766 3	1.76709 6	Partial	Partial	E	E	Ok
69	60	0	341.447 7	1.73532 9	Partial	Partial	E	E	Ok
70	60	0	363.004	1.96708	Uniform	Uniform	E	E	Ok
71	150	2	236.170	1.65202	Partial	Partial	E	E	Ok
72	150	0	339.345	1.75732	Partial	Partial	E	E	Ok
73	150	0	379.753 3	2.03304 6	Uniform	Uniform	E	E	Ok
74	150	0.5	312.879	1.73199	Partial	Partial	E	E	Ok
75	150	0.7	353.857 5	2.02510 2	Uniform	Uniform	E	E	Ok

The faulty cases are highlighted in yellow.

Table 5-7 summarizes the results of the testing cases.

Table 5-7 Summary for test results

Description	Quantity	Percentage
Total Number of Cases	75	100%
Total Successfully Type Detected Cases	73	97.3%
Total Successfully Class Detected Cases	71	94.7%
Total Successfully Detected Cases	71	94.7%

The simulation results indicated that the trained neural network is capable to detect the demagnetization faults with an overall performance of 94.7%.

CHAPTER SIX

CONCLUSIONS AND FUTURE WORK

6.1 Conclusions

To the best knowledge of the researcher, this is the first reported work on demagnetization faults which identifies the type and the class together. Also it is the first reported work on FEM using JMAG-Designer software for LSPMSM for healthy and demagnetized conditions.

This work proposes a neural based detection technique of demagnetization faults.

Thesis findings and conclusions can be summarized as follows:

- A comprehensive literature review has been accomplished on the demagnetization fault, covering both permanent magnet synchronous motors PMSM and Line Start Permanent Magnet Synchronous Motors LSPMSM. The investigations on the demagnetization faults in LSPMS motor are still premature.
- The mathematical model is developed for healthy conditions and simulated using MATLAB SIMULINK™.
- The developed mathematical model for healthy case is verified by the FEM model created using JMAG™ software. The model considers all the geometric complexities provided in the motor datasheets. Both models show very good agreement in terms of simulated results.

- The effect of demagnetization has been evaluated under different operating conditions. The motor line current and speed characteristics were discussed and their behavior was explained. The level of demagnetization considered in the simulation varied from 0% to 90%.
- A neural-based detection method of demagnetization faults is proposed utilizing the motor stator current and supply voltage. Instantaneous power is found to be the most useful feature source. Fourier transform is taken for the power signal and the selected feature was the difference between the 2nd and DC harmonic component. The detection accuracy is found to be 94.7%

6.2 Recommendations for Future Work

- To use 3D model instead of 2D model to account for end winding effect and take more accurate consideration for end rings.
- To use optimization technique in finding the optimal solution for the ANN instead of trial and error technique.
- To study the developed technique in presence of other failures in the motor like eccentricity, broken bars and short circuit.

References

- [1] S. Kahourzade, A. Mahmoudi, W. P. Hew and M. N. Uddin, "Design and performance improvement of a line-start PMSM," 2013 IEEE Energy Conversion Congress and Exposition, Denver, CO, 2013, pp. 5042-5047
- [2] Guang Yang, J. Ma, Jian-Xin Shen and Yu Wang, "Optimal design and experimental verification of a line-start permanent magnet synchronous motor," 2008 International Conference on Electrical Machines and Systems, Wuhan, 2008, pp. 3232-3236.
- [3] Li, Jian, Jungtae Song, and Yunhyun Cho. "High performance line start permanent magnet synchronous motor for pumping system." Industrial Electronics (ISIE), 2010 IEEE International Symposium on. IEEE, 2010.
- [4] Isfahani, Arash Hassanpour, and Sadegh Vaez-Zadeh. "Line start permanent magnet synchronous motors: Challenges and opportunities." *Energy* 34.11 (2009): 1755-1763.
- [5] Libert, F., J. Soulard, and J. Engstrom. "Design of a 4-pole line start permanent magnet synchronous motor." ICEM, 2002.
- [6] Sorgdrager, A. J., A. J. Grobler, and R. J. Wang. "Design procedure of a line-start permanent magnet synchronous machine." (2014).
- [7] Ong, Chee-Mun. "Dynamic simulation of electric machinery: using MATLAB/SIMULINK", Prentice Hall, p 309-310, 1998.
- [8] K. J. Binns, "Permanent magnet machines with line start capabilities: their design and application," IEE Colloquium on Permanent Magnet Machines and Drives, London, 1993, pp. 5/1-5/5.
- [9] Hanselman, Duane C., "Brushless permanent magnet motor design", The Writers' Collective, 2nd ed, p 36, 2003.
- [10] Ong, Chee-Mun., "Dynamic simulation of electric machinery: using MATLAB/SIMULINK", Prentice Hall, p 42-43, 1998.
- [11] Cullity, Bernard Dennis, and Chad D., "Graham. Introduction to magnetic materials", John Wiley & Sons, 2011.
- [12] Sjökvist, Stefan, "Demagnetization Studies on Permanent Magnets: Comparing FEM Simulations with Experiments", Diss. Acta Universitatis Upsaliensis, 2014.

- [13] Xiaomin Lu, "Dual Benefits of Adding Damper Bars in PMSMs for Electrified Vehicles: Improved Machine Dynamics and Simplified Integrated Charging", University of Windsor (2014).
- [14] Maraaba, L. S., Z. M. Al-Hamouz, and M. A. Abido. "Modeling and simulation of line start permanent magnet synchronous motors with asymmetrical stator windings." Industrial Electronics Society, IECON 2016-42nd Annual Conference of the IEEE. IEEE, 2016.
- [15] Jedryczka, Cezary, Rafal Marek Wojciechowski, and Andrzej Demenko. "Influence of squirrel cage geometry on the synchronisation of the line start permanent magnet synchronous motor." IET Science, Measurement & Technology 9.2 (2014): 197-203.
- [16] R. T. Ugale and B. N. Chaudhari, "A new rotor structure for line start permanent magnet synchronous motor," 2013 International Electric Machines & Drives Conference, Chicago, IL, 2013, pp. 1436-1442.
- [17] Y. Bao, W. Mehmood and X. Feng, "Super premium efficiency Line Start Permanent Magnet Synchronous Motor: Design, test and comparison," 2012 Petroleum and Chemical Industry Conference (PCIC), Chicago, IL, 2012, pp. 1-7.
- [18] S. Nedelcu, T. Tudorache and C. Ghita, "Influence of design parameters on a line start permanent magnet machine characteristics," 2012 13th International Conference on Optimization of Electrical and Electronic Equipment (OPTIM), Brasov, 2012, pp. 565-571.
- [19] W. Lu, M. Liu, Y. Luo and Y. Liu, "Influencing factors on the demagnetization of line-start permanent magnet synchronous motor during its starting process," 2011 International Conference on Electrical Machines and Systems, Beijing, 2011, pp. 1-4.
- [20] B. M. Dinh and H. M. Tien, "Maximum efficiency design of line start permanent magnet synchronous motor," 2016 IEEE International Conference on Sustainable Energy Technologies (ICSET), Hanoi, 2016, pp. 350-354.
- [21] Zawilak, T., and M. Gwozdziewicz. "Limitation of higher harmonics in line start permanent magnet synchronous motor by star-delta mixed stator winding." (2011): 76-77.

- [22] R. T. Ugale, G. Singh, S. Baka and B. N. Chaudhari, "Effective energy conservation for the agricultural sector using line start permanent magnet synchronous motors," TENCON 2009 - 2009 IEEE Region 10 Conference, Singapore, 2009, pp. 1-5.
- [23] W. Fei, P. C. K. Luk, J. Ma, J. X. Shen and G. Yang, "A High-Performance Line-Start Permanent Magnet Synchronous Motor Amended From a Small Industrial Three-Phase Induction Motor," in IEEE Transactions on Magnetics, vol. 45, no. 10, pp. 4724-4727, Oct. 2009.
- [24] R. T. Ugale, A. Bhanuji and B. N. Chaudhari, "A novel line start permanent magnet synchronous motor using two-part rotor," TENCON 2009 - 2009 IEEE Region 10 Conference, Singapore, 2009, pp. 1-5.
- [25] R. T. Ugale and B. N. Chaudhari, "Rotor Configurations for Improved Starting and Synchronous Performance of Line Start Permanent-Magnet Synchronous Motor," in IEEE Transactions on Industrial Electronics, vol. 64, no. 1, pp. 138-148, Jan. 2017.
- [26] X. Tang and X. Wang, "Calculation of magnets' average operating point during the starting process of line-start permanent magnet synchronous motor," 2014 17th International Conference on Electrical Machines and Systems (ICEMS), Hangzhou, 2014, pp. 2147-2150.
- [27] A. Takahashi, S. Kikuchi, H. Mikami, K. Ide and A. Binder, "d-q Space vector analysis for line-starting permanent magnet synchronous motors," 2012 XXth International Conference on Electrical Machines, Marseille, 2012, pp. 136-142.
- [28] B. Štumberger, T. Marčič, G. Štumberger, M. Hadžiselimović and M. Trlep, "Evaluation of line-start interior permanent magnet synchronous motor model parameters using finite elements," Digests of the 2010 14th Biennial IEEE Conference on Electromagnetic Field Computation, Chicago, IL, 2010, pp. 1-1.
- [29] Qing Zhao, Xiulian Wang, Shenbo Yu, Dong Zhang, Zhongliang An and Renyuan Tang, "Study and design for large line-start permanent magnet synchronous motors," Sixth International Conference on Electrical Machines and Systems, 2003. ICEMS 2003., Beijing, China, 2003, pp. 132-133 vol.1.
- [30] Krause, Paul C., et al. "Analysis of electric machinery and drive systems". Vol. 75. John Wiley & Sons, 2013.
- [31] Liu, Li, and Emmanuel Collins. "Robust fault detection and diagnosis for permanent magnet synchronous motors." Florida State University (2006).

- [32] JMAG Application Note –“Demagnetization Analysis of an SPM Motor” through [https://www.jmag-international.com/catalog/34_SPMMotor_Demagnetization.html] accessed March 24, 2017.
- [33] M. R. Mehrjou, N. Mariun, M. Karami, N. Misron and M. A. M. Radzi, "Performance analysis of line-start permanent magnet synchronous motor in presence of rotor fault," 2014 IEEE Student Conference on Research and Development, Batu Ferringhi, 2014, pp. 1-4.
- [34] H. P. Nee, L. Lefevre, P. Thelin and J. Soulard, "Determination of d and q reactances of permanent-magnet synchronous motors without measurements of the rotor position," in IEEE Transactions on Industry Applications, vol. 36, no. 5, pp. 1330-1335, Sep/Oct 2000.
- [35] X. Lu, K. L. V. Iyer, K. Mukherjee and N. C. Kar, "Development of a Novel Magnetic Circuit Model for Design of Premium Efficiency Three-Phase Line Start Permanent Magnet Machines With Improved Starting Performance," in IEEE Transactions on Magnetics, vol. 49, no. 7, pp. 3965-3968, July 2013.
- [36] V. Elistratova, M. Hecquet, P. Brochet, D. Vizireanu and M. Dessoude, "Analytical approach for optimal design of a line-start internal permanent magnet synchronous motor," 2013 15th European Conference on Power Electronics and Applications (EPE), Lille, 2013, pp. 1-7.
- [37] MA Cruz, AJ Marques Cardoso, S. "Rotor cage fault diagnosis in three-phase induction motors by extended Park's vector approach." *Electric Machines & Power Systems* 28.4 (2000): 289-299.
- [38] Wenxin Liu, Li Liu, Il-Yop Chung, David A. Cartes, Wei Zhang, “Modeling and detecting the stator winding fault of permanent magnet synchronous motors”, *Simulation Modelling Practice and Theory*, Volume 27, September 2012, Pages 1-16, ISSN 1569-190X,
- [39] Jawad Ahmed, F., Tsarafidy, R., Abdesslem, D., & Abdellatif, M. (2008). “Modelling and simulation of stator winding inter-turn faults in permanent magnet synchronous motors”, *COMPEL - The international journal for computation and mathematics in electrical and electronic engineering*, 27(4), 887-896.
- [40] Kawady, T. A., Afify, A. A., Osheiba, A. M., & Taalab, A. I. (2009). “Modeling and Experimental Investigation of Stator Winding Faults in Induction Motors”, *Electric Power Components and Systems*, 37(6), 599-611.

- [41] R. M. Tallam, T. G. Habetler and R. G. Harley, "Transient model for induction machines with stator winding turn faults," in IEEE Transactions on Industry Applications, vol. 38, no. 3, pp. 632-637, May/Jun 2002.
- [42] Sang Bin Lee, K. Younsi and G. B. Kliman, "An online technique for monitoring the insulation condition of AC machine stator windings," in IEEE Transactions on Energy Conversion, vol. 20, no. 4, pp. 737-745, Dec. 2005.
- [43] Singh, Arvind, et al. "A review of induction motor fault modeling." *Electric Power Systems Research* 133 (2016): 191-197.
- [44] Arkan, M., D. Kostic-Perovic, and P. J. Unsworth. "Modelling and simulation of induction motors with inter-turn faults for diagnostics." *Electric Power Systems Research* 75.1 (2005): 57-66.
- [45] Thomson, William T., and Ronald J. Gilmore. "Motor current signature analysis to detect faults in induction motor drives—fundamentals, data interpretation, and industrial case histories." *Proceedings of 32nd Turbo machinery Symposium*, A&M University, Texas, USA. 2003.
- [46] Khalid L Barad'ieh. "A linear algebraic based diagnosis method for broken rotor bars of line start permanent magnet synchronous motors", KFUPM, 2016.
- [47] Ibrahim Mahmoud Hussein, "A novel method for detecting eccentricity in line start permanent magnet synchronous motors", KFUPM, 2017
- [48] H. A. Toliyat, M. S. Arefeen and A. G. Parlos, "A method for dynamic simulation of air-gap eccentricity in induction machines," in IEEE Transactions on Industry Applications, vol. 32, no. 4, pp. 910-918, Jul/Aug 1996.
- [49] C. A. Lopez, A. S. Babel and E. G. Strangas, "Detecting uniform and partial demagnetization for an interior permanent magnet machine," 2016 XXII International Conference on Electrical Machines (ICEM), Lausanne, 2016, pp. 2874-2880.
- [50] Sara Hamidizadeh, "Study of Magnetic Properties and Demagnetization Models of Permanent Magnets for Electric Vehicles Application", McGill University 2016
- [51] S.S. Moosavi, A. Djerdir, Y.Ait. Amirat, D.A. Khaburi, "Demagnetization fault diagnosis in permanent magnet synchronous motors: A review of the state-of-the-art", *Journal of Magnetism and Magnetic Materials*, Volume 391, 1 October 2015, Pages 203-212, ISSN 0304-8853,

- [52] Ruoho, Sami. "Demagnetisation of permanent magnets in electrical machines." OH presentation, Helsinki University (2006).
- [53] Akar, Mehmet, and Mustafa Eker. "Demagnetization fault diagnosis in permanent magnet synchronous motors." *Przegląd Elektrotechniczny* 89.2a (2013): 229-233.
- [54] Subhadeep Chakraborty, Eric Keller, Asok Ray, Jeffrey Mayer, "Detection and estimation of demagnetization faults in permanent magnet synchronous motors", *Electric Power Systems Research*, Volume 96, March 2013, Pages 225-236, ISSN 0378-7796,
- [55] M. Zhu, W. Hu and N. C. Kar, "Torque-Ripple-Based Interior Permanent-Magnet Synchronous Machine Rotor Demagnetization Fault Detection and Current Regulation," in *IEEE Transactions on Industry Applications*, vol. 53, no. 3, pp. 2795-2804, May-June 2017.
- [56] Li, Guang-Jin, and Zi-Qiang Zhu. "Demagnetization of modular surface mounted permanent magnet machines." *Electrical Machines (ICEM)*, 2016 XXII International Conference on. IEEE, 2016.
- [57] J. C. Urresty, J. R. Riba, M. Delgado and L. Romeral, "Detection of Demagnetization Faults in Surface-Mounted Permanent Magnet Synchronous Motors by Means of the Zero-Sequence Voltage Component," in *IEEE Transactions on Energy Conversion*, vol. 27, no. 1, pp. 42-51, March 2012.
- [58] T. H. Akinaga, T. Staudt, P. Ely da Silva and A. A. Espindola, "FEA-based method for estimating PM demagnetization in electrical motor design: Development and experimental validation," 2016 XXII International Conference on Electrical Machines (ICEM), Lausanne, 2016, pp. 1749-1755.
- [59] J. H. Yoo, C. s. Park and T. U. Jung, "Demagnetization diagnosis of permanent magnet synchronous motor by using continuous wavelet transform," 2015 18th International Conference on Electrical Machines and Systems (ICEMS), Pattaya, 2015, pp. 1486-1489.
- [60] S. S. Moosavi, A. Djerdir, Y. A. Amirat and D. A. Khaburi, "Demagnetization fault investigation in permanent magnet synchronous motor," *The 5th Annual International Power Electronics, Drive Systems and Technologies Conference (PEDSTC 2014)*, Tehran, 2014, pp. 617-623.
- [61] J. D. McFarland and T. M. Jahns, "Investigation of the Rotor Demagnetization Characteristics of Interior PM Synchronous Machines During Fault Conditions," in *IEEE Transactions on Industry Applications*, vol. 50, no. 4, pp. 2768-2775, July-Aug. 2014.

- [62] W. f. Lu, H. s. Zhao and S. Liu, "Demagnetization conditions comparison for line-start permanent magnet synchronous motors," 2014 17th International Conference on Electrical Machines and Systems (ICEMS), Hangzhou, 2014, pp. 48-52.
- [63] X. Tang and X. Wang, "Research of the demagnetization mechanism of line-start permanent magnet synchronous motor under operating condition of sudden reversal," 2014 17th International Conference on Electrical Machines and Systems (ICEMS), Hangzhou, 2014, pp. 1981-1984.
- [64] J. X. Shen, P. Li, M. J. Jin and G. Yang, "Investigation and Countermeasures for Demagnetization in Line Start Permanent Magnet Synchronous Motors," in IEEE Transactions on Magnetics, vol. 49, no. 7, pp. 4068-4071, July 2013.
- [65] X. Tang, X. Wang, G. Li and M. Tian, "Demagnetization study of line-start permanent magnet synchronous motor under out-of-step and supersynchronous faults," 2016 IEEE 11th Conference on Industrial Electronics and Applications (ICIEA), Hefei, 2016, pp. 1496-1501.
- [66] X. Lu, K. L. V. Iyer, K. Mukherjee and N. C. Kar, "Study and detection of demagnetization in line start permanent magnet synchronous machines using artificial neural network," 2012 15th International Conference on Electrical Machines and Systems (ICEMS), Sapporo, 2012, pp. 1-6.
- [67] M. Seera, C. P. Lim, D. Ishak and H. Singh, "Fault Detection and Diagnosis of Induction Motors Using Motor Current Signature Analysis and a Hybrid FMM–CART Model," in IEEE Transactions on Neural Networks and Learning Systems, vol. 23, no. 1, pp. 97-108, Jan. 2012.
- [68] J. Faiz and H. Nejadi-Koti, "Demagnetization Fault Indexes in Permanent Magnet Synchronous Motors—An Overview," in IEEE Transactions on Magnetics, vol. 52, no. 4, pp. 1-11, April 2016.
- [69] J. Braun and M. Doppelbauer, "Protection against demagnetization with rotor coils for permanent magnet synchronous machines," 2016 XXII International Conference on Electrical Machines (ICEM), Lausanne, 2016, pp. 550-556.
- [70] Nathaniel Taylor, "Network Effects Of Line Start Permanent Magnet Synchronous Motors As Replacements For Induction Motors", Royal Institute Of Technology 2001.
- [71] Behbahanifard, Hamidreza, and Alireza Sadoughi. "Line Start Permanent Magnet Synchronous Motor Performance and Design; a Review." Journal of World's Electrical Engineering and Technology 2322 (2015): 5114.

- [72] Rojas, Raul, “*Neural networks, a systematic introduction*”, Springer, 1996.
- [73] B. Krose and P. Van Der Smagt, “*Introduction to neural networks*”. University of Amsterdam, 1996.
- [74] R. May, G. Dandy, and H. Maier, “Review of input variable selection methods for artificial neural networks,” *Artificial Neural Networks - Methodological Advances and Biomedical Applications*, vol. 2, no. August 2016, pp. 362–376, 2011.
- [75] B. Chebel-Morello, S. Malinowski, and H. Senoussi, “Feature selection for fault detection systems: application to the Tennessee Eastman process,” *Applied Intelligence, Springer Verlag (Germany)*, vol. 44, no. 1, pp. 111–122, 2016.
- [76] G. P. Zhang, "Neural networks for classification: a survey," in *IEEE Transactions on Systems, Man, and Cybernetics, Part C (Applications and Reviews)*, vol. 30, no. 4, pp. 451-462, Nov 2000.
- [77] Soreshjani, Mohsen Hosseinzadeh, and Alireza Sadoughi. "Conceptual comparison of Line-Start Permanent Magnet Synchronous and Induction Machines for Line-fed of different conditions." *Journal of World's Electrical Engineering and Technology* 2322 (2014): 5114.
- [78] Sadiku, Matthew NO. "Numerical techniques in electromagnetics", second edition, CRC Press (2000).
- [79] V. N. Ghate and S. V. Dudul, “Cascade neural-network-based fault classifier for three-phase induction motor,” *IEEE Transactions on Industrial Electronics*, vol. 58, no. 5, pp. 1555–1563, 2011

APPENDICES

Appendix A MOTOR PARAMETERS

A.1 Dimensions of LSPMS Motor

The detailed geometry model of the LSPMS motor and the winding diagram are shown in figure A.1.

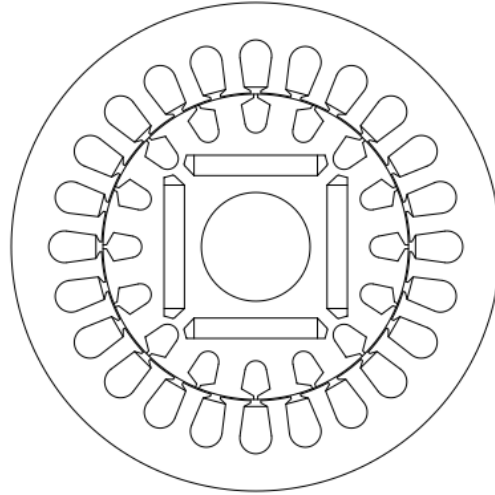


Figure A-1Geometry model of LSPMS motor.

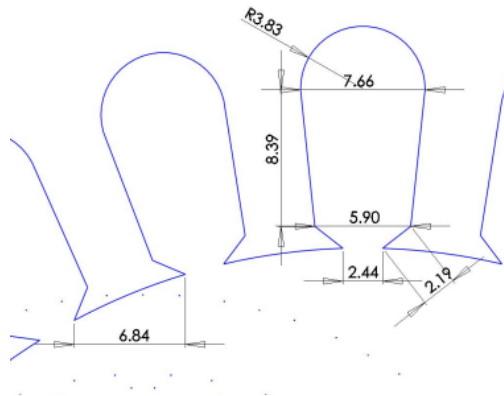


Figure A2: Dimensions of the stator slot.

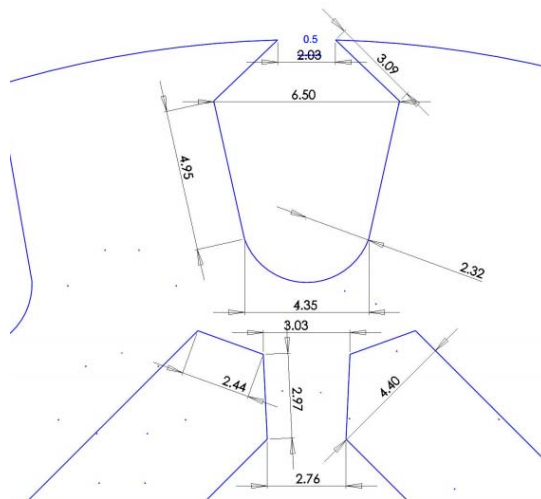


Figure A3 Dimensions of the rotor slot

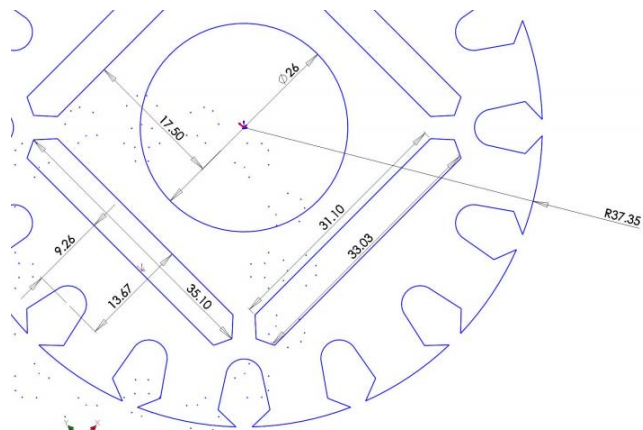


Figure A4: Dimensions of the rotor and the magnets.

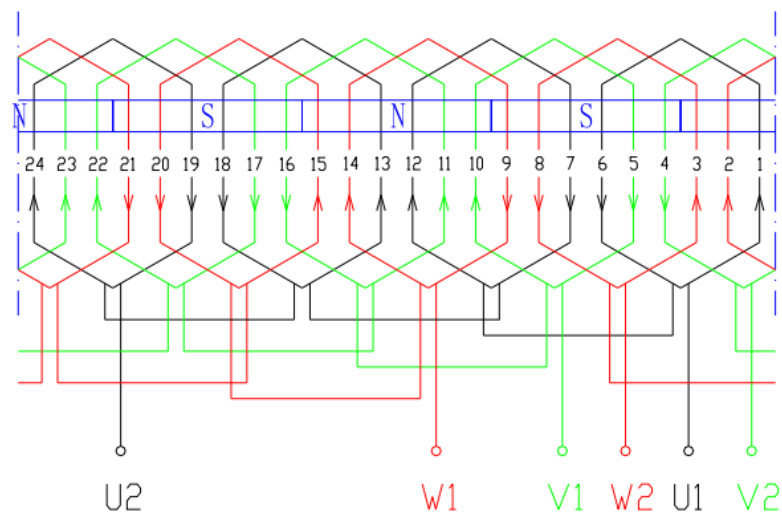


Figure A5: Stator winding diagram.

A.2 Magnets Datasheet



Recoma 24HE

Recoma® Sintered Samarium Cobalt Magnets

These are also referred to as Rare Earth or SmCo magnets. They offer a combination of high magnetic output, excellent temperature stability and moderate corrosion resistance. Please contact Arnold for additional grade information and recommendations for protective coating. Assemblies using these magnets can also be provided.

	Characteristic	Units	min.	nominal
Magnetic Properties	Br , Residual Induction	Gauss	9,700	10,200
		Tesla	0.97	1.02
	H_{cB} , Coercivity	Oersteds	8,900	9,600
		kA/m	715	765
	H_{cJ} , Intrinsic Coercivity	Oersteds	19,000	25,000
		kA/m	1,500	2,000
	BHmax , Maximum Energy Product	MGOe	22	25
		kJ/m ³	175	195

	Characteristic	Units	C //	C ⊥
Thermal Properties	Reversible Temperature Coefficients ⁽¹⁾			
	of Induction, α(Br)	%/°C		-0.035
	of Coercivity, α(H _{cj})	%/°C		-0.212
	Coefficient of Thermal Expansion ⁽²⁾	ΔL/L per °C x 10 ⁻⁶	11	13
	Thermal Conductivity	kcal/mh°C		10
	Specific Heat ⁽³⁾	cal/g°C		350
	Max. Recommended Use Temperature	°C		350
Other Properties	Curie Temperature, T _c	°C		825
	Flexural Strength	psi		17,400
		MPa		120
	Compressive Strength	psi		116,000
		MPa		800
	Young's Modulus	GPa		140
	Density	g/cm ³		8.4
	Hardness, Vickers	Hv		600
	Electrical Resistivity, ρ	μΩ • cm		90

Notes: (1) Coefficients measured between 20 and 150 °C
(2) Between 20 and 200 °C (3) Between 20 and 150 °C

Appendix B JMAG-DESIGNER VERSION 16

JMAG is an electromagnetic simulation program developed by JSOL corporation. JMAG provide a 2D/3D platform to construct the motor model. Material properties can be assigned to each part in the model. JMAG consists of material library based on commercial and industrial materials. Material properties and names are depicted from the manufacturers data sheets and brochures. Additional materials can be easily added with complete mechanical, electrical and magnetic properties. Also the available material can be customized based on the application.

JMAG software includes JMAG-EXPRESS, JMAG-DESIGNER, and JMAG-RT. The level of problem complexity decides the software package to be used. JMAG EXPRESS contains some common motor templates which can be used to generate basic characteristics. JMAG DESIGNER is considered to be the core program in the JMAG software environment and will be used in this thesis. It allows a 2D and 3D electromechanical finite element analysis and design with numerous analysis tools such as parametric analysis, optimization, and scripting.

JMAG software package supports users in developing and designing electronic and electric equipment such as motors, actuators, circuit components, and antennae. JMAG performs the following analytic functions:

- Magnetic field analysis
- Thermal analysis
- Structural analysis
- Electric field analysis
- Thermal stress analysis.

JMAG also perform the coupled analyses listed below by combining the above functions:

- Magnetic field and thermal analyses
- Magnetic field and structural analyses
- Magnetic field and thermal stress analyses
- Thermal and electric field analyses
- Thermal and structural analyses.

The analysis process in JMAG runs through the flow chart in figure B-1.



Figure B-1 JMAG Work Process Flowchart

Create Geometry

There are two types of geometry in JMAG: Full geometry and Partial geometry. In full geometry, the complete details will be clear with all dimensions. However, in partial geometry, only part of geometry will be presented. JMAG-Designer automatically convert the model from partial to full by adjusting few settings and parameters. The goal of having partial model is to reduce the required time and efforts in creating the geometry. The size of the partial model can be decided based on the smallest typical portion of the geometry. There are three methods to create the geometry in JMAG:

- 1- Through JMAG Designer Geometry Editor.
- 2- Through external CAD software like AutoCAD, SolidWorks, Solid Edge, CATIA, Pro Engineer, Parasolid, 3D IGES, NX, STEP,...etc.
- 3- Through JMAG Express software for some preconfigured motors.

Figure B-2 shown JMAG-Designer application interface. From the project manager panel, with right click on the project after saving the project, select “Geometry Editor” and chose one of the two options. If there is any existing geometry through the above-mentioned softwares, then the geometry can be imported to the project by selecting the “import” choice. Another way is to use JMAG Designer Geometry Editor to create the geometry. The third option is to use JMAG Express to create the geometry based on pre-configured adjustable motor models. Selecting the most appropriate method depends on the available data and geometry complexity.

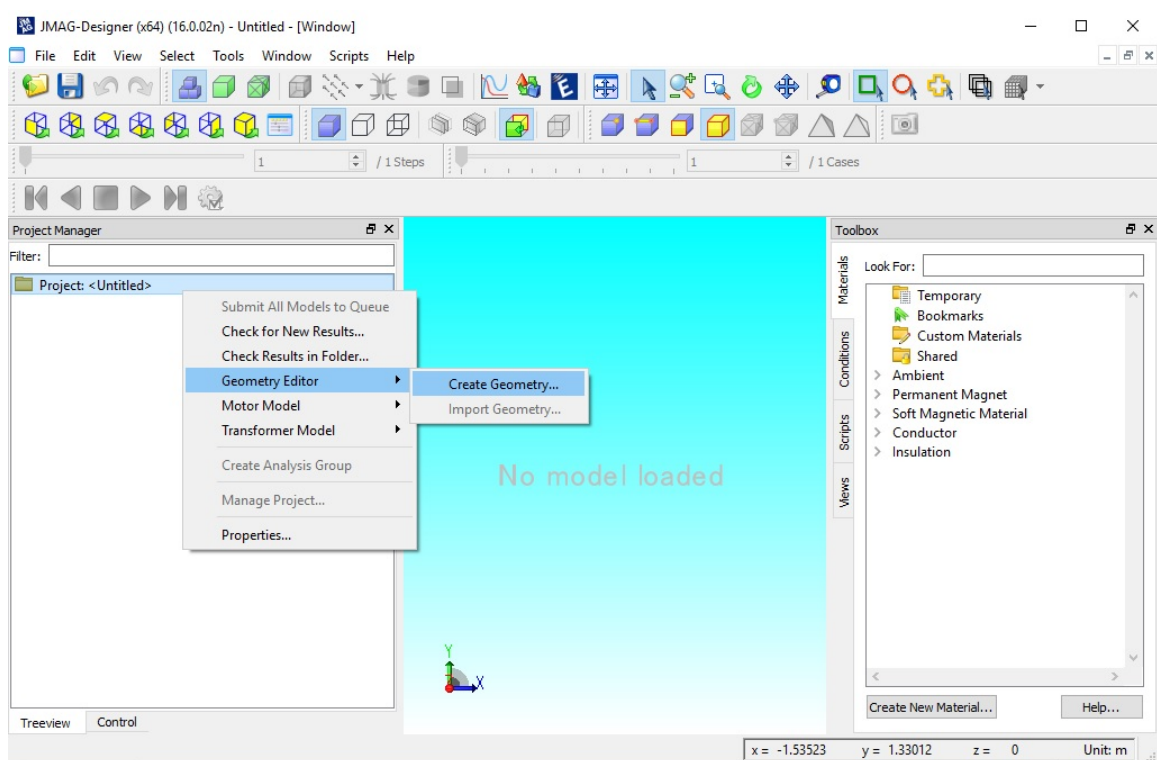


Figure B-2 JMAG-Designer Application Interface

JMAG-Designer Geometry Editor

Figure B-3 shows JAMG-Designer Geometry Editor 16.0 build date 2/02/2017, which is 2D/3D software. The work starts by selecting the plane of geometry and then “create sketch”. The LSPMSM consists of two main set parts, which are Rotor and Stator.

Each of the main parts can be drawn separately. A point worth to be mentioned, the sketch center shall be located at (0,0) and the units shall be chosen to match the available data.

The restrictions and complexity of creating the geometry, depends on the goal from creating the model. In case a solid model is being implemented to measure the performance of that model, then normal CAD geometry processes are adopted. However, in case the goal is to obtain an optimized model depends on the motor dimensions, then the sketch shall contain conditions and constraints to be used in parametric simulations.

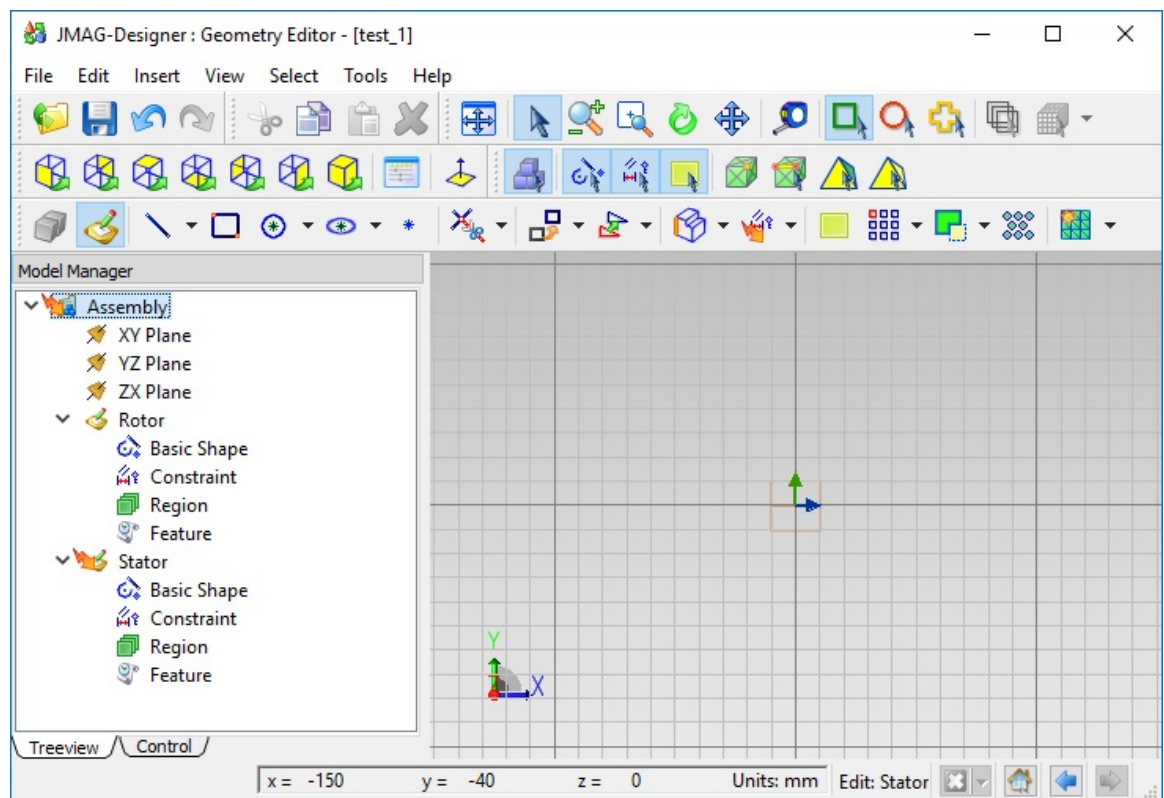


Figure B-3 JMAG-Designer Geometry Editor

Figure B-4 shows the flow chart for creating 2D geometry in JMAG-Designer Geometry Editor.

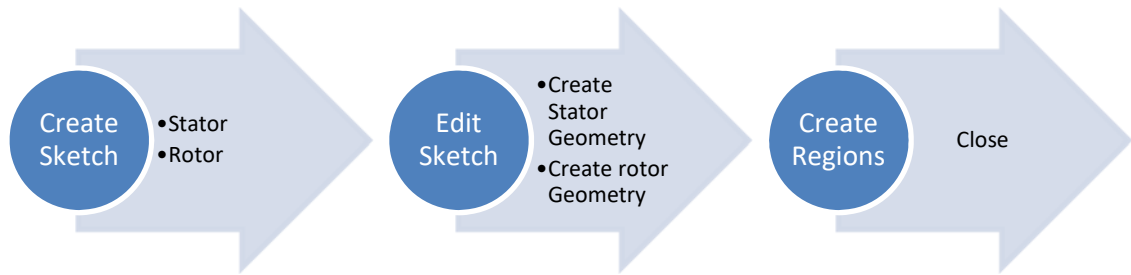


Figure B-4 Processes for creating 2D geometry in JMAG-Designer Editor

The regions represents motor parts like coils, stator core, rotor core, rotor bars, magnets, demagnetization barriers, ...etc.

Creating geometry through JMAG Express

JMAG-Express is a tool designed to create and analyze 2D motor models. It is fast and efficient software to design the following types of motors:

- Brushless Motor (IPM)
- Brushless Motor (SPM)
- Brushless Motor (Outer Rotor/IPM)
- Brushless Motor (Outer Rotor/SPM)
- Three-phase Induction Motor
- Single-phase Induction Motor
- Switched Reluctance Motor
- Brush Motor
- Externally Excited Synchronous Machine
- Wound-Field AC Synchronous Machine

- Universal Motor

The motor model can be created using JMAG-Express, and then exported to JMAG-Designer and do the detail design and conduct the analysis. Starting the design through JMAG-Express will save time and efforts. But unfortunately, LSPMSM is not yet supported and need some more works to create an initial model for that motor and then export the model to JMAG-Designer.

Create Geometry through External CAD Software

JMAG-Designer can import geometry from external CAD software like AutoCAD, SolidWorks, Solid Edge, CATIA, Pro Engineer, Parasolid, 3D IGES, NX and STEP. It depends on the user experience which CAD software he used to work with and depend on the complexity of the geometry of the motor.

JMAG can handle 2D and 3D geometry. While 3D model gives more accurate results, 2D model is much simpler and faster.

Create Study

The next step after getting the geometry ready is to create study. Selecting the study type depends on the type of analysis and the required data from simulation. The following studies are available in JMAG-Designer:

1- Magnetic field analysis:

- a. Static analysis: A magnetic field analysis (static analysis) is used when an analysis target does not have time-varying phenomena such as motion and current variations.
- b. Transient analysis: A magnetic field analysis (transient response analysis) is used when an analysis target has time-varying phenomena such as motion and current variations.

- c. Frequency analysis: A magnetic field analysis (frequency response analysis) is used when the current (voltage) varies sinusoidally with time at a single frequency.

2- Thermal analysis:

- a. Steady state analysis (3D): A thermal analysis (steady state analysis) is used when the temperature distribution does not vary with time.
- b. Transient state analysis (3D): A thermal analysis (transient state analysis) is used when the temperature distribution varies with time.

3- Structural analysis:

- a. Static analysis: A structural analysis (static analysis) is used to analyze the displacement and stress when a constant static load is applied.
- b. Frequency analysis: A structural analysis (frequency response analysis) is used to analyze the response of a structure that is constantly vibrated.
- c. Transient analysis: A structural analysis is run when obtaining displacement or stress specified with load that changes size in time.

The activated features/studies in JMAG-Designer depends on the purchased modules. User can decide which modules should be purchased based on the application, machine, required analysis, analysis speed, doing calculation on several machines, number of licenses and availability of maintenance services.

The flow chart in figure B-5 shows the processes of creating new study.

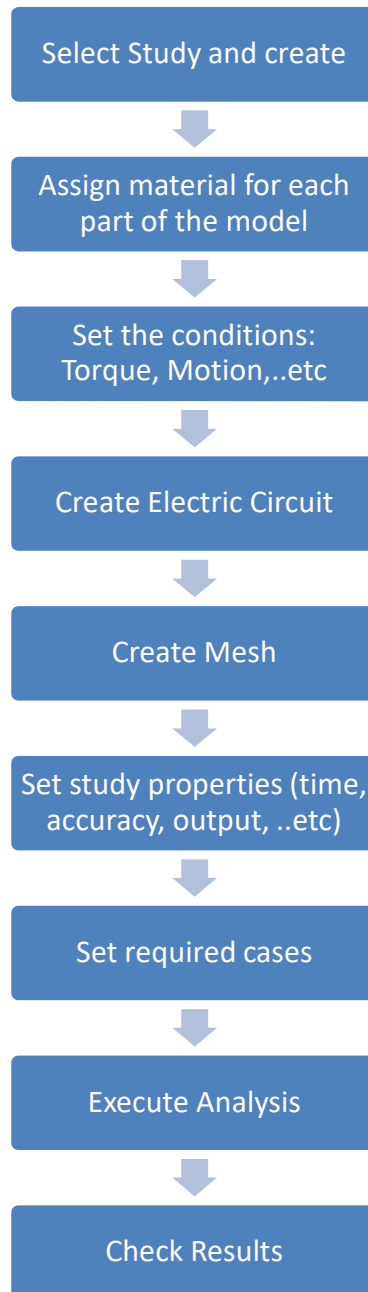


Figure B-5 Flow chart for creating study

Select Study

In our case, we are looking for magnet analysis – transient study as we have current varying in rotating machine.

Assign Material for Each Part

Different material types exist under the Toolbox in the most right side of JMAG interface. Table B-1 summaries the material and its use.

Table B-1 List of Material Groups in JMAG-Designer

Sr #	Material	Description
1	Ambient	Consists of “Air” only
2	Permanent Magnet	Consists of all known types of permanent magnets with manufacturer model number.
3	Soft Magnetic Material	Consist of material of stator core, rotor core, shaft and yoke.
4	Conductor	Consists of Aluminum and Copper for the winding, conductors and cage bars.
5	Insulation	Consists of plastic as insulation material.
6	Custom Material	Any material not available in the JMAG-Designer library can be created using the manufacturer technical properties (Electrical, Mechanical , Thermal)

Assigning the material to the parts is done by dragging the required material and drop the selection on the part on the geometry. Then customize the material properties as required. Table B-2 shows sample of selected material for LSPMSM.

Table B-2 Sample of LSPMSM Assigned Material

Sr #	Part	Material Group	Manufacturer	Selected Model
1	Shaft	Soft Magnetic Material: Steel for Structure	JSOL	S45C
2	Rotor Core	Soft Magnetic Material: Steel Sheet	JFE Steel	50JN600
3	Rotor Magnet	Permanent Magnet Sintered NdFeB	Arnold	Reversible N30AH
4	Magnet Barriers	Insulation	-	Plastic
5	Rotor Bars	Conductors	JSOL	Aluminium
6	Stator Core	Soft Magnetic Material: Steel Sheet	JFE Steel	50JN600
7	Stator Winding	Conductors	JSOL	Copper

Assigning Conditions

Figure B-6 shows the conditions list available in JMAG-Designer Version 16. The use of each condition depends on the application, the geometry and required analysis.

For our case of full model motors, we use the following: Symmetry and Slide boundary, FEM coil for windings, FEM conductor for rotor bars, rotation Motion and Nodal Force Torque. Table B-3 summarizes the entries in each condition.

Adding a condition is done by dragging the required condition and dropping it on the required part and then adjust the condition settings.

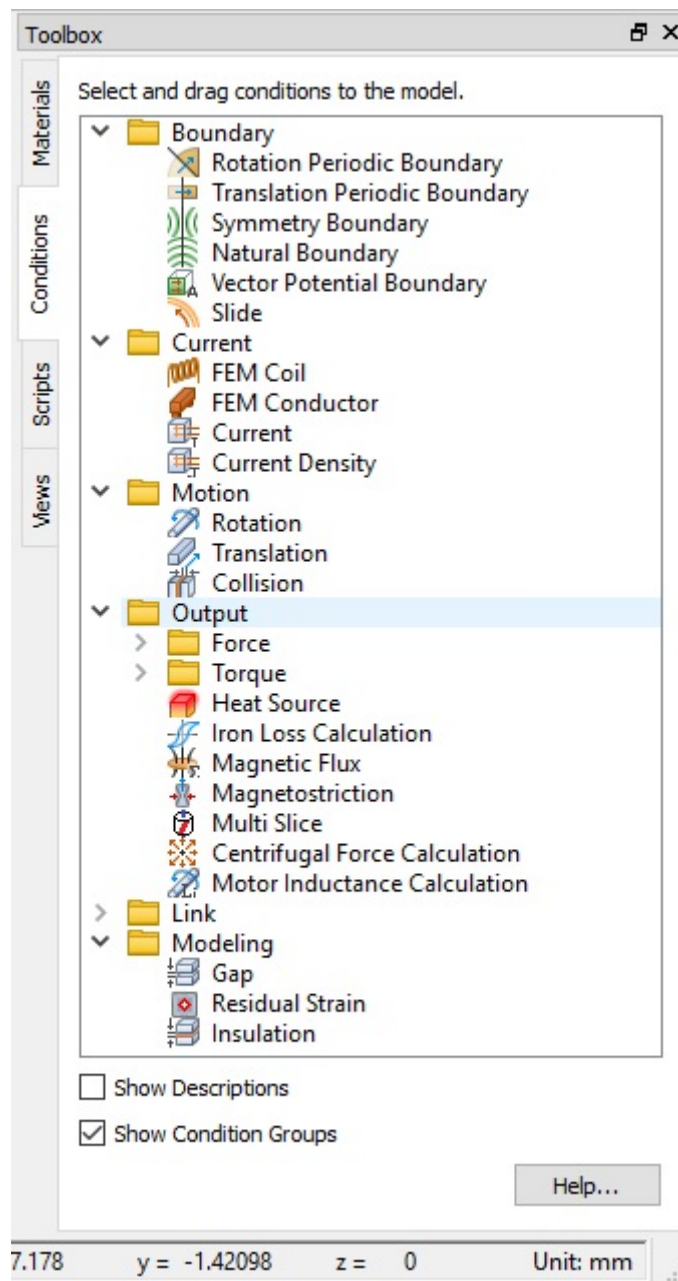


Figure B-6 JMag-Designer conditions list

Table B-3 Summary of conditions

Sr#	Condition	Part	Settings
1	FEM coil	Stator Coils	There will be three FEM coils, each of them consists of the coils per phase
2	FEM conductor	Rotor Bars	Group of rotor bars
3	Nodal Force Torque	Rotating Parts	Assigned on all rotation parts. Specify the positive torque direction.
4	rotation Motion	Rotating Parts (rotor core, shaft, magnets, rotor bars, magnet barriers)	Add all rotating parts. Select “Equation of Motion” Adjust the settings
5	Symmetry boundary	Any edge of the model vertical to the motion rotation	Automatically selected for full model when creating mesh
6	Slide boundary	Any edge of the model vertical to the motion rotation	Automatically selected for full model when creating mesh

Creating the Circuit

The “current” condition should be connected to electrical circuit to specify the electrical properties and parameters of the circuit. Coils, conductors, power supply, type of connections, probes and reference ground point should be clearly identified in the circuit. After creating the circuit, the conditions of FEM coil and FEM conductor shall be updated to connect the physical part with the related part in the circuit. Figure B-7 shows example of circuit for induction motor.

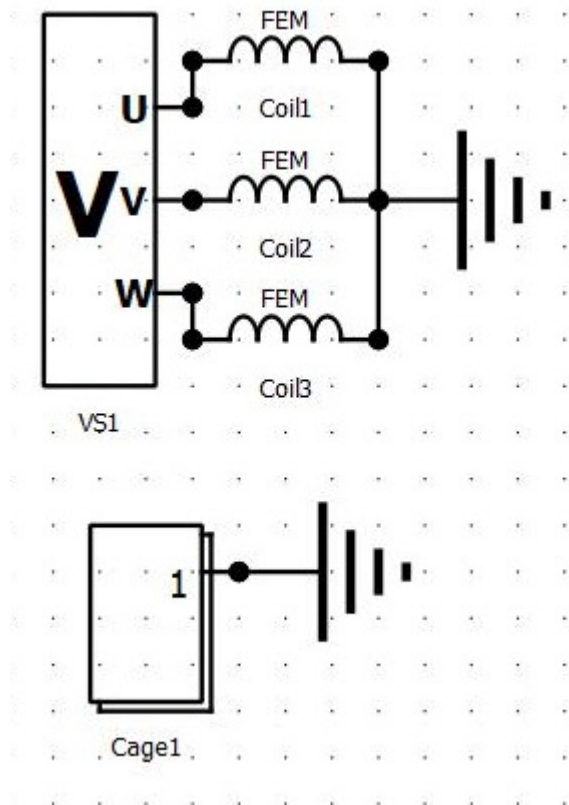


Figure B-7 Circuit of Induction Motor

Create Mesh

The idea of the FEM calculation is directly related to the mesh, which specifies the dimension of the elements in the calculations. The elements size can be set depending on the required accuracy and importance of the area. In addition, it depends on the region dimension where the mesh dimension in specific region should be smaller than the region dimension.

There are two types of meshes: Standard Mesh for non-rotational machines and Slide Mesh for rotating machines. The element size is inversely proportional to the time of simulation, the smaller the element size the simulation time becomes more and more.

Setting Study Properties

After completing the above steps, we need to decide the properties of study. In this field, the required simulation time, accuracy, iteration numbers, convergence rate, method of calculation, acceptable error and control of outputs.

Create Study Cases

Under “Case Control” tap, we can add different scenarios for the simulation by specifying the variable parameters and set different values for these variables. Variables can be material, conditions, circuit parameters, mesh properties and study parameters.

Appendix C Matlab Code for Healthy Case

```

clc
clear all
close all
warning off
NS=344;
Tl=0;
% wrslip0=-1;
wrslip0=0;
lambdads0=0;
lambdadr0=0;
%*****
Vl_rated=400;
P_rated=1;%hp
nm_rated=1800;
f=60;
vm=sqrt(2)*(Vl_rated/sqrt(3));
we=2*pi*f;
p.f=.92;
P=4;
Ns=344;
%%%%%%%%%%%%%%%%%%%%%%%%%%%%%%%%%%%%%%%%%%%%%%%%%%%%%%%%%%%%%%%%%%%%%%%%
delt0=-30*(pi/180); % starting position angle (angle between the q-
axis and a axis

%lambdam=0.591538665; %flux linkage from permanent magnets
lambdam=0.591538665;

j=0.00160119408; % Moment of inertia

rs=5.552724; %stator resistance
ls=0.0222677; % stator leakage inductance
lrd=0.00163515; %% rotor leakage inductance in d axis
lrq=0.00173515; %% rotor leakage inductance in q axis
rd=6.8879;%% rotor resistance in q axis
rq=8.8488;%% rotor resistance in q axis
wb=1;
lmd=.0653759;
lmq=.2736067;
lm=(1/3)*(lmq+lmd);
ldm=(1/3)*(lmq-lmd);

Domega=0;
Tfactor=((3*P)/(4));
%%%resistance calculation%%%%%%%%%%%%%%%%%%%%%%%%%%%%%%%%%%%%%%%%
ld=lmd+ls;
lq=lmq+ls;

b=[lmq+ls 0 lmq 0 ; 0 lmd+ls 0 lmd ; lmq 0 lmq+lrq 0 ; 0 lmd 0
lmd+lrd ];
c=[0 lambdam 0 lambdam ]';
a=inv(b);
d=a*c;
open ('lspmsmsluq.mdl')
sim ('lspmsmsluq.mdl')

```

Appendix D Training Cases

Temp	Load	Power (FFT)	Current RMS	TYPE	CLASS
60	0	336.29497	1.6810263	Partial	A
60	1	254.49287	1.4523811	Partial	A
60	2	208.29896	1.3671121	Partial	A
60	3	152.90377	1.4036881	Partial	A
60	4	106.00726	1.5225695	Partial	A
120	0	342.09034	1.7291323	Partial	A
120	1	266.81942	1.512392	Partial	A
120	2	210.36638	1.4450224	Partial	A
120	3	157.98255	1.4791383	Partial	A
120	4	113.41551	1.5891443	Partial	A
150	0	340.80631	1.7599822	Partial	A
150	1	273.16799	1.5437541	Partial	A
150	2	216.40117	1.4796575	Partial	A
150	3	161.20316	1.5243374	Partial	A
150	4	115.4944	1.6410559	Partial	A
60	0	336.12542	1.6832026	Partial	A
60	1	260.12956	1.4680509	Partial	A
60	2	211.66475	1.3841706	Partial	A
60	3	159.00401	1.417086	Partial	A
60	4	109.69194	1.55214	Partial	A
120	0	337.38063	1.7295734	Partial	A
120	1	270.14333	1.5260055	Partial	A
120	2	213.33798	1.4597741	Partial	A
120	3	161.53551	1.4993216	Partial	A
120	4	117.51893	1.6124578	Partial	A
150	0	342.74225	1.7654069	Partial	A
150	1	273.52954	1.5525183	Partial	A
150	2	217.06028	1.4909822	Partial	A
150	3	164.61196	1.5402068	Partial	A
150	4	118.4804	1.6725603	Partial	A
60	0	336.09168	1.6842589	Partial	B
60	1	261.33361	1.4708868	Partial	B
60	2	211.97676	1.3875977	Partial	B
60	3	160.11764	1.4212537	Partial	B
60	4	110.3107	1.557499	Partial	B
120	0	336.38332	1.7308771	Partial	B
120	1	270.86859	1.5292008	Partial	B
120	2	214.01804	1.4627392	Partial	B
120	3	162.01383	1.504169	Partial	B

120	4	117.99361	1.6196735	Partial	B
150	0	342.69911	1.7643359	Partial	B
150	1	272.812	1.553829	Partial	B
150	2	217.50299	1.4936884	Partial	B
150	3	165.29983	1.5441565	Partial	B
150	4	119.75542	1.6776696	Partial	B
60	0	340.17178	1.7119573	Partial	B
60	1	265.55859	1.4842128	Partial	B
60	2	212.42603	1.4145299	Partial	B
60	3	169.24716	1.4591874	Partial	B
60	4	121.4929	1.5948376	Partial	B
120	0	339.55599	1.757272	Partial	B
120	1	275.48135	1.5548507	Partial	B
120	2	219.72596	1.4934889	Partial	B
120	3	167.81005	1.54095	Partial	B
120	4	127.03039	1.6683138	Partial	B
150	0	340.71262	1.7555964	Partial	B
150	1	271.83318	1.5782718	Partial	B
150	2	219.20903	1.5251312	Partial	B
150	3	171.99326	1.578882	Partial	B
150	4	129.41045	1.7296039	Partial	B
60	0	341.17901	1.7157973	Partial	C
60	1	266.05968	1.486038	Partial	C
60	2	212.5986	1.4174157	Partial	C
60	3	169.99344	1.4628049	Partial	C
60	4	122.83512	1.5991077	Partial	C
120	0	340.02316	1.7593829	Partial	C
120	1	275.92948	1.55737	Partial	C
120	2	220.35884	1.4972841	Partial	C
120	3	168.45448	1.5448996	Partial	C
120	4	127.70247	1.6741828	Partial	C
150	0	340.2354	1.7545548	Partial	C
150	1	271.89273	1.5814209	Partial	C
150	2	219.80052	1.5298076	Partial	C
150	3	172.89729	1.5828405	Partial	C
150	4	130.68125	1.7341235	Partial	C
60	0	346.22635	1.7356055	Partial	C
60	1	266.48584	1.5063772	Partial	C
60	2	214.02627	1.4504686	Partial	C
60	3	175.31056	1.4974239	Partial	C
60	4	135.03338	1.6474139	Partial	C
120	0	343.18605	1.7666871	Partial	C

120	1	277.35746	1.5824047	Partial	C
120	2	225.33274	1.5327047	Partial	C
120	3	176.66129	1.5863103	Partial	C
120	4	136.46782	1.7248953	Partial	C
150	0	337.97353	1.7513457	Partial	C
150	1	275.61432	1.6187967	Partial	C
150	2	223.86244	1.5741563	Partial	C
150	3	180.15264	1.626493	Partial	C
150	4	141.37612	1.7767301	Partial	C
60	0	346.43317	1.7362494	Partial	D
60	1	265.9942	1.5080566	Partial	D
60	2	214.46996	1.4541391	Partial	D
60	3	175.9387	1.500676	Partial	D
60	4	135.95219	1.6529339	Partial	D
120	0	343.0308	1.7665353	Partial	D
120	1	277.68347	1.5859392	Partial	D
120	2	225.8272	1.5373359	Partial	D
120	3	177.75305	1.5911652	Partial	D
120	4	137.62856	1.7309426	Partial	D
150	0	337.7521	1.7513667	Partial	D
150	1	275.9347	1.6229269	Partial	D
150	2	224.79756	1.5797115	Partial	D
150	3	181.23815	1.6317103	Partial	D
150	4	142.56267	1.7823033	Partial	D
60	0	342.93111	1.7357607	Partial	D
60	1	268.74143	1.5421368	Partial	D
60	2	220.31454	1.4983846	Partial	D
60	3	181.93221	1.5453892	Partial	D
60	4	146.40124	1.6946666	Partial	D
120	0	343.35402	1.7675896	Partial	D
120	1	278.53336	1.6210415	Partial	D
120	2	233.14184	1.5837628	Partial	D
120	3	188.63725	1.6431527	Partial	D
120	4	150.05735	1.7885992	Partial	D
150	0	337.81606	1.753226	Partial	D
150	1	280.82222	1.6658603	Partial	D
150	2	233.22266	1.63315	Partial	D
150	3	192.78829	1.6856588	Partial	D
150	4	157.04285	1.8332226	Partial	D
60	0	342.62804	1.7354783	Partial	E
60	1	268.90118	1.5441881	Partial	E
60	2	220.59347	1.5009535	Partial	E

60	3	182.35481	1.5482328	Partial	E
60	4	146.95462	1.6954826	Partial	E
120	0	343.29368	1.7675289	Partial	E
120	1	278.64877	1.6232378	Partial	E
120	2	233.61756	1.5868716	Partial	E
120	3	189.34381	1.6463838	Partial	E
120	4	150.74343	1.7915458	Partial	E
150	0	337.81449	1.7534142	Partial	E
150	1	281.06551	1.6682056	Partial	E
150	2	233.70101	1.6362546	Partial	E
150	3	193.47186	1.6892208	Partial	E
150	4	157.8584	1.8361777	Partial	E
60	0	342.49113	1.7355158	Partial	E
60	1	269.01787	1.5461224	Partial	E
60	2	220.87313	1.503442	Partial	E
60	3	182.82903	1.551075	Partial	E
60	4	147.55273	1.6963171	Partial	E
120	0	343.26926	1.7675966	Partial	E
120	1	278.73248	1.6251	Partial	E
120	2	234.04696	1.5899184	Partial	E
120	3	190.06844	1.6496613	Partial	E
120	4	152.05719	1.7991711	Partial	E
150	0	337.77536	1.7534395	Partial	E
150	1	281.27611	1.670548	Partial	E
150	2	234.17965	1.6393286	Partial	E
150	3	194.14407	1.6927907	Partial	E
150	4	158.75381	1.8395854	Partial	E
60	0	340.02239	1.7402651	Partial	E
60	1	270.88605	1.585924	Partial	E
60	2	227.54927	1.5598489	Partial	E
60	3	194.26389	1.6110127	Partial	E
60	4	162.49076	1.7550864	Partial	E
120	0	343.75515	1.7725991	Partial	E
120	1	281.45302	1.6680007	Partial	E
120	2	242.78473	1.6514997	Partial	E
120	3	204.61928	1.7188384	Partial	E
120	4	168.44066	1.8611644	Partial	E
150	0	339.59231	1.7588102	Partial	E
150	1	284.27344	1.7114006	Partial	E
150	2	244.30531	1.7029811	Partial	E
150	3	207.76047	1.7633335	Partial	E
150	4	177.01309	1.9070261	Partial	E

60	0	336.29497	1.6810257	Uniform	A
60	1	254.49306	1.452381	Uniform	A
60	2	208.30077	1.3671148	Uniform	A
60	3	152.90331	1.403689	Uniform	A
60	4	106.00743	1.5225706	Uniform	A
120	0	342.08692	1.7291236	Uniform	A
120	1	266.8191	1.5123912	Uniform	A
120	2	210.36661	1.4450225	Uniform	A
120	3	157.98249	1.4791382	Uniform	A
120	4	113.41557	1.5891436	Uniform	A
150	0	340.79131	1.7598507	Uniform	A
150	1	273.17304	1.5437622	Uniform	A
150	2	216.40087	1.4796585	Uniform	A
150	3	161.20303	1.5243376	Uniform	A
150	4	115.49449	1.6410563	Uniform	A
60	0	335.93744	1.7304041	Uniform	A
60	1	270.9419	1.5284766	Uniform	A
60	2	213.29975	1.459094	Uniform	A
60	3	158.57261	1.4977795	Uniform	A
60	4	114.59033	1.6200046	Uniform	A
120	0	336.70864	1.7475662	Uniform	A
120	1	271.98601	1.5829147	Uniform	A
120	2	213.38878	1.5262215	Uniform	A
120	3	165.31153	1.5703762	Uniform	A
120	4	122.76242	1.7181014	Uniform	A
150	0	343.08956	1.7628969	Uniform	A
150	1	280.36998	1.6195826	Uniform	A
150	2	217.21835	1.568133	Uniform	A
150	3	164.52139	1.6259501	Uniform	A
150	4	133.66239	1.7538699	Uniform	A
60	0	339.6889	1.7559287	Uniform	B
60	1	274.17873	1.5434438	Uniform	B
60	2	216.38928	1.4760892	Uniform	B
60	3	160.47862	1.5202656	Uniform	B
60	4	115.16092	1.6401418	Uniform	B
120	0	338.65962	1.7547768	Uniform	B
120	1	277.18181	1.6055851	Uniform	B
120	2	214.60907	1.5479291	Uniform	B
120	3	164.5038	1.5983669	Uniform	B
120	4	129.43278	1.741355	Uniform	B
150	0	345.50911	1.7619428	Uniform	B
150	1	280.5882	1.6266716	Uniform	B

150	2	219.63841	1.5874892	Uniform	B
150	3	167.30805	1.6517777	Uniform	B
150	4	136.7706	1.7794608	Uniform	B
60	0	343.42711	1.7569049	Uniform	B
60	1	284.77696	1.706436	Uniform	B
60	2	224.90442	1.6936696	Uniform	B
60	3	183.90622	1.7520768	Uniform	B
60	4	161.75445	1.8970095	Uniform	B
120	0	346.15466	1.7742605	Uniform	B
120	1	282.37588	1.7431233	Uniform	B
120	2	235.34286	1.7417844	Uniform	B
120	3	202.01653	1.8228005	Uniform	B
120	4	175.28368	1.9789352	Uniform	B
150	0	350.41792	1.7717966	Uniform	B
150	1	287.50867	1.7708553	Uniform	B
150	2	239.31271	1.774935	Uniform	B
150	3	210.14616	1.8444279	Uniform	B
150	4	184.94719	2.0226815	Uniform	B
60	0	344.45623	1.7603008	Uniform	C
60	1	284.84726	1.7152393	Uniform	C
60	2	230.84702	1.7161817	Uniform	C
60	3	189.05026	1.7833686	Uniform	C
60	4	168.25618	1.9166706	Uniform	C
120	0	342.37295	1.7727935	Uniform	C
120	1	285.26483	1.7613781	Uniform	C
120	2	237.97584	1.7653609	Uniform	C
120	3	207.85535	1.8384548	Uniform	C
120	4	181.69022	2.0123927	Uniform	C
150	0	350.47151	1.7693009	Uniform	C
150	1	292.00415	1.7829043	Uniform	C
150	2	245.55385	1.796437	Uniform	C
150	3	213.37828	1.8692413	Uniform	C
150	4	192.3555	2.0443887	Uniform	C
60	0	362.28124	1.8779548	Uniform	C
60	1	304.12624	1.8189954	Uniform	C
60	2	272.67718	1.8962061	Uniform	C
60	3	241.57086	1.9959758	Uniform	C
60	4	225.81934	2.1953898	Uniform	C
120	0	373.67578	2.127751	Uniform	C
120	1	310.83058	1.8243359	Uniform	C
120	2	284.25961	1.9228087	Uniform	C
120	3	253.71493	2.0607185	Uniform	C

120	4	233.81799	2.2442059	Uniform	C
150	0	359.91137	1.8401685	Uniform	C
150	1	311.11024	1.8326956	Uniform	C
150	2	286.3208	1.934189	Uniform	C
150	3	261.94904	2.0773588	Uniform	C
150	4	237.42923	2.2878443	Uniform	C
60	0	368.49322	1.9647785	Uniform	D
60	1	308.95021	1.8239675	Uniform	D
60	2	280.48651	1.9148912	Uniform	D
60	3	245.63402	2.0328438	Uniform	D
60	4	231.56283	2.2116451	Uniform	D
120	0	370.54916	1.9496497	Uniform	D
120	1	311.06949	1.8317625	Uniform	D
120	2	286.10676	1.9333991	Uniform	D
120	3	261.62718	2.07691	Uniform	D
120	4	237.18051	2.2859473	Uniform	D
150	0	358.67515	1.858543	Uniform	D
150	1	312.68976	1.8470638	Uniform	D
150	2	288.78282	1.959448	Uniform	D
150	3	266.11683	2.0847809	Uniform	D
150	4	243.56211	2.3190801	Uniform	D
60	0	354.98924	1.9440097	Uniform	D
60	1	336.74165	1.9428195	Uniform	D
60	2	315.86643	2.0826042	Uniform	D
60	3	280.60374	2.2589179	Uniform	D
60	4	259.99813	2.4784024	Uniform	D
120	0	363.03526	1.9690434	Uniform	D
120	1	342.85924	1.9524983	Uniform	D
120	2	319.62439	2.0963825	Uniform	D
120	3	286.00526	2.2994213	Uniform	D
120	4	258.73239	2.5201197	Uniform	D
150	0	366.00365	1.9661967	Uniform	D
150	1	343.02557	1.9514232	Uniform	D
150	2	319.05341	2.1001245	Uniform	D
150	3	289.06708	2.3088388	Uniform	D
150	4	260.70978	2.5427316	Uniform	D
60	0	357.42711	1.9553471	Uniform	E
60	1	340.20856	1.9498942	Uniform	E
60	2	318.37786	2.091565	Uniform	E
60	3	282.43365	2.2783275	Uniform	E
60	4	259.60782	2.4876752	Uniform	E
120	0	365.45887	1.9704701	Uniform	E

120	1	342.7247	1.9510082	Uniform	E
120	2	319.10409	2.0968975	Uniform	E
120	3	288.54399	2.3088072	Uniform	E
120	4	259.94373	2.5396338	Uniform	E
150	0	365.23979	1.9611913	Uniform	E
150	1	341.78823	1.9542919	Uniform	E
150	2	317.15276	2.1063174	Uniform	E
150	3	290.2565	2.3113311	Uniform	E
150	4	262.92417	2.5584974	Uniform	E
60	0	361.51739	1.9662931	Uniform	E
60	1	342.14969	1.9517437	Uniform	E
60	2	319.56965	2.0935522	Uniform	E
60	3	284.94808	2.296974	Uniform	E
60	4	258.69769	2.5102022	Uniform	E
120	0	365.41001	1.965611	Uniform	E
120	1	341.95068	1.954043	Uniform	E
120	2	317.18319	2.1055504	Uniform	E
120	3	290.04344	2.3089893	Uniform	E
120	4	262.12745	2.5566654	Uniform	E
150	0	363.58676	1.9606179	Uniform	E
150	1	341.78549	1.9620247	Uniform	E
150	2	315.61209	2.1219703	Uniform	E
150	3	290.1189	2.3088582	Uniform	E
150	4	265.54515	2.5659858	Uniform	E
60	0	377.45365	2.0495595	Uniform	E
60	1	351.39569	2.0781873	Uniform	E
60	2	324.33718	2.2318493	Uniform	E
60	3	298.18709	2.452807	Uniform	E
60	4	473.70891	3.6157874	Uniform	E
120	0	379.58632	2.059967	Uniform	E
120	1	350.68229	2.0794343	Uniform	E
120	2	322.40501	2.2443752	Uniform	E
120	3	296.98602	2.4535155	Uniform	E
120	4	436.36083	3.43673	Uniform	E
150	0	380.80035	2.0648009	Uniform	E
150	1	349.25483	2.0817595	Uniform	E
150	2	322.57053	2.2509552	Uniform	E
150	3	296.17168	2.4630034	Uniform	E
150	4	420.32644	3.3288287	Uniform	E

Appendix E Testing Cases

Temperature	Load	Power FFT	Current rms	Demag (F/P)	Demag. Class
60	3	152.90397	1.40369	Partial	A
60	4	106.00717	1.52257	Partial	A
60	3	152.9037	1.40369	Uniform	A
60	4	106.00634	1.52262	Uniform	A
60	3.5	132.19312	1.43889	Partial	A
60	3.8	116.33637	1.47526	Partial	A
60	3.3	141.07381	1.42215	Uniform	A
60	3.7	122.02431	1.45999	Uniform	A
60	2	209.54737	1.37354	Partial	A
60	2	209.802	1.39557	Uniform	A
60	2.5	179.75211	1.37377	Partial	A
60	2.8	168.33452	1.41437	Uniform	A
60	0	336.38685	1.68144	Partial	A
60	0	344.2194	1.72637	Uniform	A
60	0.5	287.45514	1.57275	Partial	A
60	0.7	283.41734	1.55199	Uniform	A
60	1	259.01379	1.46466	Partial	A
60	1	267.8159	1.51673	Uniform	A
60	1.5	231.75222	1.4031	Partial	A
60	1.3	253.56735	1.4836	Uniform	A
60	0	336.07752	1.68849	Partial	B
60	0	337.65363	1.74706	Uniform	B
120	2	219.96627	1.59103	Uniform	B
120	1	274.06299	1.54479	Partial	B
120	1	285.53546	1.71051	Uniform	B
120	1.5	239.21472	1.49111	Partial	B
120	1.3	263.0631	1.6911	Uniform	B
60	0	338.83105	1.70483	Partial	B
60	0	340.93853	1.74343	Uniform	B
120	2	230.02244	1.71293	Uniform	B
120	2	219.72608	1.49349	Partial	B
120	2	235.34222	1.74178	Uniform	B
120	2.5	192.22128	1.49769	Partial	B
120	2.8	206.80336	1.80359	Uniform	B
120	0	341.96672	1.76548	Partial	C
120	0	352.49964	1.85259	Uniform	C
120	0.5	302.82103	1.63104	Partial	C
120	0.7	308.67906	1.78493	Uniform	C
120	4	132.69338	1.70369	Partial	C

120	4	213.51301	2.16663	Uniform	C
120	3.8	141.14003	1.66882	Partial	C
120	3.7	217.58254	2.09664	Uniform	C
120	3	174.50079	1.577	Partial	C
120	3	241.40237	2.00012	Uniform	C
60	0	345.96566	1.73408	Partial	C
60	0	352.24146	1.85462	Uniform	C
120	2	224.36544	1.52397	Partial	C
120	3.5	155.05472	1.6321	Partial	C
120	3.3	233.39168	2.06006	Uniform	C
150	1	276.9189	1.63224	Partial	D
150	1	326.82277	1.88556	Uniform	D
150	1.5	257.06016	1.60381	Partial	D
150	1.3	316.12852	1.91608	Uniform	D
150	4	148.00372	1.80338	Partial	D
150	4	250.30189	2.40615	Uniform	D
150	3.8	153.4623	1.76826	Partial	D
150	3.7	259.54097	2.31473	Uniform	D
60	0	345.09902	1.73669	Partial	D
60	0	365.012	1.90458	Uniform	D
150	2	229.07098	1.60587	Partial	D
150	2	230.83953	1.61757	Partial	D
150	2	312.93833	2.07181	Uniform	D
150	2.5	210.34915	1.63889	Partial	D
150	2.8	287.97238	2.18766	Uniform	D
150	3	195.45628	1.70009	Partial	E
150	3	287.27188	2.3324	Uniform	E
150	3.5	173.76635	1.7671	Partial	E
150	3.3	279.1364	2.4164	Uniform	E
60	0	341.44766	1.73533	Partial	E
60	0	363.00439	1.96709	Uniform	E
150	2	236.1708	1.65203	Partial	E
150	0	339.34581	1.75732	Partial	E
150	0	379.75332	2.03305	Uniform	E
150	0.5	312.87962	1.73199	Partial	E
150	0.7	353.85746	2.0251	Uniform	E

Vitae

Name :ABDULAZIZ SALEH MILHEM

Nationality :Palestinian

Date of Birth :1/24/1983

Email :milhem83@gmail.com

Address :Jenin - Palestine

Academic Background :Bachelor Degree in Electrical Engineering from An-Najah National University - Palestine in 2006

Master of Science in Electrical Engineering from King Fahd University of Petroleum and Minerals (KFUPM) – Saudi Arabia in 2017.